The role of IQGAP3 in cell cycle progression

Die Rolle von IQGAP3 in der Zellzyklusprogression

Der Naturwissenschaftlichen Fakultät

der Friedrich-Alexander-Universität Erlangen-Nürnberg

zur

Erlangung des Doktorgrades Dr. rer. nat.

vorgelegt von

Marina Leone

aus

Neapel, Italien

Als Dissertation genehmigt von der Naturwissenschaftlichen

Fakultät der Friedrich-Alexander-Universität

Erlangen-Nürnberg

Tag der mündlichen Prüfung: 29.10.2015

Vorsitzender der

Promotionsorgans: Prof. Dr. Jörn Wilms

Gutachter/in: Prof. Dr. Manfred Frasch

Prof. Dr. med. Kerstin Amann

SUPERVISED BY

Prof. Dr. Felix B. Engel
Experimental Renal and Cardiovascular Research
Department of Nephropathology
Institute of Pathology
Friedrich-Alexander-Universität Erlangen-Nürnberg (FAU)
Erlangen, Germany

Prof. Dr. Manfred Frasch
Developmental Biology
Department of Biology
Friedrich-Alexander-Universität Erlangen-Nürnberg (FAU)
Erlangen, Germany

To my superhero,

To Mom and Stefy

Contents

Abbreviations

°C	Degree Celsius
Ac	Acetylated
Amp R	Ampicillin resistance
bp	Base pairs
BSA	Bovine serum albumin
ca.	Circa
$CaCl_2$	Calcium chloride
cDNA	Complementary DNA
CH	Calponin homology domain
CH_3COOK	Potassium acetate
CMV	Cytomegalovirus
DAPI	4’,6-diamidin-2-phenylindol
ddH_2O	Double distilled water
DMEM	Dulbecco’s modified eagle medium
DMSO	Dimethyl sulfoxide
DNA	Deoxyribonucleic acid
dNTP	Deoxyribonucleotide triphosphate
E	Embryonic day
E. coli	*Escherichia coli*
ECL	Enhanced chemiluminiscence
EDTA	Ethylenediaminetetraacetic acid
ERK	Extracellular receptor kinase
EtBr	Ethidium bromide
FACS	Fluorescence activated cell sorting
F-actin	Filamentous actin
FBS	Fetal bovine serum

FGF1	Fibroblast growth factor 1
FISH	Fluorescence in situ hybridization
fwd	Forward
g	Acceleration of gravity
g	Gram
G418	Geneticin sulphate
GAPDH	Glyceraldheydes-3-phosphate dehydrogenase
GFP	Green fluorescent protein
GTP	Guanosine 5‘-triphosphate
h	Hour
HCl	Hydrochloric acid
HEPES	4-(2-hydroxyethyl)-1-piperazineethanesulfonic acid
HRP	Horseradish peroxidase
HS	Horse serum
IF	Immunofluorescence
IR	Internal repeats
Kan R	Kanamycin resistance
KCl	Potassium chloride
kDa	Kilodalton
KH_2PO_4	Monopotassium phosphate
l	Liter
LB	Lysogeny broth
LDS	Lithium dodecyl sulphate
M	Molar
MAPK	Mitogen-activated protein kinase
mCherry	Monomeric cherry fluorescent protein
mg	Milligram
$MgCl_2$	Magnesium chloride

$MgSO_4$	Magnesium sulphate
min	Minute
ml	Milliliter
mM	Millimolar
MMLV	Moloney murine leukemia virus
MOPS	3-(*N*-morpholino) propanesulfonic acid
mRNA	Messenger RNA
Na_2HPO_4	Disodium phosphate
$Na_3C_6H_5O_7$	Trisodium citrate
NaCl	Sodium chloride
NaH_2PO_4	Monosodium phosphate
NaN_3	Sodium azide
NaOH	Sodium hydroxide
Neo R	Neomycin resistance
ng	Nanogram
NP40	Nonidet 40
O.D.	Optical density
P	Postnatal day
PBS	Phosphate buffered saline
PCR	Polymerase chain reaction
pH	Negative logarithm of hydrogen ions concentration
PI	Propidium iodide
PIPES	Piperazine-1,4-bis(2-ethanesulfonic acid)
p38i	p38 mitogen-activated protein (MAP) kinase inhibitor
q.s.	Quantum sufficiat (as much as suffices)
RasGAP	Ras GTPase activating proteins
RNA	Ribonucleic acid
RNase	Ribonuclease

rpm	Revolutions per minute
RT	Room temperature
RT-PCR	Reverse transcription followed by polymerase chain reaction
rv	Reverse
SDS	Sodium dodecyl sulphate
sec	Second
siRNA	Small interfering RNA (duplexes)
TAE	Tris-acetate-EDTA
Taq	*Thermus aquaticus*
TBST	Tris buffered saline with Tween 20
U	Unit
UV	Ultraviolet
V	Voltage
v/v	Volume/volume
W	Watt
w/v	Weight/volume
WB	Western blot
WW	Armadillo repeats
µg	Microgram
µl	Microliter
µM	Micromolar

Summary

The cell cycle is a critical process for organism development and tissue homeostasis. In addition, it is required for organ regeneration and its mis-regulation is known to lead to cancer. Thus, tight regulation of the cell cycle is of fundamental importance.

In the heart, cardiomyocytes proliferate during early mammalian development while they reach a post-mitotic state after birth. This state can be reversed in postnatal day 3 cardiomyocytes by treating them with fibroblast growth factor 1 (FGF1) and an inhibitor of p38 mitogen-activated protein kinase (p38i). In addition tumors derived from cardiomyocytes are extremely rare in adults. These characteristics make cardiomyocytes a good model to identify novel cell cycle regulators. Therefore, the aim of this PhD thesis was to identify a new cell cycle regulator, by comparing gene expression data from heart development and cardiomyocyte cell cycle reentry. Candidate genes from the heart development database were chosen from a cluster of similar temporal expression profiles enriched in mitotic genes. Subsequently, it was assessed which of the candidate genes is reexpressed upon FGF1/p38i stimulation. A literature-based analysis identified *Iqgap3* as a possible candidate gene. Immunofluorescence analyses showed that IQGAP3 is mainly expressed in mitosis. It concentrates at the cleavage furrow, at the stem body of the midbody and later at the midbody remnant due to its N-terminal part. Gene silencing experiments have demonstrated that IQGAP3 is required for cell cycle progression because its depletion results in a decreased proliferation rate and a delay in S and G2/M phase progression. Time-lapse movies indicated that IQGAP3 depletion caused a mitotic delay from pro-metaphase to abscission. However, IQGAP3-depleted HeLa cells did not exhibit any alterations in the localization of proteins known to be important for cytokinesis suggesting that IQGAP3 is not required for cytokinesis, also because no binucleation was observed. Closer analyses of time-lapse movies have highlighted the presence of mitotic multipoles in IQGAP3-depleted HeLa cells. In addition, FISH analysis has demonstrated that IQGAP3-depleted cell cultures accumulate over time aneuploid cells. These data demonstrate that IQGAP3 is a novel cell cycle factor playing a possible role in chromosome segregation preventing aneuploidy.

Zusammenfassung

Der Zellzyklus ist ein kritischer Prozeß für die Entwicklung eines Organismus und die Gewebshomöostase. Zudem ist er für die Organregeneration erforderlich und seine Fehlregulation führt bekannter Weise zu Krebs. Daher ist die enge Regulierung des Zellzyklus von grundlegender Bedeutung. Im Herzen proliferieren Herzmuskelzellen während der frühen Säugetierentwicklung während sie nach der Geburt einen post-mitotischen Zustand einnehmen. Dieser Zustand kann in postnatalen Tag 3 Herzmuskelzellen durch Behandlung mit Fibroblasten-Wachstumsfaktor 1 (FGF1) und einem Inhibitor der p38 Mitogen-aktivierten Proteinkinase (p38i) umgekehrt werden. Ferner sind Tumore die von Herzmuskelzellen abgeleitet sind bei Erwachsenen extrem selten. Diese Eigenschaften machen Herzmuskelzellen zu einem guten Modell, um neue Zellzyklusregulatoren zu identifizieren. Daher war das Ziel dieser Doktorarbeit einen neuen Zellzyklus-Regulator zu identifizieren durch den Vergleich von Genexpressionsdaten aus der Herzentwicklung und Herzmuskelzellzyklus-Wiedereintritt. Kandidatengene aus der Herzentwicklungsdatenbank wurden aus einem Cluster zeitlich ähnlicher Expressionsprofile ausgewählt, das in mitotischen Genen angereichert war. Anschließend wurde untersucht, welche der Kandidatengene nach FGF1/p38i Stimulation reexprimiert werden. Eine Literatur-basierte Analyse identifizierte *Iqgap3* als mögliches Kandidatengen. Immunfluoreszenz-Analysen zeigten, daß IQGAP3 hauptsächlich in der Mitose exprimiert wird. Es konzentriert sich aufgrund seines N-terminalen Teils an der Teilungsfurche, am Flemming-Körper und später am Rest des Flemming-Körpers. Gen-Silencing-Experimente zeigten, dass IQGAP3 für die Zellzyklusprogression benötigt wird, da seine Depletierung in einer verringerten Proliferationsrate und einer Verzögerung der S und G2/M-Progression resultierte. Lebendzellbeobachtungen deuteten darauf hin, dass IQGAP3 Depletierung eine mitotische Verzögerung von Prometaphase bis zur Abschnürung verursacht. Allerdings wiesen IQGAP3-depletierte HeLa-Zellen keine Veränderungen in der Lokalisierung von für die Zellteilung wichtigen Proteinen auf. Dies deutete darauf hin, daß IQGAP3 nicht für die Zytokinese erforderlich ist, da auch keine Binukleation beobachtet wurde. Eine nähere Analyse von Lebendzellbeobachtungen hat das Vorhandensein von mitotischen Multipolen in IQGAP3-depletierten HeLa-Zellen hervorgehoben. Darüber hinaus hat eine FISH Analyse gezeigt, daß IQGAP3-depletierte Zellkulturen über die Zeit aneuploide Zellen akkumulieren. Diese Daten

zeigen, daß IQGAP3 ein neuer Zellzyklus-Faktor ist, der möglicherweise eine Rolle in der Chromosomensegregation spielt um Aneuploidie zu verhindern.

1 Introduction

1.1 The mitotic cell cycle

The mitotic cell cycle is comprised of a series temporally distinct phases that a somatic cell passes through prior to undergoing division. Thus, it is required for processes such as tissue homeostasis and organ regeneration. Mis-regulation of cell cycle progression is known to lead to cancer formation. Thus, identifying novel cell cycle proteins and investigating new mechanisms regulating cell cycle progression is important.

The mitotic cell cycle consists of four phases: gap phase 1 (G1), synthesis phase (S), gap phase 2 (G2), and mitotic (M) phase (or mitosis) (Figure 1.1). In G1 phase a cell starts to grow preparing for the duplication of its DNA occurring in S phase. After S phase the cell enters G2 phase where the cell checks if DNA synthesis has been completed and prepares itself for entering in mitosis including an increased microtubule dynamic[1]. Mitosis is composed by two events, karyokinesis (DNA separation) and cytokinesis (cell separation), that act in parallel. During mitotic karyokinesis sister chromatids (replicated chromosomes) segregate to opposite poles of the cell due to forces generated by a bipolar spindle.

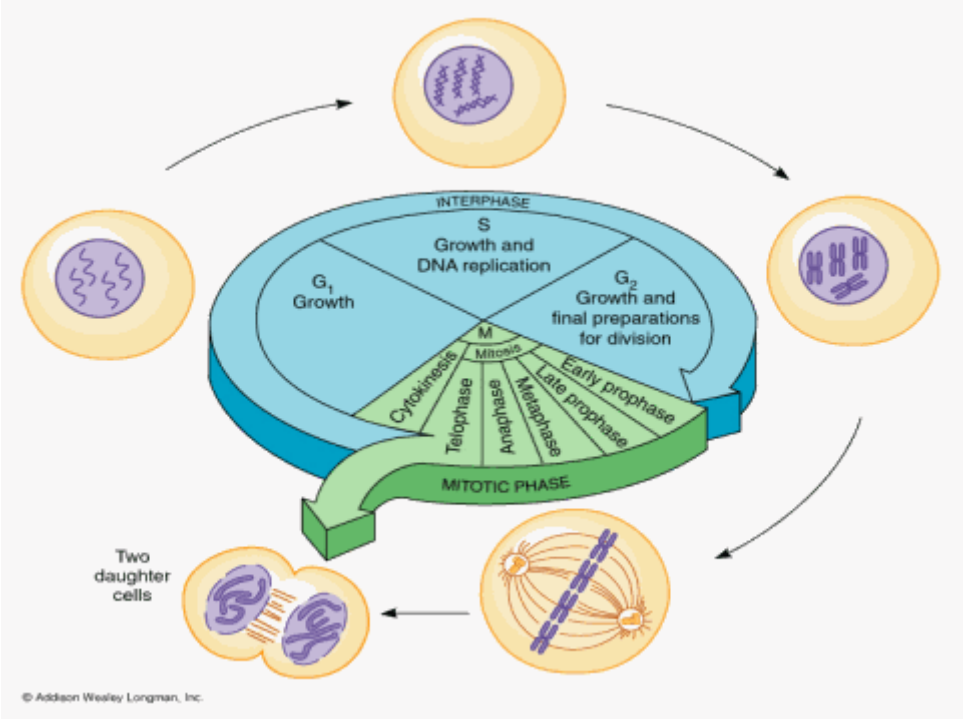

Figure 1.1: Mitotic cell cycle representation. The mitotic cell cycle consists of four phases (G1, S, G2 and M). In G1 phase the cell undergoes a growth process preparing itself for DNA replication that occurs in the following phase, the S phase. After DNA replication the cell

passes through the G2 phase in which it checks if the DNA synthesis occurred without any errors. The M phase or mitosis starts at the end of G2 phase. The mitotic phase is composed by two major events, karyokinesis (DNA separation) and cytokinesis (cell separation), that act in a synchronic way. During mitotic karyokinesis (from prophase to telophase) sister chromatids (replicated chromosomes) segregate to opposite poles of the cell due to forces generated by a bipolar spindle. Figure adopted from Addison-Wesley.

The bipolar spindle is a structure made of several proteins that include kinesin and dynein molecular motors and microtubules which are attached to sister chromatids by a complex called "kinetochore"[2]. Polymerization and depolymerization of microtubules causes chromosome segregation[3]. The polymerization of microtubules is organized by the microtubule organizing center (MTOC) that consists of one centrosome[4].

Cell cycle progression is tightly regulated by checkpoints that ensure upon division, the cell has the correct genetic complement. The two classical checkpoints exist at G1/S and G2/M transition phases[5-8]. Recently, another checkpoint was discovered in mitosis. The NoCut pathway driven by aurora B temporally coordinates the completion of chromosome segregation and abscission timing.[9,10]

Synchronized to the cell cycle the centrosome cycle takes place (Figure 1.2). The centrosome is an organelle that regulates chromosome segregation being part of the MTOC in mitosis[4] and regulates the G1/S transition due to cyclin A and cyclin E centriolar localization[11]. The centrosome is formed by two centrioles, one mother and one daughter and it is surrounded by a matrix of proteins called the pericentriolar material (PCM)[12]. In G1 phase the two centrioles, mother and daughter, separate from each other (disengagement) becoming two independent mother centrioles, linked by a group of proteins called "linker fibers" such as C-Nap1 and rootletin (linker establishment)**.** In S phase the mother centriole duplicates creating a daughter centriole that elongates until the end of S phase (duplication and elongation). In G2 phase centrosomes mature by losing the linker fiber and thus separating from each other (linker dissolution). At the beginning of mitosis the separated mature centrosomes migrate at opposite poles respectively and they generate the bipolar spindle by acting as a functional MTOC[13,14].

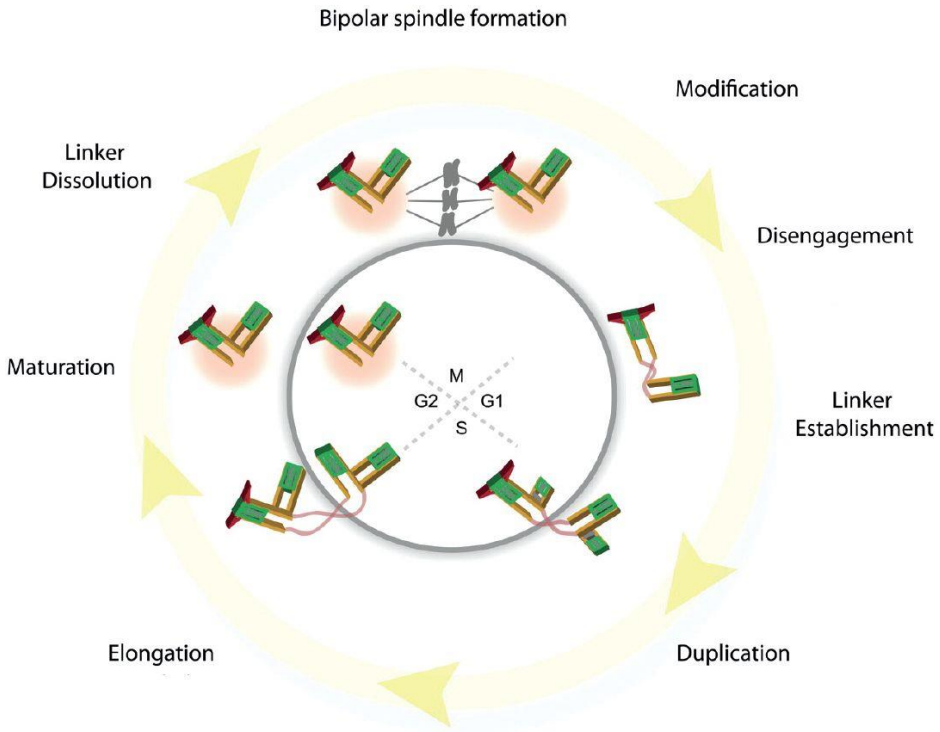

Figure 1.2: The centrosome cycle of animal cells. The centrosome is formed by two centrioles, one mother (it has distal appendages, red triangles in the figure) and one daughter and it is surrounded by a matrix of proteins called the pericentriolar material (PCM) (orange circle in the figure). In G1 phase the two centrioles, mother and daughter, separate from each other (disengagement) becoming two independent mother centrioles, linked by a group of proteins called "linker fibers" such as C-Nap1 and rootletin (linker establishment)**.** In S phase the mother centriole duplicates creating a daughter centriole that elongates until the end of S phase (duplication and elongation). In G2 phase centrosomes mature by losing the linker fiber and thus separating from each other (linker dissolution). At the beginning of mitosis the separated mature centrosomes migrate at opposite poles respectively and they generate the bipolar spindle by acting as a functional MTOC. Figure adopted and modified from Mardin B.R. *et al.*, 2012[130].

1.2 Cardiomyocyte proliferation during heart development

Cell cycle progression is fundamental for organ development including heart development. In mouse, the cardiac crescent is formed at embryonic day (E) 7.5 by the primary heart field, a mesodermal bilateral region consisting of precursors of cardiac lineages[15]. At E 8.0 the cardiac crescent forms the heart tube, which then elongates[16,17] and undergoes looping through a second group of progenitor cells, the second heart field. The looping generates structures, which develop later into the four cardiac chambers (E 13.5)[18]. After the completion of these structural processes the heart grows mainly due to cardiomyocyte proliferation until birth[19,20]. After birth most

mammalian cardiomyocytes reach a post-mitotic state characterized by incomplete cytokinesis resulting in bi- or poly-nucleation or polyploidy (Figures 1.3)[21-25]. In fact adult mouse and rat hearts consist of >90% of bi- or polynucleated cardiomyocytes[22,25] while the adult human heart contains >60% of mononucleated cardiomyocytes; among them ca. 50% being polyploid[26].

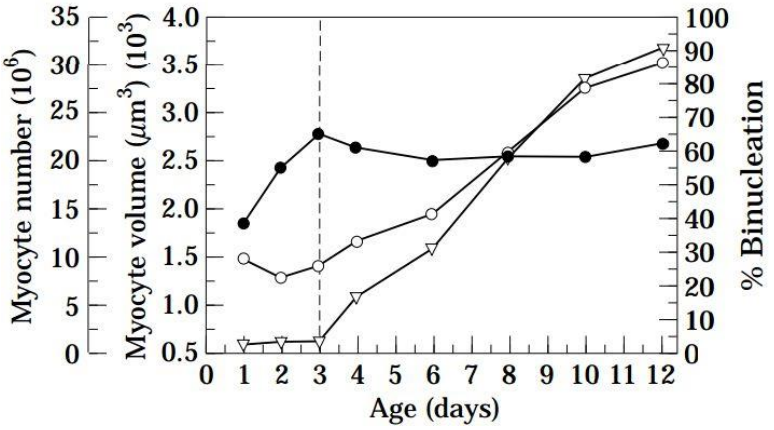

Figure 1.3: Changes of myocyte number, volume and per cent nucleation during postnatal rat heart development. Figure adopted from Li F. *et al.*, 1996[25].

Early studies demonstrated that the post-mitotic status of cardiomyocytes after birth is associated with downregulation of positive cell cycle regulators such as cyclin dependent kinase 2 (CDK2)[27], CDK4[27], cyclin D2, cyclin D3, cyclin E[28], and cyclin A[29] as well as upregulation of negative cell cycle regulators such as the CDK inhibitors $p21^{cip1}$ and $p27^{kip1}$ [30,31,28,32]. The group of MacLellan has provided evidence that indicates that the members Rb and p130 of the retinoblastoma protein family recruit the heterochromatin protein 1-γ (HP1-γ) to silence proliferation promoting genes by heterochromatin formation[33]. Yet, what induces these biological and molecular mechanisms causing the post-mitotic status and why are still unknown. One possible explanation is the loss of centrosome integrity. Zebrowski *et al.* have shown that centrosomes start splitting shortly after birth (postnatal day (P) 3). This phenomenon is coupled with the translocation of some centrosome proteins around the nucleus that thus acquires MTOC function[34].

The fact that cardiomyocytes proliferate during early development and progress after birth through a final incomplete cell cycle, makes them an interesting model to identify novel cell cycle proteins. Moreover, it is possible to induce cell cycle reentry and cell division in P3 cardiomyocytes by stimulation with both fibroblast growth factor 1 (FGF1) and an inhibitor of the p38 mitogen-activated protein (MAP)

kinase (p38i)[35]. The comparison of gene expression data from heart development and cardiomyocyte cell cycle reentry can be used to identify inversely correlated genes as potential candidates for novel cell cycle-related genes.

1.3 Mitosis and cytokinesis

Cardiomyocytes, as well as all the other mammalian cell types, undergo mitosis. Although most of mammalian cells go through karyokinesis (separation of DNA), some of them fail to undergo cytokinesis (separation of the cell) (*e.g.* cardiomyocytes). Mitosis can be separated into prophase, pro-metaphase, metaphase, anaphase and telophase. In prophase, chromatin condenses in chromosomes and at the end of this phase the nuclear membrane breaks down. In pro-metaphase microtubules attach to the kinetochores. In metaphase, chromosomes are aligned along the metaphase plate and in anaphase sister chromatids segregate to opposite ends of the cell due to the forces generated by the two spindle poles. In telophase the nuclear membrane reforms and karyokinesis is completed[36]. In general, cytokinesis, which divides the cytoplasm and organelles, occurs in concert with karyokinesis. The timing of these two events is crucial, in fact it is regulated by the activity of four major proteins[37], anaphase promoting complex (APC)[38], CDK1[39], polo-like kinase 1 (Plk1)[40,41] and aurora B[9,42,43]. During early anaphase the formation of a midzone is the first feature of cytokinesis (Figure 1.4)[44]. The midzone is characterized by the central spindle, a tightly packed bundle of antiparallel microtubules formed by dimers of globular proteins, α-tubulin and β-tubulin. To stabilize microtubules some post-translational modifications on tubulin subunits occurs such as acetylation[45].

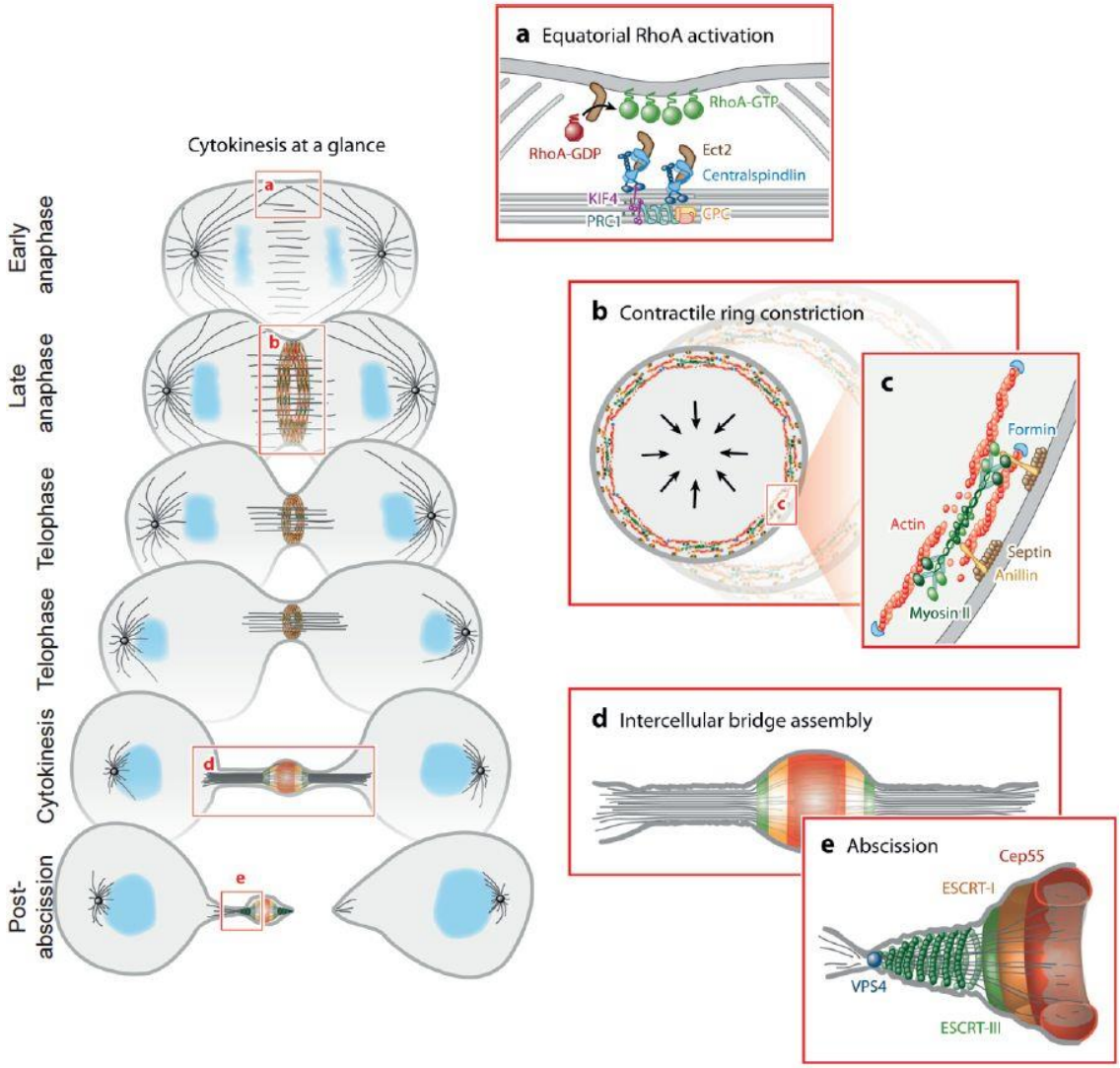

Figure 1.4: Events correlated with cytokinesis. (a) In early anaphase cytokinesis starts with the cross-talk between the proteins (*e.g.* Ect2, MKLP1, aurora B) recruited at the midzone (a narrow zone of bundled microtubules) and the cortex, the cytoplasm layer on the inner face of the plasma membrane, in order to generate an equatorial Rho A activation. (b and c) The activated Rho A assembles the contractile ring formed by actin and myosin type II filaments that constricts the microtubule bundle. These shape changes of the contractile ring are tightly organized and regulated by several proteins such as anillin. (d) During telophase and cytokinesis the constriction of the furrow due to the contractile ring narrowing causes the formation of the midbody from the compaction of the previous midzone. (e) The last step of the cytokinesis is a process called abscission (physical detachment of the two daughter cells). This process is regulated by a complex called endosomal sorting complex required for transport-III (ESCRT-III). Cep55 recruits ESCRT-I at the midbody allowing the assembling of ESCRT-III complex and thus the cell scission. Figure adopted and modified from Green R.A. *et al.*, 2012[44].

Central spindle formation is initiated and regulated by a complex signaling network. Initiation of central spindle formation requires mainly two proteins, protein regulator of cytokinesis 1 (PRC1) and kinesin family member 4 (KIF4). PRC1 cross-links the microtubule in an antiparallel direction, while KIF4 stops the elongation of microtubules that make up the central spindle [44]. Loss of KIF4 results in mis-alignment of microtubules at the midzone leading to cytokinesis failure[46]. Central spindle formation requires two complexes known as centralspindlin and the Chromosome Passenger Complex (CPC). Centralspindlin consists kinesin-6 (MKLP1) and two molecules of CYK-4-GAP (known as MgcRacGAP), while CPC consists of aurora B (AIM1), INCENP, survivin and borealin. The CPC localizes centraspindlin complex to the midzone via phosphorylation of MKLP1. Here, Ect2-GEF activates Rho A protein (Rho-GTP) by binding to the N-terminal part of CYK-4-GAP protein[47]. The binding of Ect2-GEF to CYK-4-GAP protein and the recruitment of Ect2-GEF to the central spindle is regulated by Plk1[44]. In fact, Plk1 inhibitor stops cytokinesis by abolishing Rho A localization and thus the contractile ring formation[41]. Currently, it is hypothesized that CYK-4-GAP inactivates Rho A through exchanging the GTP molecule to GDP[44]. Rho A is the master regulator of the activation and regulation of the contractile ring that allows the formation of a cleavage furrow that occurs between late anaphase and cytokinesis[48]. The contractile ring is an actomyosin ring made of actin and myosin filaments. Rho A activates actin polymerization and myosin filaments to create the contractile ring[49,50]. The dynamics of the actomyosin ring is due to a concerted effort of several proteins, such as nonmuscle myosin II, actin, septins and anillin[51]. Anillin interacts with both myosin and actin filaments through its two domains at its N-terminal part, while it interacts with Rho A and septins through its C-terminal part[52]. Until now, anillin is the only protein known to connect the actomyosin ring and the cortex, the cytoplasm layer on the inner face of the plasma membrane. The coordination between constriction of the cortex and the actomyosin ring is fundamental for a proper cell division. A visible sign of constriction of the cortex is the cleavage furrow. When the cleavage furrow occurs, the antiparallel microtubule bundle undergoes constriction and compaction allowing the formation of the midbody, a single compacted microtubule bundle (called also intracellular bridge) with an electrodense bulge called stem body (Figure 1.5)[53]. In

this transition the recognition of the different stages from late anaphase to cytokinesis is helped by the different stages of compaction of the microtubule bundle.

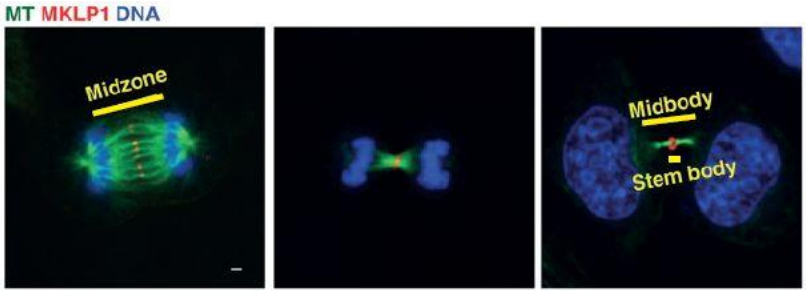

Figure 1.5: Cells in consecutive mitotic stages (from left to right). Cleavage furrow constricts and compacts the antiparallel microtubule bundle (midzone) allowing the formation of the midbody, a single compacted microtubule bundle with an electrodense bulge called stem body. Figure adopted and modified from Hu C.K. *et al.*, 2012[53].

The proteins that form the midbody can be divided into three different groups based on their relative immunohistochemically-defined localizations at the midbody (Figure 1.6). The first group, often referred to as “bulge proteins”, localizes at the stem body of the midbody and includes MKLP1, Cep55 and Ect2. The second group localize adjacent to the stem body (or dark zone), and include PRC1 and KIF4. The third group flanks the previous two groups and includes aurora B, which localize at the two edges of the midbody known as midbody arms[53]. Upon formation of the midbody, a scission of the plasma membrane occurs resulting in cellular abscission, pulling a part the two edges of the microtubule bundle. This process completes cytokinesis and causes the formation of a midbody remnant from the stem body of the previous midbody[44].

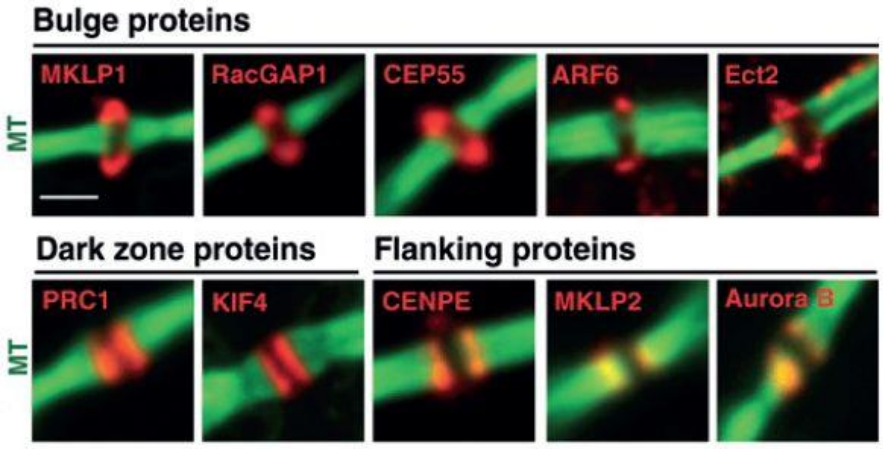

Figure 1.6: Localization of different proteins at the midbody. Midbody proteins are divided into three groups based on their localization at the midbody. The bulge proteins (*e.g.* MKLP1, Cep55, and Ect2) concentrate at the stem body. The second group consists of the

so-called dark zone proteins (*e.g.* PRC1). The flanking proteins (*e.g.* aurora B) are localized at the midbody arms. Figure adopted from Hu C.K. *et al.*, 2012[53].

Abscission, the last step of cytokinesis, is a tightly regulated process (Figure 1.4e). The endosomal sorting complex required for transport-III (ESCRT-III) complex formed by CHMP proteins such as CHMP4B is required for abscission and is localized at both sides of the midbody dark zone. It is recruited to the midbody by ESCRT-I (known also as Tsg101), which is first recruited by Cep55[54,55]. The localization of Cep55 at the midbody is negatively regulated by Plk1. Thus, Plk1 degradation is a necessary step for the recruitment of Cep55 to the midbody and thus the activation of abscission[56]. The ESCRT-III complex polymerizes due to the activity of vacuolar protein sorting-associated protein 4 (VPS4) and migrates to the abscission site where it constricts the intracellular bridge. The last step of abscission is the plasma membrane modelling done by the protein spastin at the abscission site followed by the final physical detachment separation of the two daughter cells[54,55,57]. Abscission can happen either at one side of the midbody, allowing the inheritance of the midbody remnants to one of the two daughter cells, or at both sides causing the release of the midbody remnant to the extracellular space. In this case it can happen that the midbody gets engulfed into another cell, either one of the two daughter cells or a neighbor cell[58]. The microtubule edge next to the midbody can be positively stained for tubulin immediately after abscission[58]. In addition, the midbody remnant can be detected for several hours after abscission by staining for MKLP1 and Cep55[59]. The lifespan of a midbody remnant is around 11 hours before it is degraded by lysosomal and authophagic activity[58].

1.4 Mitotic multipoles and aneuploidy

A required process for generating two genomic balanced daughter cells from one cell is the formation of a bipolar spindle[2]. Several scenarios are known to cause multipole formation (Figure 1.7)[60]. For example, failure of cytokinesis results in binucleation and thus cells containing two nuclei, or one polyploid nucleus[61], and two centrosomes. Induction of mitosis in binucleated or polyploid cells can result in the formation of mitotic multipoles (multipolarity with centrosome amplification). Instead of the presence of a normal bipolar spindle in metaphase (two centrosomes, one at each pole) the mitotic multipolar spindle is formed by the presence of three or more

spindle poles due to the presence of the supernumerary centrosomes. Mitotic poles can experimentally be induced, for example, by Cytochalisin D, an inhibitor of actin polymerization[62]. Cytochalisin D (2 µM) induces cytokinesis failure by inhibiting the formation of the actomyosin contractile ring resulting in mitotic multipoles after several generations in culture[63]. Besides cytokinesis failure, multipolarity with centrosome amplification is caused by centriole overduplication, *e.g.* the rosette phenotype (several daughter centrioles formed from one mother centriole)[60]. Several experimental treatments are known to induce the formation of the rosette phenotype[64,65], such as overexpression of Plk4[66].

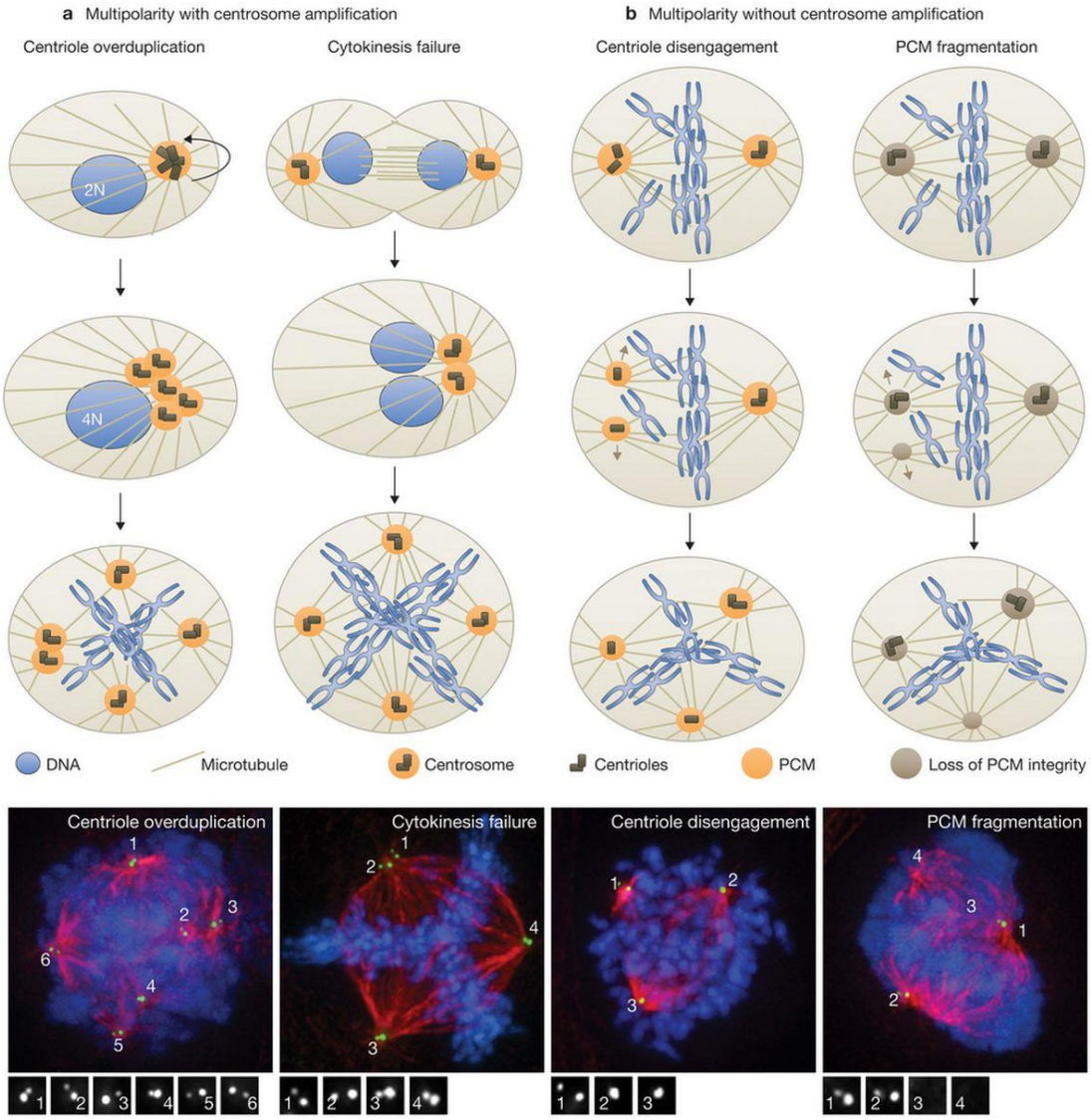

Figure 1.7: Schematic representation of the main causes of mitotic multipolar spindles with and without centrosome amplification. At the bottom of the scheme immunofluorescence analysis of HeLa stably overexpressing EGFP-centrin-2 (green) stained

for α-tubulin (red) and DNA (blue) represent the four conditions explained in the above scheme. Figures are adopted and manipulated from Maiato H. *et al.*, 2014[60].

Multipolarity can also be caused by mechanisms that are independent from centrosome amplification such as premature centriole disengagement and PCM fragmentation[60]. In late mitosis a protein called separase, a protease that controls also chromatid sister cohesion, induces disengagement of the mother centriole from its daughter centriole[67-69]. To prevent premature centriole disengagement and uncoordinated sister chromatid segregation, separase is regulated by two layers of negative regulation. Separase is inhibited by binding to securin[65] and phosphorylation of cyclin-CDK complexes[70]. Multipoles caused by premature centriole disengagement are characterized by the presence of single centrioles at the spindle poles. It remains, however, unclear whether multipolarity in this case is due to premature centriole disengagement or mitotic delay caused by uncoordinated sister chromatid separation[60,71,72]. In fact it has been shown that mitotic delay, induced by the proteasome inhibitor MG132, causes uncoordinated chromatid segregation followed by centriole disengagement and multipolarity[72]. Thus, centriole disengagement can cause loss of spindle pole integrity (uncoordinated sister chromatid segregation) that cause mitotic multiple formation. Another cause of multipolarity without centrosome amplification is the loss of spindle pole integrity due to PCM fragmentation[60]. Several studies have demonstrated that depletion of proteins involved in the formation of the PCM causes mitotic multipoles characterized by acentriolar poles[73-75]. One cause of PCM fragmentation is for example an imbalance of traction forces exerted by kinetochore activity which influences and is influenced by spindle pole organization. Recently, it has been shown that CLIP-associating proteins (CLASPs) and ninein confer spindle pole resistance to these traction forces. Depletion of CLASP proteins leads to three main spindle abnormalities: monopolarity, short spindles and multipolarity. Multipolarity was in around 70% due to fragmentation of pre-existing poles (acentriolar poles) and in around 30% due to premature centriole disengagement (mono-centriolar poles). Loss of spindle pole integrity was preceded by the presence of mis-aligned chromosomes in metaphase. This observation led to the finding that CLASP1/2 depletion caused multipolarity dependent on CENP-E- and/or Kid-mediated forces at kinetochores/chromosome arms. Thus, CLASPs are required for spindle pole resistance to CENP-E-mediated forces[63].

Spindle multipolarity can cause aneuploidy due to failure of faithful chromosome segregation (abnormality in chromosome number)[76-78]. Generally, aneuploidy results in cell death[79,80]. However, occasionally, aneuploidy can be tolerated, and is a defining feature of nearly cancer cells[81]. Previously, it was believed that spindle multipolarity can be utilized to detect pathological mitosis in human tumors[82]. Yet, nowadays, it has been proven that mitotic multipoles are rare events in tumors compared to the "typical bipolar division"[83]. This "failure to detect multipoles" is due to a pro-survival mechanism of tumor cells with centrosome amplification. They cluster extra centrosomes to mimic a semi-normal bipolar spindle that is called "pseudo bipolar spindle". This centrosome clustering allows balanced chromatid segregation and thus the survival of daughter cells[84,85]. However, recent data have demonstrated that tumor cells can form intermediate multipolar spindles before the extra centrosomes are efficiently clustered. The formation of intermediate multipolar spindles causes an accumulation of merotelic attachment (microtubules emanating from both poles attach to a single kinetochore[86]) leading to the presence of lagging chromosomes (chromosomes that lag behind while all the other chromosomes segregate to the spindle poles during anaphase). This phenomenon results in daughter cells with an aneuploidy phenotype that generally permits survival[79,80,87]. In contrast, lack of centrosome clustering results in multipole formation (3 or more poles) and the generation of daughter cells with a poor survival rate due to a severe aneuploidy phenotype[79,88]. However, it has recently been shown that spindle multipolarity caused by centriole disengagement (depletion of astrin[89]) or PCM fragmentation (depletion of CLAPSs proteins[63]) results in daughter cells with a high survival rate. The influence of spindle multipolarity on aneuploidy is to date poorly understood.

1.5 IQGAP family

The IQ motif containing GTPase Activating Protein (IQGAP) family is a well conserved protein family among different species (*Schizosaccharomyces pombe, Saccharomyces cerevisiae, Candida albicans and Ashbya gossypii, Dictyostelium discoideum and* mammalians). While in yeast *(S. pombe and S. cerevisiae)* and fungus *(C. albicans and A. gossypii)* this protein family has only one member, in amoeba (*D. discoideum)* and mammalians there are three members, DdIQGAP1-3

and IQGAP1-3, respectively. In mammalians, the IQGAP family contains three members: IQGAP1, IQGAP2 and IQGAP3[90,91]. These proteins share a common protein structure with five domains (Figure 1.8)[90-92]. The N-terminal part contains calponin-homology domain (CH) and internal repeats (IR). Between the N- and C-terminals exist armadillo repeats (WW) and IQ domains. The C-terminal part contains a RasGAP domain. The similarity between the three mammalian IQGAP family members is around 49% between IQGAP1 and IQGAP2 and 57% between IQGAP1 and IQGAP3[92]. IQGAP1, being the first member to be studied, is the best understood IQGAP family member.

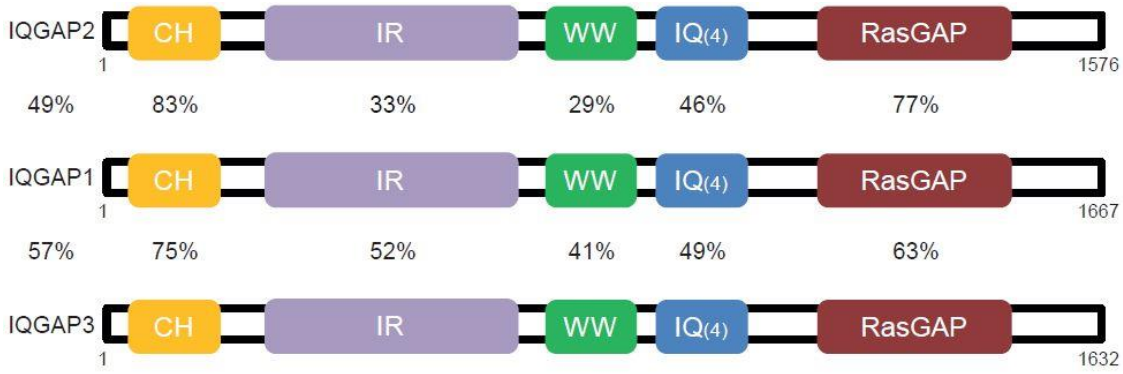

Figure 1.8: Schematic representation of mammalian IQGAP family members, IQGAP2, IQGAP1 and IQGAP3 and their similarity (percentage) in their amino acid sequence homology. CH = Calponin homology domain; IR = Internal repeats; WW = Armadillo repeats; IQ = IQ domains; RasGAP = Ras GAP-related domain.

IQGAP1 has a variety of functions in the cell that can be grouped into four major categories: cell proliferation; cell migration; exocytosis; cell signaling. IQGAP1 modulates cell proliferation in different ways. Johnson *et al.* have shown that it is localized in the nucleus in the G1/S transition[93]. IQGAP1 knockdown in a synchronous HeLa (human epithelial cervix adenocarcinoma cell line) population caused a S phase delay, most probably due to its binding to the two DNA replication factors replication protein A2, 32 KDa (RPA32) and proliferating cell nuclear antigen (PCNA)[93,94]. In addition, IQGAP1 is associated with cytokinesis, even though its role is uncertain. This possible involvement of IQGAP1, or more in general of mammalian IQGAP proteins, in cytokinesis is not surprising as their othologs are required for cytokinesis in *D. discoideum* and yeast[91,95,96]. In HeLa cells, overexpression of a truncated form of IQGAP1 containing IR domain and WW repeats caused increased numbers of bi- or multinucleated cells compared to control cells[97]. In addition it has

been shown that IQGAP1 interacts with Tsg101[98]. Moreover proteomic analysis of isolated midbodies and following immunofluorescence analyses revealed the presence of IQGAP1 at the flanking regions of the midbody in CHO cells (Chinese hamster ovary cell line)[99]. In contrast, another group has shown by immunofluorescence analyses using two different antibodies that IQGAP1 is present at the bulge region of the midbody in both HeLa and NIH3T3 cells (mouse embryonic fibroblast cell line)[100]. However, it has recently been suggested that IQGAP1 does not localize to the midbody[101]. Taken together, these findings highlight that the role of IQGAP1 related to cytokinesis is poorly understood.

In contrast to cytokinesis, the role of IQGAP1 in cell migration is well known. On one hand IQGAP1 has a fundamental function in lamellipodia formation and on the other hand it modulates microtubule dynamics. Lamellipodia are a characteristic feature at the front, leading edge, of motile cells and are generated by actin nucleation. IQGAP1 is involved in this process by interacting with neuronal wiskott-aldrich syndrome protein (N-Wasp) and filamentous actin (F-actin) through its CH domain and thus stabilizing the F-actin structure at the edge of the lamellipodia[102]. In addition, IQGAP1 links microtubules to actin filaments at the front of migrating cell by interacting with CLASP2, a microtubule dynamic regulator[103]. Besides its function in migration, the role of IQGAP1 in exocytosis is well characterized. IQGAP1 is known to bind to exocyst complex protein 70 (EXO70) and septin 2 (SEPT2) via its IR domain and WW repeats[104]. Finally, IQGAP1 is a platform for different cell signaling pathways such as MAP kinases, mammalian target of rapamycin (mTOR) and AKT signaling[91]. This variety of feature can explain how IQGAP1 can be involved in several biological processes such as tumor proliferation, invasion and metastasis[105].

Regarding the role of IQGAP1 in heart development or disease, Sbroggiò *et al.* have not observed a heart phenotype in IQGAP1-null mice under physiological conditions. However, when these mice were exposed to prolonged pressure overload they exhibited left ventricular remodeling. This study has suggested that IQGAP1 regulates cardiac hypertrophy and survival through extracellular signal-regulated kinase 1/2 (ERK1/2) and PI3 kinase-AKT pathways[106,107].

The function of IQGAP2 is in contrast to IQGAP1 less characterized. It has been suggested that it acts as tumor suppressor in gastric[108], liver[109,110] and prostate cancer[111]. This conclusion has been drawn from the observation that IQGAP2 expression is decreased in gastric[108] and liver[110] cancer compared to normal tissues.

In addition, ectopic expression of IQGAP2 decreased the proliferation rate of the prostate cancer cell lines DU145 and PC3 as well as the invasiveness of DU145[111]. Moreover, IQGAP2 is involved as IQGAP1 in cell migration. The IQ domains of IQGAP2 are phosphorylated by A-kinase anchor protein 220 (AKAP220) that binds cAMP-dependent protein kinases (PKA). This post-translational modification of IQGAP2 increases the presence of actin-rich membrane ruffles at the periphery of HEK 293 cells (human embryonic kidney cell line)[112]. Finally, IQGAP2 is involved in colonic inflammation[113] and podocyte structure and function[114].

IQGAP3 is the least studied member of the IQGAP family with the first study published less than a decade ago. As the other family members IQGAP3 has shown to exhibit a variety of cellular functions that can be grouped into three major categories: cell growth and proliferation; cell migration; and tumor invasiveness. The first evidence of IQGAP3 playing a role in regulating cell growth was provided by Wang *et al*. The authors have shown that IQGAP3 binds F-actin by its CH domain as well as guanosintriphophat-cell division control protein 42 (GTP-Cdc42) and guanosintriphophat-ras-related C3 botulinum toxin substrate 1 (GTP-Rac1). In addition, they have discovered that depletion of IQGAP3 impairs Cdc42 and Rac1-dependent neurite outgrowth in PC12 cells (rat pheocromocytoma cell line)[115]. Subsequently, Nojima *et al.* have reported that IQGAP3, but not IQGAP1 and IQGAP2, is expressed in proliferative cells in the crypts of both colon and small intestine and proliferating Eph4 cells (mouse epithelial cell line). Depletion of IQGAP3 impaired proliferation of Eph4 cells, possibly through activation of the rat sarcoma protein (Ras)-dependent ERK pathway[92]. Moreover, it has been shown that IQGAP3, but again not IQGAP1 and IQGAP2, is also expressed in proliferating mouse hepatocytes during development as well as regeneration after partial hepatectomy or CCl_4-induced injury[116]. Furthermore, Yang *et al.* have shown that IQGAP3 suppression decreases the proliferative capacity of A549 cells, a lung cancer cell line. In addition, IQGAP3 depletion in A549 cells reduced their tumorigenicity *in vivo* after intravenous injection[117]. Recently, Adachi *et al.* have suggested a possible role of mammalian IQGAP proteins in cytokinesis of HeLa cells. The authors have shown that IQGAP3 protein expression is increased in G2/M phase, while the expression of IQGAP1 remained unchanged during mitosis. Immunofluorescence analysis revealed that IQGAP3 localizes during mitosis to the cleavage furrow and midbody. The localization at the cleavage furrow was dependent on Rho A and Ect2. Furthermore,

the authors suggest that the N-terminal part of IQGAP3 interacts with anillin via its myosin and actin binding domains. This was supported by the observation that loss of anillin resulted in the mis-localization of IQGAP3 at the cleavage furrow. Functional analyses have shown that suppression of IQGAP3 causes an increase of 5% of multinucleated cells compared to control cells, while silencing both IQGAP3 and IQGAP1 increased multinucleation to 10%. Time-lapse movies finally demonstrated that the reason of binucleation is furrow regression due to a possible mis-localization of anillin and Rho A at the cleavage furrow[101].

IQGAP3, as the other members of the IQGAP protein family, is associated with cell migration. Yang *et al*. have shown that IQGAP3 depletion impaired migration and reduced invasiveness of A549 cells. In addition, overexpression of IQGAP3 in HeLa cell line caused an increase of both migration and invasion capacity[117]. Moreover, high protein levels of IQGAP3 have been associated with the invasive capacity of squamous cell carcinoma (SCC)[118]. However, even though IQGAP3 is correlated with several tumor tissues (bone marrow, breast, large intestine, lung, ovary and stomach[117]) and processes important for cancer such as migration and invasion, the role of IQGAP3 in cancer is still poorly understood.

1.6 Aim of the study

Cardiomyocytes proliferate during early development and progress after birth through a final incomplete cell cycle. In addition, cardiac tumors of the adult heart based on cardiomyocytes are extremely rare, if they exist at all. These features make cardiomyocytes an interesting model to identify novel cell cycle regulators. Moreover, it is possible to induce cell cycle reentry and cell division in P3 cardiomyocytes by stimulation with both FGF1 and p38i. In order to identify cell cycle regulators it appears promising to compare gene expression data describing heart development from E11 to P10.5 in intervals of 12 hours with gene expression data describing cardiomyocyte cell cycle reentry within 72 hours after FGF1/p38i stimulation[35]. Gene expression profiles of the developmental study were grouped in 42 clusters based on their similar temporal expression profiles by using a Bayesian clustering algorithm (Ferrazzi *et al.*, unpublished). Subsequently the functional enrichment of the clusters performed with DAVID identified the cell cycle-related Gene Ontology (GO) terms in each cluster. The aim of this study was to identify and characterize a novel cell cycle regulator by analyzing genes of a cluster enriched in the GO term “M phase”. Candidate genes were obtained by literature analysis and comparison to the FGF1/p38i expression data, in which candidate gene of the developmental data have to be inversely correlated. The specific aims of this study were:

Aim 1: Identifying candidates as novel cell cycle genes by cross-matching the two microarray datasets

Aim 2: Characterization of one candidate gene expression pattern

Aim 3: Elucidating the requirement of one candidate gene for cell cycle progression

Aim 4: Determining the cellular and functional role of one candidate gene

2 Materials

2.1 Equipment

2.1.1 Miscellaneous equipment

Table 1: List of used equipment

Equipment	Model	Supplier
Agarose gel electrophoresis chamber	PerfectBlue Gelsystem Mini	peqlab
Agarose gel electrophoresis chamber	B2 Separationsystem	Owl
Balance	ABJ	KERN
Balance	Pioneer	Ohaus
Belly dancer	Rotamax 120	Heidolph
Chemical hood	EN 14175	Arge
CO_2 incubator	BB15	Thermo Scientific
Digital Gas Mixing system and Heating incubator	INUF-KI4	Tokai Hit
Electronic contact thermometer	ETS-D5	IKA
Electronic pipette	Accu-jet pro	Brand
Electronic pipette	peqMATE	peqlab
FACS	FACS Canto TM II	BD Biosciences
Heating block	LSE Digital dry bath heater	Corning
Laminar flow	MSC-ADVANTAGE	Thermo Scientific
Magnetic stirrer	D-6010	neoLab
Magnetic stirrer with heating	C-MAG HS7	IKA
Manual pipette 2,5 µl; 10 µl; 100 µl; 1000 µl	Reference	Eppendorf
Manual pipette 2,5µl; 10 µl;100 µl;1000 µl	pipetman	Gilson
Microwave	MWG 722	Europa
Microwave	MM817ASM	Siemens
Multilabel Plate Reader	VICTORTM X3	PerkinElmer
MyECL Imager	MyECL Imager	Thermo Scientific
Oven	Memmert	Kirsch
PCR thermocycler	Veriti	Applied Biosystems
pH Meter	pH 221 Microprocessor pH Meter	Hanna Instruments
Power supply	EV231, EV43	Consort
Rocker	Rocker 2D	IKA
SDS-Page electrophoresis chamber	X Cell Sure Lock	Invitrogen

Spectrophotometer	Basic BioSpectrophometer	Eppendorf
Thermomixer	Thermomixer 5435	Eppendorf
Thermomixer	Thermomixer comfort	Eppendorf
Transfer chamber	X Cell II Blot Module	Invitrogen
Vacuum aspirator	AP 04	DITABIS
Vortex	VV3	VWR
Water bath	TW20	Julabo
Water bath	U3	Julabo
Water bath	1083	GFL

2.1.2 Microscopes

Table 2: List of used microscopes

Microscope type	Models	Supplier
Binocular and bright field	DMi1	Leica
Bright field/ Epifluorescence	EVOS FL Imaging System	Life Technology
Confocal	LSM 710	Carl Zeiss
Confocal	TCS SP8	Leica
Epifluorescence	BZ-9000	Keyence
Epifluorescence	DM6000B	Leica

2.1.3 Centrifuges

Table 3: List of used centrifuges

Centrifuge type	Models	Supplier
Centrifuge	Heraeus, Multifuge X1R	Thermo Scientific
Cooling table centrifuge	Biofuge fresco, Haraeus	Thermo Scientific

2.2 Miscellaneous materials

2.2.1 Disposables

Table 4: List of used disposable materials

Materials	Type	Supplier
Butan	C 206 GLS	Campingaz
Cell counter	R80	IVO
Cell Scraper	Cell Scraper 28 cm length	Greiner Bio-one
Cell Scraper	Cell Scraper 25 cm 2-position blade	Sarstedt
Disposal bags	Sekuroka®	Carl Roth
Filter paper	Chromatography Paper	Whatman

Fixogum	290117000	Marabu
Gloves	SensiCare Ice, Powder-Free Nitrile Exam	MEDLINE
Manuel pipettor tip	2 ml; 5 ml; 10 ml; 25 ml; Serological Pipette; CELLSTAR	Greiner Bio-one
Microscope slides	Super Frost WEISS, cut edges	Carl Roth
Needle	Sterican 26G x 1/2	Braun
Needle	Microlance 3.30G x 1/2	BD
Needle	Neolus 23Gx1 1/4	Terumo
Nitrocellulose transfer membrane	Whatman Protan BA 85, 0,45µm	GE Healthcare Life Sciences
Parafilm	807	Laboratory Film
PCR tubes	I1402-8108	Star Lab
Pipette filter tips	1000 µl TipOne (steril)	Star Lab
Pipette filter tips	100 µl FT100	Greiner Bio-one
Pipette filter tips	10 µl SafeSeal-Tips professional	Biozym
Pipette tips	100 µl; 1000 µl	Sarstedt
Pipette tips	10 µl TipOne	Star Lab
Precision wipes	05511	Kimberly-Clark
Reaction tubes	15 ml; 50 ml	Greiner Bio-one
Reaction tubes	1.5 ml; 2.0 ml; Safe Lock Tubes	Eppendorf
Reaction tubes	14 ml (sterile)	Greiner Bio-one
Syringe	Omnifix U-40 Insulin	Braun
Tissue	2069600	Starline
Western blot detection solutions	Immobilon™ Western Chemiluminescent HRP Substrate	Millipore
Western blot gels (PAGE)	NuPAGE 4-12% Bis-Tris Gel, 1.0 mm x 10 well	Novex life technologies

2.2.2 Non disposables

Table 5: List of used non disposable materials

Materials	**Type / Purpose**	**Supplier**
Coplin jars	472800	Brand
Corex tubes	214,588-2	Sigma Aldrich
Forceps	No 4	Dumont & Fils
Glass bottles	DURAN	Schott
Glass Erlenmeyer flasks	DURAN	Schott
Glass Measuring cylinder	DURAN	Hirschmann
Magnetic micro stir bar	58948-397	VWR
Scissors	RS-6845; RS-5910	ROBOZ
Surgical Disposable Scalpels	No 10	Braun

2.3 Chemicals

Table 6: List of used chemicals

Product	Supplier	Product	Supplier
100 bp DNA ladder	NEB	3-(*N*-morpholino) propanesulfonic acid (MOPS)	Carl Roth
1Kb DNA ladder	NEB	Buffer solution pH 4	Carl Roth
2-Propanol ROTIPURAN® ≥ 99.8%	Carl Roth	Buffer solution pH 7	Carl Roth
Albumin Fraction V	Carl Roth	Buffer solution pH 9	Carl Roth
Acetic acid, ROTIPURAN®	Carl Roth	$CaCl_2$	Sigma Aldrich
Acetone	Fluka	Citric acid	Carl Roth
Agarose NEEO ultra-quality	Carl Roth	DABCO	Sigma Aldrich
Ampicillin sodium	Carl Roth	DAPI stock solution	Sigma Aldrich
cOmplete ULTRA Tablets	Roche	Ethidium bromide solution 1%	Carl Roth
dNTP Mix with dTTP	A&B System	Glycerol	Sigma Aldrich
Ethanol denaturated	Carl Roth	HCl	Carl Roth
Ethanol ROTIPURAN® ≥ 99.8%	Carl Roth	HEPES	Sigma Aldrich
Ethylendiamintetraacetic acid	Sigma Aldrich	Immersion oil	Nikon
Formaldehyde solution 37%	Sigma Aldrich	KCl	Sigma Aldrich
Kanamycin sulphate	Carl Roth	KCl	Carl Roth
LDS Sample buffed (4x), NuPAGE	Invitrogen	KH_2PO_4	Carl Roth
Methanol, EMPLURA®	Merck	$MgCl_2$	Carl Roth
NaOH	Carl Roth	$MgSO_4$	Sigma Aldrich
Nonidet P40	Sigma Aldrich	Mowiol 40-88	Sigma Aldrich
Oligo $(dT)_{12-18}$ primer	Invitrogen	Na_2HPO_4 (dibasic)	Carl Roth
PageRuler Plus Protein Ladder	Thermo Scientific	$Na_3C_6H_5O_7$	Carl Roth
Potassium acetate	Carl Roth	NaCl	Carl Roth
Powdered Milk, low fat	Carl Roth	NaCl	Carl Roth
Propidium iodide (PI) stock solution	Sigma Aldrich	NaH_2PO_4 (monobasic)	Carl Roth
RNase A stock solution	Thermo Scientific	NaN3	Carl Roth

Sample Reducing Agent (10x), NuPAGE	Invitrogen	Pepsin from porcine gastric mucosa	Sigma Aldrich
Sodium dodecyl sulphate (SDS)	Sigma Aldrich	PIPES PUFFERAN® ≥99%	Carl Roth
Tris base	Fisher BioReagents	Polyethylene glycol (PEG 3500)	Sigma Aldrich
Triton X-100	Carl Roth	Ponceau S	Carl Roth
Tween 20	Carl Roth	Tris	Carl Roth

2.4 Buffers, media and solutions

Table 7: List of used buffers, media and solutions

Buffer/Medium/Solution	Composition (final concentration)	
10x PBS (1l) (pH 7.4)	80 g 2 g 14.4 g 2.4 g	NaCl KCl Na_2HPO_4 KH_2PO_4
10x TBST (pH 7.5)	200 mM 1.5 mM (1% [v/v])	Tris base NaCl Tween 20
10x Transfer buffer (pH 7.5)	200 mM 1.5 M 1% [v/v]	Tris base NaCl Tween 20
1x MOPS running buffer (1l)	50 ml 950 ml	20x MOPS Running Buffer ddH_2O
1x PBS (1l)	100 ml 900 ml	10x PBS ddH_2O
1x TAE buffer (1l)	20 ml 980 ml	50x TAE buffer ddH_2O
1x TBST (1l)	100 ml 900 ml	10x TBST ddH_2O
1x Transfer buffer	100 ml 900 ml	10x Transfer Buffer ddH_2O
1x wash buffer I	0.4x 0.3% [v/v]	SSC Nonidet P40
1x wash buffer II	2x 0.1% [v/v]	SSC Nonidet P40
20x MOPS running buffer	50 mM 50 mM 0.1% [v/v]) 1 mM	MOPS Tris base SDS EDTA (pH 7.7)
20x SSC (pH 7.0)	3 M 0.3 M	NaCl $Na_3C_6H_5O_7$
2x SSC (1l)	100 ml 900 ml	20x SSC ddH_2O
3.7% formaldehyde (50 ml)	5 ml 45 ml	37% formaldehyde ddH_2O
50x TAE buffer (1l)(pH 8.5)	242 g	Tris base

	57.1 ml 100 ml	Acetic acid 0.5 M EDTA (pH 8.0)
5x KSM buffer	500 mM 150 mM 250 mM 21.7 ml	KCl $CaCl_2$ $MgCl_2$ ddH_2O
70% Methanol	70 ml 30 ml	Methanol H_2O
85% Methanol	85 ml 15 ml	Methanol H_2O
Blocking buffer BSA	5% [w/v]	BSA in 1x TBST
Blocking buffer milk	5% [w/v]	Milk in 1xTBST
Carnoy's fixative	3:1	Methanol:Acetic acid
Complete DNA staining buffer	223 µl 15 µl 12 µl	DNA staining buffer RNase A stock solution Propidium iodide stock solution
DAPI working solution	49.95 ml 50 µl	0.1% Nonidet P40 DAPI stock solution
DNA staining buffer (pH 6.8)	10 mM 100 mM 2 mM 0.1% [v/v] 0.02% [v/v]	PIPES NaCl $MgCl_2$ Triton X-100 NaN_3
Hypotonic solution	0.8% [w/v]	Sodium citrate
IF blocking solution	5% [w/v] 0.2% [v/v]	BSA Tween 20 in 1x PBS
IF washing solution	0.1% [v/v]	Nonidet P40 in 1x PBS
LB agar	35 g	in 1 l H_2O
LB medium	20 g	in 1 l H_2O
Mounting medium (30 ml)	4 g 10 ml 750 mg 20 ml	Mowiol 40-88 Glycerol DABCO 0.2 M Tris-HCl (pH 8.5)
P1 buffer	50 mM 10 mM 400 µg/ml	Tris base 0.5 M EDTA (pH 8.0) RNase A
P2 buffer	0.2 M 1% [v/v]	NaOH SDS
P3 buffer	3 M	Potassium acetate adjust the pH 5.5 with acetic acid
Permeabilization buffer	0.5% [v/v]	Triton X-100 in 1x PBS
PI extraction buffer (pH 7.8)	9:1 0.1% [v/v] 0.01% [v/v]	50 mM Na_2HPO_4: 25 mM citric acid Triton X-100 NaN_3
PI fixation buffer	1 part 6 parts	Ethanol (70% [v/v]) PBS (15% [v/v])

Ponceau S Solution	0.1% [w/v] 5% [v/v]	Ponceau S Acetic acid
TSB buffer	10% [v/v] 5% [v/v] 10 mM 10 mM 100 ml	PEG 3500 DMSO $MgCl_2$ $MgSO_4$ LB medium

2.5 Cell culture-related materials and media

2.5.1 Cell culture chemicals and materials

Table 8: List of used cell culture chemicals and materials

Product	Supplier
µ-Slide 4-well chamber	Ibidi
1.8 ml Conical Cryovial	Star Lab
12 mm coverslip	Thermo Scientific
CELL STAR® 10 cm dishes	Cell Star Greiner Bio-one
CELL STAR® 24 well plates	Cell Star Greiner Bio-one
CELL STAR® 6 well plates	Cell star Greiner Bio-one
CELL STAR® 96 well plates	Cell star Greiner Bio-one
Claycomb medium	Sigma Aldrich
Collagenase type II	Invitrogen
Dimethyl sulfoxide (DMSO)	Carl Roth
DMEM/F-12 (1:1)+GlutaMAX™ –I medium	Gibco, Life Technologies
DNase I	Roche
DPBS, steril filtered, Ca^{2+}/Mg^{2+}-free	Gibco, Life Technologies
Dulbecco's Modified Eagle's Medium-GlutaMAX™ (DMEM-GlutaMAX™) medium	Gibco, Life Technologies
FBS (for HL-1 cell line)	Sigma Aldrich
Fetal bovine serum (FBS)	Biowest
FGF1	R&D Systems
Fibronectin (1mg/ml)	Sigma Aldrich
Gelatin from bovine skin	Sigma Aldrich
Geneticin disulphate (G418)-solution, CELLPURE	Carl Roth
Glass Pasteur pipette	Dojindo
Horse serum (HS)	Invitrogen
L-Ascorbic acid, Sodium Salt	Sigma Aldrich
L-Glutamine	Sigma Aldrich
Lipofectam®2000	Life Technologies
Lipofectamine®LTX with PLUS™ Reagent	Life Technologies
Lipofectamine®RNAiMAX Transfection Reagent	Life Technologies
Norepinephrine	Sigma Aldrich
Opti-MEM®, GlutaMAX™ supplement	Gibco, Life Technologies
p38 inhibitor (SB203580)	Tocris
Pancreatin	Sigma Aldrich
Penicillin/Streptomycin (Pen/Strep) (100	Gibco, Life Technologies

U/ml:100 µg/ml)	
Scienceware® cloning discs size 3 mm	Sigma Aldrich
T25 flask	Cell star Greiner Bio-one
T75 flask	Cell star Greiner Bio-one
Thymidine (100 mM) solution	Sigma Aldrich
Trypsin-EDTA solution	Sigma Aldrich

2.5.2 Cell culture media, supplements and coating solutions

Table 9: List of used cell culture media, supplements and coating solutions

Product	**Formulation (final concentration)**
Cardiomyocyte digestion buffer	20 mM HEPES-NaOH (pH 7.6) 130 mM NaCl 3 mM KCl 1 mM NaH_2PO_4 4 mM Glucose 0.14 mg/ml Collagenase II 0.50 mg/ml Pancreatin 10 mg/ml DNase I
Cardiomyocyte pre-plating medium	DMEM/F-12 (1:1)+GlutaMAX™–I medium supplemented with: 10% [v/v] FBS 1% [v/v] Pen/Strep 2 mM L-Glutamine
Cell Culture Freezing Medium	DMEM-GlutaMAX™ medium supplemented with: 10% [v/v] DMSO 20% [v/v] FBS
Cell culture medium	DMEM-GlutaMAX™ medium supplemented with: 10% [v/v] FBS 1% [v/v] Pen/Strep
Complete cardiomyocyte medium	DMEM/F-12 (1:1)+GlutaMAX™–I medium supplemented with: 1% [v/v] Pen/Strep 1% [v/v] HS
Complete Claycomb medium	Claycomb medium supplemented with: 10% [v/v] FBS 1% [v/v] Pen/Strep 0.1 M norepinephrine 2 mM L-Glutamine
DNase I solution	100 mg DNase I dissolved in 10µM $MgCl_2$ solution
FGF1	50 ng/ml dissolved in 0.1% [w/v] BSA in PBS
HL-1 coating solution	0.02%[w/v] gelatin 0.005 mg/ml fibronectin
Norepinephrine stock solution	80 g norepinephrine in 25 ml L-Ascorbic Acid (30 mM) => 10 µM stock solution

p38 inhibitor (SB203580)	10 µM in ddH_2O

2.6 Plasmids

Table 10: List of used and created plasmids

Protein/Gene name	Backbone vector	Bacterial resistance to	Mammalian resistance to	Plasmid Name
IQGAP3	pCMV6-AC-GFP	Ampicillin	G418	IQGAP3-GFP
IQGAP3	pCMV6-Entry	Kanamycin	G418	IQGAP3-myc
	pCMV6-AC-GFP	Ampicillin	G418	pCMV-AC-GFP
C-terminal part of IQGAP3	pCMV6-Entry	Kanamycin	G418	mutB-myc
C-terminal part of IQGAP3	pCMV6-AC-GFP	Kanamycin	G418	mutB-GFP
N-terminal part of IQGAP3	pCMV6-Entry	Kanamycin	G418	mutA-myc
N-terminal part of IQGAP3	pCMV6-AC-GFP	Ampicillin	G418	mutA-GFP

2.7 Enzymes

Table 11: List of used enzymes

Product	Supplier	Product	Supplier
HotStar HiFidelity DNA polymerase	QIAGEN	*Kpn*I restriction enzyme	NEB
M-MLV Reverse Transcriptase	Sigma-Aldrich	*Mlu*I restriction enzyme	NEB
T4 DNA Ligase	Promega	*Not*I restriction enzyme	NEB
T4 DNA Polymerase	NEB	*Psi*I restriction enzyme	NEB
TopTaq DNA Polymerase	QIAGEN	*Sgf*I restriction enzyme	NEB

2.8 Antibiotics

Table 12: List of used antibiotics

Antibiotics	Working concentration	
	Liquid culture	Agar plate
Ampicillin	100 µg/ml	100 µg/ml
Kanamycin sulphate	20 µg/ml	20 µg/ml
Geneticin disulphate (G418) solution, CELLPURE	400 ng/ml	

2.9 Kits

Table 13: List of used kits

Kit	Purpose	Supplier
BCA Protein Assay Kit	Protein quantification	Merck Millipore
Cell Counting Kit-8	Cell proliferation assay	Dojindo
Immobilon Western HRP Substrate	HRP detection	Merck Millipore
QIAGEN Plasmid Midi Kit	Plasmid isolation from 100 ml of bacterial culture	QIAGEN
QIAquick Gel Extraction Kit	DNA extraction from agarose gel	QIAGEN
QIAquick PCR Purification Kit	PCR purification	QIAGEN

2.10 Competent cells

Table 14: List of used competent cells

Bacterial strain	Specification
XL1-Blue	Competent cells

2.11 Software

Table 15: List of used software

Software	Application
Adobe Photoshop, Illustrator	Figure presentation
FlowJo	FACS data analysis
Geneious	Plasmid building
GraphPad Prism	Graphical representation and Fisher's exact test calculation
ImageJ, Fiji, BZ-II Analyzer	Video analysis and preparation
Microsoft Excel, Word, PowerPoint	Data analysis, documentation and p-value calculation

3 Methods

3.1 Cell culture-related methods

3.1.1 Cell lines and reagents

Human epithelial cervix carcinoma cell line HeLa and HeLa stably transfected with mCherry-α-tubulin (a gift from Prof. Gaubatz, Würzburg University), mouse embryonic fibroblast cell line NIH3T3 (ATCC, Mannasas, VA) and human colon tumor cell line HCT116 (ATCC, Mannasas, VA) were maintained in supplemented Dulbecco's Modified Eagle's Medium-GlutaMAX^{TM} (DMEM-GlutaMAX^{TM}) (cell culture medium). Mouse atrial muscle cell line HL-1 was cultivated in completed Claycomb medium. Before passaging HL-1 cells plates were coated with gelatin/fibronectin (HL-1 coating solution). Cells were grown at 37°C in a humidified atmosphere of 5% CO_2. The pH of the culture medium was monitored by the color of phenol red present in the medium. Dependent on the purposes of the experiments cells were plated in different concentrations either in 6-well plates, in 24-well plates, in µ-Slide 4-well Ibidi chambers or in 96-well plates (Table 16).

Table 16: Cell-chambers utilized in this thesis and correlated cell numbers

HeLa cell line		
Experiment/ Figure number	Culture plate	Cell number per well
FACS experiment	6-well plate	600,000
Proliferation assay	24-well plate	170,000
Proliferation assay	96-well plate	6,000
IF staining	24-well plate	120,000
IF staining plus transfection	24-well plate	170,000
HeLa stably transfected with mCherry-α-tubulin cell line		
Experiment/ Figure number	Culture plate	Cell number per well
IQ3-GFP transfection	24-well plate	160,000
IQ3-GFP transfection	µ-Slide 4-well plate	50,000
siIQ3#1/si ctrl transfection	24-well plate	140,000
siIQ3#1/si ctrl transfection	µ-Slide 4-well plate	50,000
mutA/B-GFP transfection	24-well plate	160,000
mutA/B-GFP transfection	µ-Slide 4-well plate	50,000

HCT116 cell line		
Experiment/ Figure number	Culture plate	Cell number per well
FISH analysis	6-well plate	600,000

3.1.2 Isolation of neonatal rat cardiomyocytes and reagents

Postnatal day 3 (P3) rats were decapitated and the heart was extracted from the opened chest by using curved forceps. The isolated hearts were immediately placed in a petri dish with 10 ml of cold PBS without Ca^{2+} and Mg^{2+} containing 5 mM glucose on ice. The aorta and the atria were removed with a scalpel and the remaining ventricles were first gently squeezed with forceps to remove the blood and then minced in small pieces. The minced ventricle tissue was collected with forceps and placed in a Corex glass tube containing 2 magnetic micro stir bars with 15 ml of cardiomyocyte digestion buffer. The Corex tube was incubated in a 37°C water bath on a magnetic stirrer (200-300 rpm). After 3 min the tube was taken out of the water bath to let the heart tissue settle for 3 min in a tube rack under the hood. Afterwards the supernatant was discarded. This washing step was repeated one more time. Subsequently seven digestion steps were consecutively performed. The first and the second ones consisted of 10 min of digestion and stirring followed by 5 min of settling. During the last five digestions steps the hearts were digested 8 min instead of 10 min. At the end of every of the seven digestion steps the supernatant was collected in a total of four 50 ml plastic tubes containing each 4 ml of HS placed in ice. The four tubes were centrifuged at 330 × *g* for 3 min at 4°C. The supernatant was aspirated and the pellets were resuspended in pre-warmed cardiomyocytes pre-plating medium (20 ml per 10 hearts). The cell suspension was plated in 10 cm petri dishes (10 ml/dish) and incubated at 37°C (5% CO_2). During this time non-myocytes attach to the dish, while cardiomyocytes remain in the medium. After 2 h the supernatant was collected in 50 ml plastic tubes, which were then centrifuged at 330 × *g* for 3 min at 4°C. Carefully the supernatant was aspirated and the pellet was resuspended in completed cardiomyocyte medium. Per well 120,000 cardiomyocytes were plated on fibronectin-coated 12 mm coverslips.

All drug stimulations were started after two days from the isolation, because during this time cardiomyocytes attach properly to the plate. The cardiomyocytes were stimulated with either p38 inhibitor (SB203580, added every 24 h) or FGF1

(added every 24 h) or 20% FBS (added once) for three days. Subsequently they were fixed for consecutive immunofluorescence analyses.

3.1.3 siRNA molecules and transient transfection

In order to understand the role and the function of a gene, gene knockdown *in vitro* is a valid method. One way to knockdown a gene is through siRNA molecules that target a 19 bp RNA-specific sequence with dTdT overhangs (Table 17).

Table 17: siRNAs utilized in this thesis

Name	Target	Sequence (5'-3')
si ctrl	Control siRNA	TGGTTTACATGTCGACTAA
si IQ3#1	siRNA binds 3'UTR region of IQGAP3	CACTAACTCACCACTGTGC
si IQ3#3	siRNA binds an internal region of IQGAP3	GCAGCCTTCTCTTCATTAC

Transient transfections were performed with the following products: Lipofectamine 2000, RNAiMAX, and LTX with Plus reagent. The technology of Lipofectamine is based on liposome formation that entraps the transfection materials (either plasmid or siRNA molecules). Lipofectamine 2000 and Lipofectamine RNAiMAX were used for siRNA transfections, while Lipofectamine LTX with Plus reagent was mainly utilized for DNA transfections. The transfection efficiency varies significantly among cell lines. Thus, different protocols depending on the cell line were utilized. In case of HeLa cells in 1.5 ml reaction tubes were used: one contained either the DNA with Plus reagent or siRNA (final concentration: 100 nM); the other one contained the Lipofectamine reagents. Subsequently, the content of the first reaction tube was mixed with the second reaction tube containing the diluted Lipofectamine. After 5 min at room temperature (RT) (incubation time) the total reaction volume was added dropwise to the dish. Regarding the HCT116 cells, the incubation time was extended up to 20 min. Even if the protocols changed between cell lines, the quantity of Lipofectamine reagent, Plus reagent, DNA and siRNA didn't change (Table 18).

Table 18: Transfection methods utilized in this thesis

Plate	Lipo fectamine reagent	Plus reagent (1:1 with µg of DNA)	DNA	siRNA (100 µM)	Total reaction volume
24-well	2 µl			0.5 µl	50 µl
24-well	2 µl	0.5 µl	0.5 µg		50 µl
6-well	5 µl			2 µl	300 µl
6-well	5 µl	2.5 µl	2.5 µl		300 µl

3.1.4 Creating HeLa stably transfected with IQ3-myc

To create a cell line that stably expresses a gene of interest requires the integration of this gene, generally linked with either one or more tags, in the genome of a cell. This is normally characterized by two major steps: 1) Linearizing and transfecting the plasmid into the cell line and 2) selection of the positive colonies via antibiotic resistance. The plasmid was linearized by digesting IQ3-myc plasmid (6 µg) with *Psi*I restriction enzyme for 3 h at 37°C. The linearized plasmid was then purified according to the instructions of a PCR purification kit and the efficiency of the linearization was assessed by agarose gel electrophoresis. Afterwards the linearized vector was transfected into HeLa cells by Lipofectamine LTX with Plus Reagent. The cells were expanded in 10 cm petri dishes and positively selected by using 400 ng of geneticin (G418) diluted in growth medium for 3 weeks, as the IQ3-myc plasmid contains a Neomycin cassette that makes successfully transfected cells resistant to G418. Non-transfected cells die upon G418 treatment. Individual positive colonies were isolated by using cloning discs and cultivated in 96-well plates for a second round of positive selections. After two weeks the surviving colonies were trypsinized and plated in both 12 mm coverslips and 6-well dishes to verify IQ3-myc expression by immunofluorescence and western blot. Three clones (clone O, K and G) positive for IQ3-myc were obtained. They were kept in culture and each two days fresh antibiotic was added to the cell culture medium.

3.1.5 Life cell imaging

Cells were placed in a µ-Slide 4-well glass bottom (Ibidi) to a final concentration of 50,000 cells per well. The slide was placed in a humid chamber (Tokai Hit) to allow the cells to survive during the length of the video-recording. Between 10 and 20 spots per each condition were video-recorded and the interval between two photos was 4

to 9 min. Since the spindle axis of HeLa cells is not parallel to the bottom, a Z-stack of pictures was recorded at every time point. A stack covered between 3 and 6 µm. The video was analyzed by both BZ-II Analyzer software (Keyence) and Fiji software.

3.2 RNA-related methods

3.2.1 Reverse transcription reaction

Ventricles were isolated from E11 to P10 in intervals of 12 h and their RNA was isolated by Trizol (Ferrazzi F. *et al.*, unpublished). To start the reverse transcription reaction from RNA the M-MLV reverse transcriptase enzyme was used. In a 1.5 ml RNase-free reaction tube the following reagents were mixed: 1 µg of RNA, 200 µM dNTPs, 0.5 µg/µl of Oligo (dT) 12-18mer primer, and RNase-free water q.s. to 10 µl. This mixture was incubated for 5 min at 65°C and then kept on ice for 1 min. Subsequently the following reagents were added to the previous mixture: 1x M-MLV Reverse Transcriptase buffer, 1 µl of M-MLV reverse transcriptase and RNase-free water q.s. to 20 µl. The tube was kept at RT for 1 min and then incubated for 50 min at 37°C. To inactivate the reaction the tube was kept for 10 min at 80°C. After a short centrifugation step 80 µl of RNase-free water was added to the cDNA to reach a final concentration of approximately 10 ng/µl.

3.3 DNA-related methods

3.3.1 *Iqgap3*, *Iqgap1* and *Iqgap2* gene amplification from rat cDNA

For analyzing the gene expression profiles of *Iqgap3*, *Iqgap1* and *Iqgap2* during rat heart development, a standard PCR reaction was set up. The enzyme TopTaq DNA polymerase and 1 µl of cDNA as template were used. A master mix was prepared by adding 1x TopTaq PCR Buffer, 200 µM dNTPs, 1x CoralLoad Concentrate, either 0.25 µM of IQGAP1 and IQGAP2 forward and revers primers or 0.5 µM of IQGAP3 and GAPDH forward and revers primers (Table 19), 1.25 U of TopTaq DNA polymerase in a final volume of 20 µl.

Table 19: Primers utilized in this thesis

Name	Primers	Sequence (5'-3')	Annealing Temperature	Product size (bp)
Iqgap1	IQ1_R_fwd	GCGTCTTCAAGGTCTCTGCTC	60.9°C	691
	IQ1_R_rv	CGAGAGCTCGTTAGCCAGGA		
Iqgap2	IQ2_R_fwd	CAGGGGTCCAGTGCCTCTCA	57°C	681
	IQ2_R_rv	GCGATGTTCTGTCGCCTCCT		
Iqgap3	IQ3_R_fwd	CACCAAACAGATGCTGGCC	60°C	650
	IQ3_R_rv	CCCAGGAACTTGGCATTGACG		
Gapdh	GAPDH_R_fwd	CAGAAGACTGTGGATGGCCC	59°C	279
	GAPDH_R_rv	AGTGTAGCCCAGGATGCCCT		

The cycling program that was used had the following conditions: initial denaturation step 3 min at 94°C, 30 cycles of 30 sec at 94°C, 30 sec annealing at 57°C to 60°C and an extension time of 1 min at 72°C. After the last cycle there was a final extension step of 10 min at 72°C. Then the temperature was lowered to and kept at 4°C until the samples were collected.

3.3.2 Agarose gel electrophoresis

DNA (PCR or digested plasmid) was analyzed by electrophoresis utilizing 1-1.5% agarose gels prepared with 1% TAE buffer containing ethidium bromide (EtBr, 1:50000 dilution). The electrophoresis was run for 30-40 min at 130V in 1% TAE buffer. The DNA was visualized under UV light, ʎ =306 nm.

3.3.3 DNA band extraction from agarose gels

The DNA band extraction from agarose gels was done according to the manufacturer's instructions for the "QIAquick gel extraction kit". At the elution step, 20 µl of ddH2O was added to the column and after 1 min samples were centrifuged at maximum speed to increase the concentration of either the plasmid or PCR product.

3.3.4 PCR purification with column

Either PCR product or digested plasmids were purified by following the manufacturer's instructions for the "QIAquick PCR purification kit". At the elution step 20 µl of ddH2O was added to the column and after 1 min samples were centrifuged at maximum speed to increase the concentration of either the plasmid or PCR product.

3.3.5 Determination of the concentration of nucleic acids

The concentration of DNA and RNA was determined with a Basic BioSpectrophotometer (Eppendorf). Samples (2 µl) were placed in an Eppendorf µCuvette G1.0. Absorbance at 260 nm was measured and the concentration was calculated based on the law of Lambert-Beer's: A = E*C*L (E = coefficient of absorbance, C = concentration, L = optical path length). The purity was measured via the ratio 260 nm : 280 nm (protein contamination) and 260 nm : 230 nm (other kind of contaminations). Both of these ratios should be between 1.8 and 2.0 in case of samples with a proper purity.

3.3.6 Cloning

3.3.6.1 IQGAP3-GFP, IQGAP3-myc, and pCMV-AC-GFP

A plasmid encoding IQGAP3 tagged with TurboGFP at the C-terminus of the protein was purchased from OriGENE through Amsbio company. Subsequently, *IQGAP3* was released from the plasmid by digesting IQGAP3-GFP (IQ3-GFP) with *Sgf*I and *Mlu*I restriction enzymes and ligated into the backbone vector pCMV6-Entry (OriGENE) following the instructions from OriGENE. The resulting plasmid encodes IQGAP3 tagged with a myc and a Flag tag at its C-terminus (IQ3-myc) (Figure 3.1).

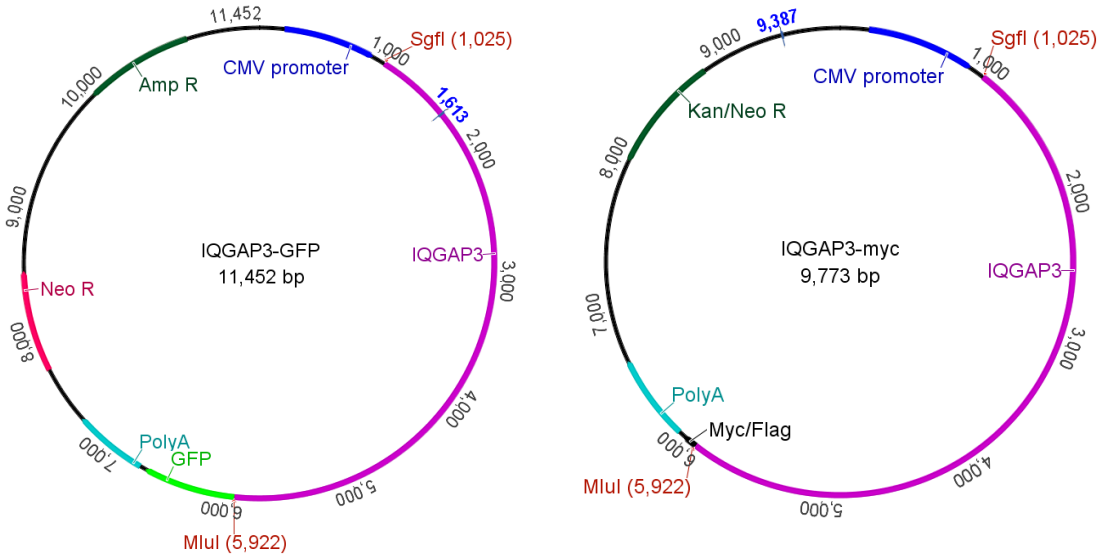

Figure 3.1: Plasmid maps of IQGAP3-GFP and IQGAP3-myc. *Mlu*I and *Sgf*I restriction sites used for the cloning process are highlighted. CMV = cytomegalovirus promoter; Amp R = ampicillin resistance cassette; Kan R = kanamycin resistance cassette; Neo R = neomycin resistance cassette; PolyA = poly-adenylation signals.

As a control vector for IQGAP3-GFP the IQ3-GFP plasmid was digested with *Kpn*I and *Not*I restriction enzyme for 3 h at 37°C to remove *IQGAP3*. The digestion reaction was run on 1.5% agarose gels and the backbone vector band (6.6 Kb) was extracted from the agarose by using the "QIAquick gel extraction kit". Since both *Not*I and *Kpn*I cut the DNA creating non-complementary "overhangs" the linearized plasmid was "blunted" before self-ligation. For this purpose the backbone of the digested IQGAP3-GFP plasmid was incubated with the enzyme T4 DNA polymerase (3 U/µl), 1x Buffer 2, 200 µM dNTPs for 30 min at 37°C. Once the vector had "blunt ends", it was self-ligated by using 100 ng of the vector, T4 DNA ligase enzyme (0.5 U) and 1x ligase buffer at 4°C overnight resulting in the Plasmid pCMV-AC-GFP (Figure 3.2).

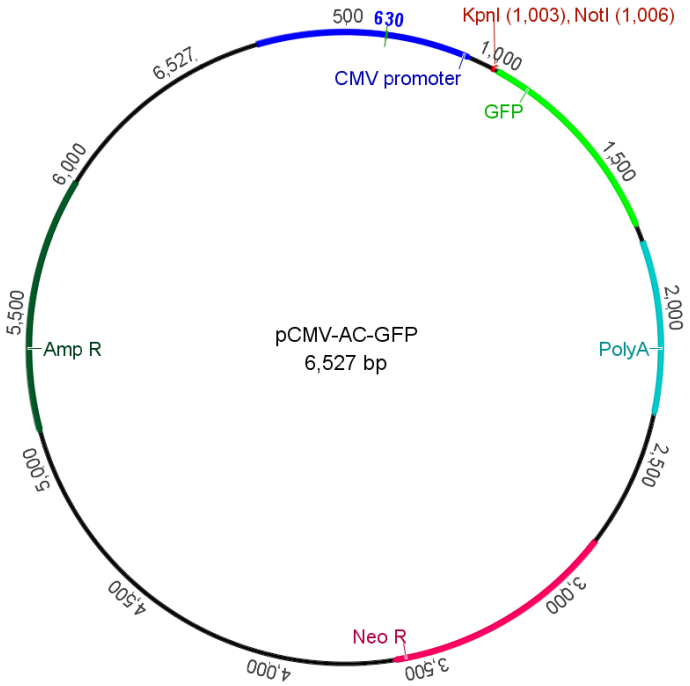

Figure 3.2: Plasmid map of pCMV-AC-GFP. *Kpn*I and *Not*I restriction sites used for the cloning process are highlighted. CMV = cytomegalovirus promoter; Amp R = ampicillin resistance cassette; Neo R = neomycin resistance cassette; PolyA = poly-adenylation signals.

3.3.6.2 mutA-GFP, mutB-GFP, mutA-myc and mutB-myc

The two truncated forms, mutA and mutB, were created by amplifying the N- and C-terminal parts of the *IQGAP3* gene from the plasmid IQ3-GFP with primers containing *Sgf*I (primer fwd) and *Mlu*I (primer rv) cutting sites. Since it was fundamental not to have mutations inserted in both the amplified sequences, a High Fidelity DNA Polymerase was used. For this aim a PCR reaction was set up by adding the HotStar HiFidelity DNA polymerase (2.5 U), 1x HotStar HiFidelity PCR buffer, 1 µM of both forward and reverse primers (Table 20), and 10 pg of IQ3-GFP. The cycling program had the following conditions: initial denaturation step for 5 min at 95°C, 30 cycles of 15 sec at 94°C, 1 min annealing at 54°C, and extension for 1 min at 72°C. After the last cycle there was a final extension step of 10 min at 72°C. Then the temperature was lowered to and kept at 4°C until the samples were collected.

Table 20: Primers used for the generation of IQGAP3 truncated forms

Name	Primers	Sequence (5'-3')	Product size (bp)
mutA	mutA_fwd	ATAGCGATCGCATGGAGAGG	2100
	mutA_rv	CAGACGCGTATAGGCAGCAG	
mutB	mutB_fwd	ATAGCGATCGCATGACCAAGGTCACT	2700
	mutB_rv	CATACGCGTCTTCCGCAAA	

Both PCR products were then purified by the "QIAquick PCR purification kit", digested with *Sgf*I and *Mlu*I restriction enzymes and ligated into both pCMV6-AC-GFP and pCMV6-Entry previously digested with the same enzymes (Figure 3.3). The ligation was performed by using 100 ng of the vector, 0.5 µl of T4 DNA ligase enzyme, 1x ligase buffer, and a quantity of insert based on a 1:3 molar ratio of vector: insert DNA at 4°C overnight.

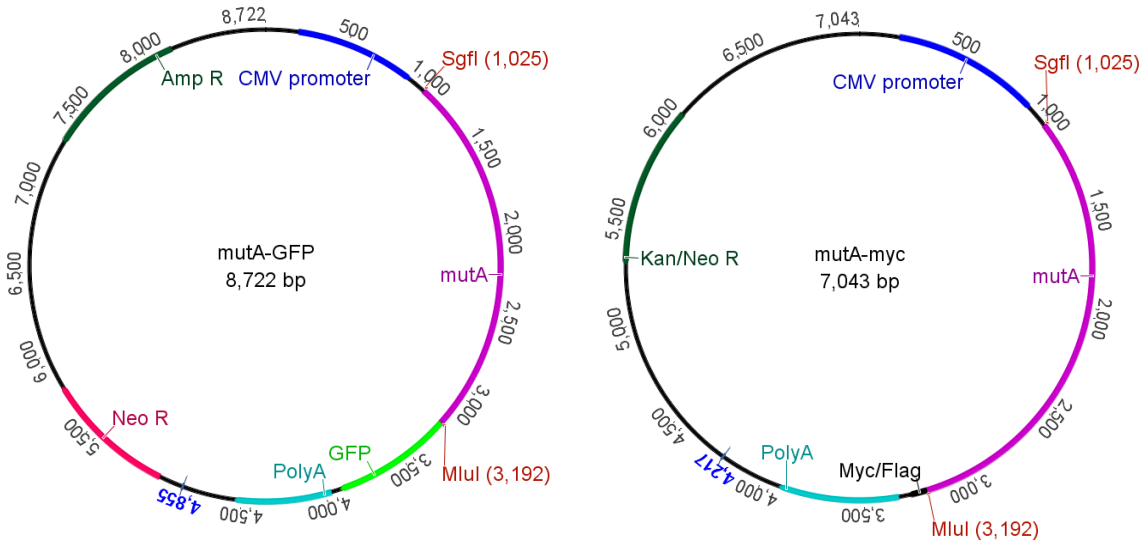

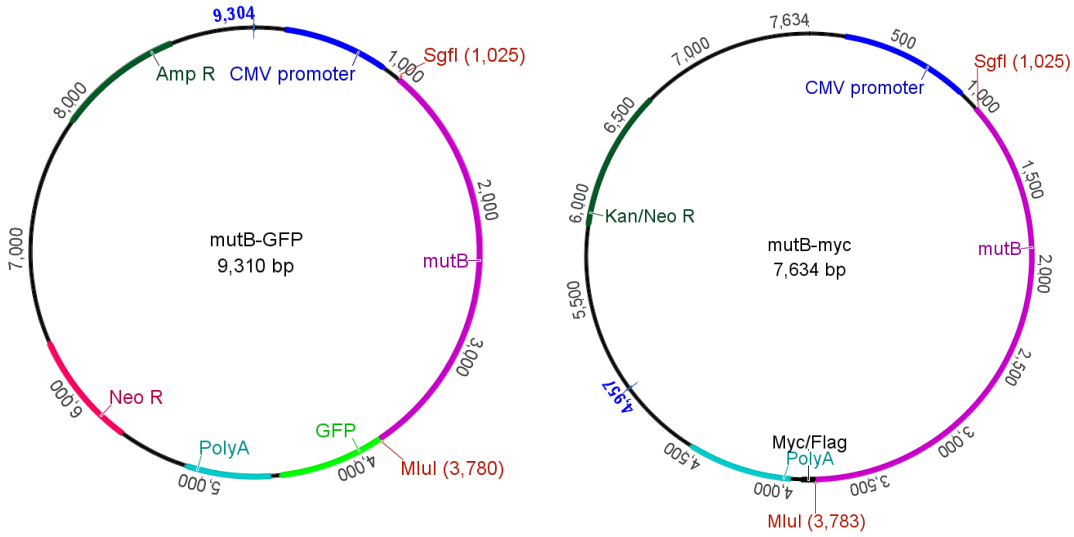

Figure 3.3: Plasmids generated to overexpress the two truncated forms of IQGAP3.
*Mlu*I and *Sgf*I restriction sites used for the cloning process are highlighted. CMV = cytomegalovirus promoter; Amp R = ampicillin resistance cassette; Kan R = kanamycin resistance cassette; Neo R = neomycin resistance cassette; PolyA = poly-adenylation signals.

3.3.7 Plasmid DNA isolation

After cloning, minipreparation of the cloned plasmids was used as fast technique to isolate plasmid DNA simultaneously from different colonies in order to screen colonies positive for successful cloning.

Single colonies were picked, inoculated in 5 ml of LB medium plus a specific antibiotic and grown overnight at 37°C under constant shaking (180 rpm). Bacteria of 2 ml of the overnight culture were pelleted for 3 min at 4000 rpm at RT and the supernatant was removed. The pellet was resuspended in 250 µl of P1 buffer and then 250 µl of P2 buffer were added. The sample was inverted 4-5 times and was incubated for 5 min at RT. After this time 500 µl of ice-cold P3 buffer was added and the tube was inverted 4-5 times. Subsequently the tube was kept on ice for 20 min and then centrifuged for 15 min at 4°C at 13000 rpm. At this step three solutions were formed, a transparent (upper), a white (middle) and a viscous one (down). The transparent one was collected, placed in a fresh 1.5 ml reaction tube and incubated with 700 µl of ice-cold isopropanol. The tube was kept on ice for 30 min and then centrifuged for 20 min at 4°C at 13000 rpm. The supernatant was removed and the pellet was resuspended in 300 µl of 70% ethanol. The tube was again centrifuged for 10 min at 4°C at 13000 rpm. Finally the pellet was air dried and resuspended in 20 µl

of ddH2O. Larger amounts of plasmid were prepared by incubating 500 µl of a 5 ml overnight culture (minipreparation) in 100 ml of LB medium plus the specific antibiotic overnight at 37°C under constant shaking (100 rpm). The plasmid was isolated using the QIAGEN Midi kit according to the manufacturer's instructions. At the final step the air-dried pellet was resuspended in 100 µl of ddH2O to have a final concentration of plasmid between 1500-3000 ng/µl.

3.3.8 Sequencing of DNA

In order to verify inserted sequences all the created plasmids were sequenced by Source BioScience according to the Sanger sequencing method**.**

3.4 Bacterial-related techniques

3.4.1 Preparation of competent cells

One bacteria colony (XL1 Blue) was isolated from an agar plate and inoculated in 5 ml of LB medium at 37°C overnight under continuous shaking. At the next day, 4 ml from this culture were added to 250 ml LB medium and grown to an early logarithmic phase (O.D.600 = 0.3 to 0.6). The culture was centrifuged for 10 min at 2500 rpm at 4°C to pellet the bacteria, which were subsequently resuspended in 25 ml of cold TSB buffer. After incubation on ice for 10 min, 0.1 ml and 0.5 ml aliquots were snap-frozen in liquid nitrogen.

3.4.2 Transformation of *E. coli* competent cells (XL1 Blue)

Either part of a ligation reaction (5 µl) or 40 ng of a plasmid were mixed together with 1x KCM buffer and 100 µl of *E. coli* competent cells. This mixture was kept on ice for 20 min and then at RT for 10 min. After this time 1 ml of LB medium (without antibiotics) was added to the transformation reaction and shaked (200 rpm) for 1 h at 37°C. Afterwards the bacteria were pellet by centrifugation (3000 rpm, 3 min), supernatant discarded, except for 100 µl, resuspended in this amount of supernatant, plated on a LB agar plate containing specific antibiotics for positively selection, and grown overnight at 37°C.

3.5 Protein-related methods

3.5.1 Protein collection

Cells in 6-well dishes were washed once with ice-cold 1x PBS and covered with 200 µl of RIPA buffer containing 1x proteinase inhibitor after PBS was removed. The cells were kept on ice for 10 min and during this time the dish was swirled around 4 to 5 times. Afterwards the cells were scraped from the plate, sonicated for 10 sec with 30% of power and centrifuged for 10 min at 13000 rpm at 4°C. The supernatant was transferred into a new 1.5 ml reaction tube and stored at -20°C.

3.5.2 Quantification of protein

Protein concentration was measured with the BCA protein assay kit because this kit can also be utilized in presence of lysis buffer such as RIPA buffer that contain strong detergents. A standard curve with a gradual increase of BSA concentration was created. Subsequently, 5 µl of total protein lysate was mixed with 1 ml of BCA solution and 20 µl of 4% Cupric sulfate in a 1.5 ml reaction tube. This mixture was incubated for 30 min at 37°C, transferred in a cuvette and its protein concentration was assessed with the BioSpectrometer.

3.5.3 Western blot

Samples were prepared by adding 30-50 µg of protein lysate, 1x LDS sample buffer, and 1x sample reducing agent and incubated for 10 min at 70°C. Afterwards a maximum of 27 µl of sample per each well was loaded in a 4-12% Bis-Tris protein gel (10-well, 1 mm). Once all samples were loaded together with a protein ladder, the gel was run constantly at 125 mA in 1x MOPS running buffer for ca. 1 h by using a SDS-Page electrophoresis chamber. After the gel electrophoresis step proteins were blotted on a nitrocellulose membrane (blotting step). A nitrocellulose membrane, pads, and filter papers were equilibrated with 1% transfer buffer (equilibration step). Depending on how many gels had to be transferred the quantity of methanol in the transfer buffer changed. For 1 gel 10% methanol and for 2 gels 20% methanol was used. After the equilibration step, the blotting chamber was assembled in the order shown in Figure 3.4. Starting from the cathode core to the anode core: 2 blotting pads, 2 filter papers, gel, nitrocellulose membrane, 2 filter papers and 2 blotting pads.

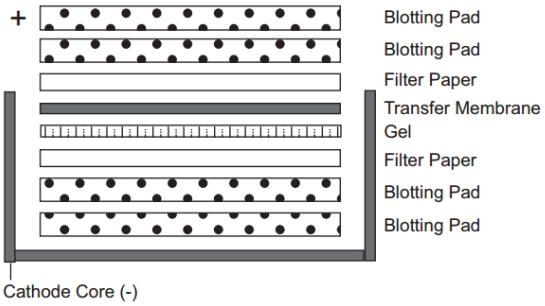

Figure 3.4: Scheme describing the blotting step of a western blot analysis. Figure adopted from "XCell II Blot Module" (Invitrogen).

The blotting chamber was closed tight and put into a blotting module. Then it was filled with 1x transfer buffer plus methanol and the electrotransfer was done for 1 h 45 min at constant voltage of 50 V for 1 gel or 2 h 30 min at 50 V for 2 gels. During this time the blotting module was kept on ice. After the blotting, the membrane was stained with Ponseau S solution and washed once with 1x TBST. Subsequently the membrane was blocked with either 5% milk or 5% BSA diluted in 1x TBST (blocking buffers) for 1 h at RT on a rocker. Once the free binding sites were blocked, the membrane was incubated with primary antibodies (Table 21) diluted in blocking buffer for either 2 h at RT or overnight at 4°C on a rocker. Subsequently the membrane was washed three times with 1x TBST for 5 min on a belly dancer and then incubated with horseradish peroxidase linked-IgG (Amersham) diluted in blocking buffer (1:10000) as secondary antibody for 1 h at RT on a rocker. Later on the membrane was washed again three times with 1x TBST for 5 min. The complexes of first and second antibodies were visualized using Chemiluminescent HRP substrate (Millipore) according to the manufacturer's instructions. Images were acquired by myECL Imager and processed with the software Adobe Photoshop CS5.

Table 21: Primary antibodies utilized in this thesis

Antibody, clone name	Catalog number/ company	Species	Working dilution	MW (kDa)
IQGAP1 (M01)	H00008826-M01, Abnova	Mouse	1:1000 in milk	189
IQGAP3	ab103372, Abcam	Rabbit	1:3000 in milk	185
Myc-Tag (9B11)	#2276, Cell Signaling	Mouse	1:3000 in milk	
Pan-actin	#4968, Cell Signaling	Rabbit	1:4000 in BSA	45

3.5.4 Stripping of membranes

Stripping membranes means to remove the previous primary/secondary complexes allowing the re-probing of the membrane with other antibodies. Membranes were stripped with the Restore™ Western Blot Stripping Buffer for 15 min at RT on a rocker. Subsequently, the stripping buffer was removed and replaced with 1x TBST. The membrane was again blocked with blocking solution for 1 h at RT and then incubated with the desired primary antibody.

3.5.5 Immunofluorescence

A first antibody recognizes one particular epitope (monoclonal antibodies) or several epitopes (polyclonal antibodies) of a protein. The availability of such epitopes depends on the conformation of a protein and thus also the fixation method used for immunofluorescence stainings. Fixation reagents can be dived into two main groups: alcohol-based (methanol, ethanol, and methanol/acetone) and aldehyde-based (3.7% formalin) fixatives. Alcohols dehydrate a sample and thus proteins are separated from each other (alcohol-based fixatives generally permeabilize the cellular membrane). In contrast, aldehyde-based fixatives cross-link proteins and a permeabilization step is required before proceeding with the staining. Cells on 12 mm coverslips were fixed either in 3.7% formalin for 20 min at RT, in ice-cold methanol for 5 min at -20°C, or in ice-cold methanol/acetone (1:1) for 10 min at -20°C. After both methanol and methanol/acetone fixation the coverslips were air-dried and then washed with 1x PBS, while after 3.7% formalin fixation the coverslips were directly washed. In all cases the coverslips could be stored up to 2 weeks at 4°C in PBS. The formalin-fixed coverslips were permeabilized with permeabilization buffer for 10 min at RT. Then, formalin-fixed, methanol-fixed, and methanol/acetone-fixed coverslips were incubated in IF blocking solution for 20 min at RT to reduce the unspecific binding of the utilized antibodies. Subsequently, the coverslips were incubated with a primary antibody (Table 22) diluted in IF blocking solution for 1 h at RT in a humid chamber.

Table 22: Primary antibodies utilized for immunofluorescence stainings

Antibody, clone name	Catalog number, Company	Species	Dilution	Fixation Method	Recognized species
IQGAP3	ab103372, Abcam	Rabbit	1:300	Methanol/ Acetone	Human
IQGAP3	Tsukita's laboratory	Rabbit	1:200	3.7% Formalin	Mouse
IQGAP1 (M01)	H00008826-M01, Abnova	Mouse	1:400	3.7% Formalin	Human
Myc-Tag (9B11)	#2276, Cell signaling	Mouse	1:500	3.7% Formalin, Methanol, Methanol/ Acetone	
Alpha-acetylated tubulin	sc-23950, Santa Cruz	Mouse	1:500	3.7% Formalin, Methanol, Methanol/ Acetone	Human, Mouse, Rat
Tubulin (YL1/2)	ab6160, Abcam	Rat	1:500	3.7% Formalin, Methanol, Methanol/ Acetone	Human, Mouse, Rat
MKLP1	sc-867, Santa Cruz	Rabbit	1:500	Methanol	Human
Cep55	H00055165-A01, Abnova	Mouse	1:500	Methanol	Human
Ect2 (C-20)	Sc-1005, Santa Cruz	Rabbit	1:200	Methanol/ Acetone	Human
Anillin	A301-406A, Bethyl	Rabbit	1:100	Methanol	Human
AIM1	611083,BD Biosciences	Mouse	1:500	3.7% Formalin, Methanol	Human, Mouse, Rat
Phalloidin	A34055, Life technology		1:500	3.7% Formalin	Human, Mouse, Rat
TrpI	Santa Cruz	Rabbit	1:500	3.7% Formalin, Methanol	Rat
alpha-sarcomeric-actinin	ab9465, Abcam	Mouse	1:500	3.7% Formalin, Methanol	Rat
γ-tubulin	sc-51715, Santa Cruz	Mouse	1:500	Methanol	Human
Odf2	12058-1-AP, Proteintech EU	Rabbit	1:500	Methanol	Human
Centrobin	HPA023321, Sigma	Rabbit	1:500	Methanol	Human

After the primary antibody incubation the coverslips were washed three times with IF washing solution for 5 min at RT. Afterwards the coverslips were incubated with a secondary antibody linked to a fluorophore (Table 23) diluted in IF blocking

solution (1:500) for 45 min at RT in a dark place. Then the cells were washed again three times with IF washing solution for 5 min at RT. By adding DAPI working solution for 10 min at RT the DNA was labeled. Finally coverslips were mounted on a microscope slide with mounting medium.

Table 23: Secondary antibodies utilized for immunofluorescence stainings

Antibody	Fluorophor	Company
Goat anti-mouse	594	Life technology
Goat anti-mouse	488	Life technology
Goat anti-rabbit	594	Life technology
Goat anti-rabbit	488	Life technology
Goat anti-rat	594	Life technology
Donkey anti-mouse	594	Life technology
Donkey anti-mouse	488	Life technology
Donkey anti-rabbit	594	Life technology
Donkey anti-rabbit	488	Life technology

3.6 Chromosome-related methods

3.6.1 Fluorescence in situ hybridization (FISH)

Cell suspension preparation for FISH slides

HCT116 cells treated with either si ctrl or si IQ3#1 were trypsinized and passed through a 1000 µl tip to avoid clump formation that can interfere with the following staining. Subsequently the cells were centrifuged for 3 min at 1000 rpm and the cell pellet was washed with cell culture medium and centrifuged again. The supernatant was aspirated except for a small quantity (1 cm from the cell pellet) and the cell pellet was resuspended in the remaining cell culture medium. Then, cells were incubated in 5 ml pre-warmed hypotonic solution for 30 min in a 37°C warm water bath in order to isolate the nuclei. After this time the solution was centrifuged for 3 min at 1000 rpm and the supernatant was aspirated. Subsequently, the nuclei pellet was resuspended in 5 ml freshly mixed Carnoy's fixative added dropwise and incubated overnight at -20°C. At the next day, the nuclei were again centrifuged (1000 rpm for 10 min) and resuspended in 1 to 2 ml freshly Carnoy's fixative. Finally, the nuclei were immobilized on microscope slides through the following procedure. Microscope slides

were placed in ddH2O. Two drops of 7 µl of the nuclei suspension were released in a fast way consecutively next to each other on the wet microscope slide. Immediately afterwards the fixative was removed from the microscope slide by shaking it off. The slide was swayed two or three times through the air and dried under the fume hood. After this step the slides with the fixed nuclei could be stored for several months.

Pretreatment

Dried samples on microscope slides were pretreated for 2 min in 2x SSC (pH 7.0) at 37°C and incubated for 10 min at 37°C in 0.005% pepsin solution diluted in 0.01 M HCl. Afterwards microscope slides were washed for 3 min in 1x PBS at RT and post-fixed in 1% buffered formaldehyde in 1x PBS/ 20 mM $MgCl_2$ for 10 min at RT. Again microscope slides were washed for 3 min in 1x PBS and dehydrated in 70%, 85% and 100% ethanol for 1 min each. As a final step they were air-dried at RT.

Co-denaturation

Probe-mix (KBI-20031, Kreatech) (3 µl per sample) was pipetted on 12 mm coverslips. The coverslips were then put on the top of the fixed nuclei and everything was sealed with fixogum. To denature the DNA of the nuclei, samples were placed in an oven for 5 min at 75°C.

Hybridization

The denatured samples were incubated overnight at 37°C in a humidified chamber to allow the probes to hybridize to the denatured DNA.

Post-hybridization wash

The fixogum was manually removed. Thus the coverslips were not sealed anymore and could be slided off from the microscope slide. At this point the microscope slide was washed in 1x wash buffer II for 2 min at RT, then in 1x wash buffer I for 2 min both at 72°C without agitation and finally in 1x wash buffer II for 1 min at RT without agitation. This step is critical for a good performance because too strong washing steps could wash away the bound probes. Afterwards the microscope slides was dehydrated in 70%, 85% and 100% ethanol for 1 min each and air-dried at RT.

Counterstaining

DAPI working solution (10 µl) was applied to the samples for 15 min at RT in a dark place. After removing the DAPI solution the commercial available mounting medium (Flouromount-G, eBioscience) was applied and a coverslip was used to cover the sample. To seal the coverslip polish nail was used.

3.7 Cell cycle-related techniques

3.7.1 Cell proliferation kit

HeLa cells were placed in a 24-well plate (170,000/well), transfected with either si ctrl, or si IQ3#1, or si IQ3#3 and then transferred into a 96-well plate (6,000/well) to perform the proliferation assay. Cell numbers were measured each day for a total of four days after transfection. Each day the cell culture medium was aspirated and replaced with Opti-MEM (100 µl/well). Subsequently the CCK-8 solution (10 µl) was added. After 3 h incubation at 37°C (5% CO2), the absorbance (450 nm) was measured with a microplate reader (PerkinElmer). Per each condition 4 wells of a 96-well plate were measured and their average calculated. As a blank four empty wells containing only Opti-MEM were used. The absorbance of blank was subtracted from the average of each condition.

3.7.2 Propidium iodide (PI) staining and Fluorescence activated cell sorting (FACS)

HeLa cells transfected with either si ctrl or si IQ#1 were cultured for three days after transfection. On the third day the cells were washed in PBS, trypsinized, and fixed in ice-cold PI fixation buffer. Subsequently, the fixed cells were centrifuged for 10 min at 500 × *g* at 4°C and the supernatant was discarded. The cell pellet was resupended in PBS and centrifuged again. After discarding the supernatant the cells were resuspended in PI extraction buffer and incubated for 15 min at RT. After another centrifugation step the cells were incubated in 250 µl of complete DNA staining buffer for 30 min at RT. Afterwards the cell suspension was moved to a FACS tube and 150 µl of PBS was added to each tube. 10000 events per sample were then analyzed by BD FACSCanto II (BD Transduction). Data were analyzed by FlowJo software.

3.8 Statistical analysis

Data are expressed as mean ± either S.E.M. or S.D. of at least three independent experiments. Only one experiment was performed for FISH analysis. In order to compare two conditions in one experiment statistical significance was calculated by two-tailed T-test (Excel program, Microsoft). To compare multiple conditions *vs* control sample in one experiment one-way ANOVA test was performed (GraphPad Prism). p-values of < 0.05 were considered statistically significant.

4 Results

4.1 *Iqgap3* gene expression is correlated to cardiomyocyte proliferation

During development cardiomyocytes reduce their proliferation rate until they stop dividing after birth. Thus, genes that positively influence cell cycle progression are upregulated in early development and downregulated in postnatal development. In order to find novel cell cycle regulators a microarray dataset describing rat heart development from E11 to P10.5 was analyzed. Genes had been clustered based on their temporal expression profiles in 42 clusters utilizing a Bayesian clustering algorithm and enrichment of the clusters in cell cycle-related GO term were performed with DAVID[119] (Ferrazzi *et al.*, unpublished). This study focused on cluster 10, which was enriched in the GO term "M phase" (p-value = 0.0105) and contained known and fundamental cell cycle genes such as *Anln*[51] and *Dlgap5*[120]. Subsequently, it was assessed which of the candidate genes is reexpressed upon p38i/FGF1 stimulation, which is known to induce cardiomyocyte proliferation. For this purpose a previously published microarray dataset was utilized[35]. The result of this analysis is represented in table 24.

Table 24: Genes of cluster 10 reexpressed upon p38i/FGF1 treatment. The expression is represented as Log2 ratio of FGF1/p381 treatment *vs* DMSO (ctrl).

	Experiment 1			Experiment 2		
Gene	**p38i**	**FGF1**	**p38i/FGF1**	**p38i**	**FGF1**	**p38i/FGF1**
Anln	1.1609	1.7304	2.4072	1.0264	0.8949	1.8035
Msn	-0.1312	1.1534	1.9086	-0.2104	1.2455	1.8938
Top2a	1.4689	0.8676	1.6375	1.5401	0.7475	2.0160
Foxm1	0.3834	-0.3146	0.9160	2.8918	0.7613	2.6581
Knstrn	1.0407	0.9346	1.7757	1.1596	0.9090	1.7390
Tk1	1.0108	0.6272	1.7296	0.8217	0.9512	1.7020
Iqgap3	0.4865	0.5197	1.5414	0.8646	0.5727	1.6898

The first gene in this list is *Anln*, a gene encoding the known pro-proliferative protein anillin. It is the most upregulated gene in proliferating cardiomyocytes upon

FGF1/p38i stimulation (enriched in mitotic genes) compared to cardiomyocytes treated with either FGF1 (induces mainly S phase) or p38i (does not induce cell cycle reentry) alone. Based on a literature-based analysis several other important cell cycle genes follow *Anln* in the list such as *Tk1*, which encodes thymidine kinase 1. The first gene on this list that was at the time of this analysis not known to regulate cell cycle progression was *Iqgap3* (Figure 4.1). Thus, it was chosen as a possible candidate gene for further investigation.

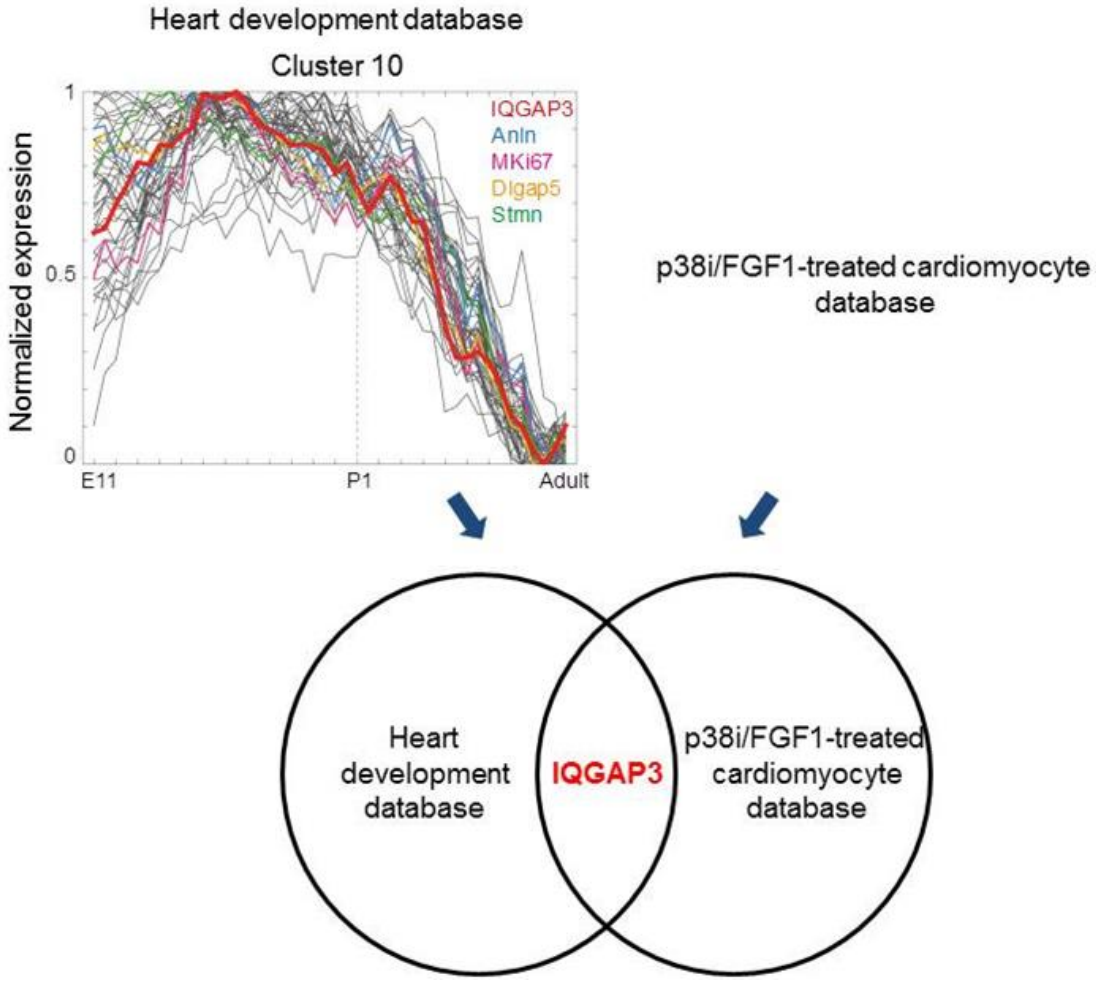

Figure 4.1: Schematic representation of the performed comparison between the rat heart development microarray dataset and the p38i/FGF1-treated rat cardiomyocyte dataset leading to the choice of *Iqgap3* as a possible novel cell cycle regulator. Cardiomyocytes proliferate during early mammalian heart development while they reach a post-mitotic status after birth. This post-mitotic status can be reversed by treating P3 cardiomyocytes with p38i/FGF1 that induce proliferation. In order to find novel cell cycle regulators two datasets, rat heart development (form E11 to P10.5) expression dataset and p38i/FGF1-treated cardiomyocyte dataset, were compared. For the heart development database genes had been clustered based on their temporal expression profiles in 42 clusters utilizing a Bayesian clustering algorithm and enrichment of the clusters in cell cycle-

related GO terms were performed with DAVID (Ferrazzi *et al.*, unpublished). This study focused on cluster 10, which was enriched in the GO term “M phase” (p-value = 0.0105) and contained known and fundamental cell cycle genes such as *Anln* and *Dlgap5*. For a better representation gene expression levels were smoothed and normalized between 0 and 1. Candidate genes from cluster 10 were subsequently screened by literature analysis and it was determined which of these genes exhibited an inversely correlated expression profile in the p38i/FGF1 database. This bioinformatics screen suggested *Iqgap3* as a possible candidate gene.

Then a literature search was performed to analyze the knowledge regarding *Iqgap3* and subsequently a gene homology analysis among different species was done. IQGAP3 belongs to the IQGAP family, which contains two other family members, IQGAP1 and IQGAP2. An analysis of the developmental microarray dataset revealed that IQGAP3 is the only family member whose expression is downregulated after birth being absent in adulthood. In contrast, IQGAP1 expression slowly increases during heart development reaching its expression maximum in adulthood. IQGAP2 was barely detectable during heart development. Subsequently, the gene expression profiles of the three IQGAP family members were validated by RT-PCR using a set of RNA different from the one used for the heart development dataset (Figure 4.2).

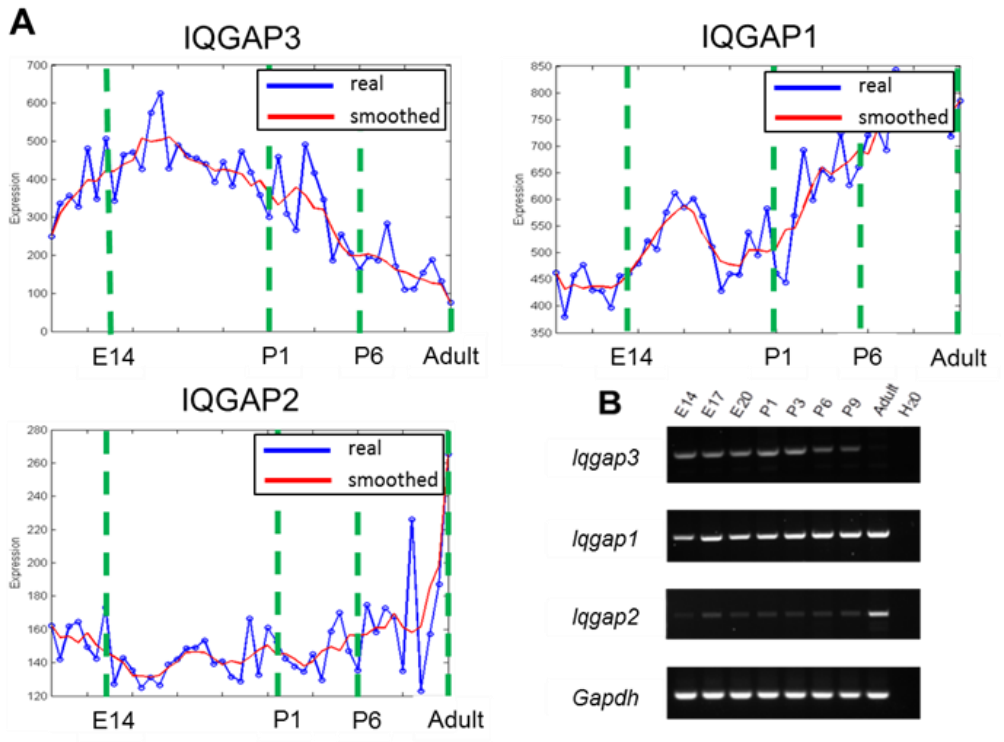

Figure 4.2: *Iqgap3* is the only IQGAP member whose gene expression decreases after birth (P1). (A) Gene expression profiles of IQGAP family members (*Iqgap3*, *Iqgap1* and *Iqgap2*). In all graphs the real (blue) and smoothed (red) profiles are shown. (B) Validation of microarray profiles by RT-PCR. GAPDH was used as loading control.

Taken together, the comparison of the two microarray datasets describing heart development and cardiomyocyte proliferation suggest *Iqgap3* as a novel cell cycle-related gene.

4.2 Iqgap3 expression and localization during cardiomyocyte cell cycle progression

Isolation of primary neonatal rat cardiomyocyte is a technique that results in a high cardiomyocyte purity (≥ 90%), but still 10% of the cells in culture are non-myocytes[121]. Thus, Iqgap3 expression was analyzed in cardiomyocytes of different cell cycle stages. For this purpose immunofluorescence analysis was performed of both dividing P3 isolated cardiomyocytes, treated with p38 inhibitor and FGF1, and binucleating P3 cardiomyocytes, stimulated with 10% FBS for 72 h. Subsequently cells were stained for endogenous Iqgap3 (green), a microtubule marker (acetylated (Ac)-α-tubulin) and a cardiac-specific marker (Troponin I). The analysis of these stainings revealed that Iqgap3 is expressed during mitosis in cardiomyocytes. Iqgap3 was observed at the spindle midzone in proliferating as well as binucleating cardiomyocytes, which exhibit a symmetric and asymmetric furrow ingression, respectively (Figure 4.3). Iqgap3 localization highlights the asymmetrical furrow ingression (yellow arrow) characteristic for binucleating cardiomyocytes as shown by Engel and coworkers[21].

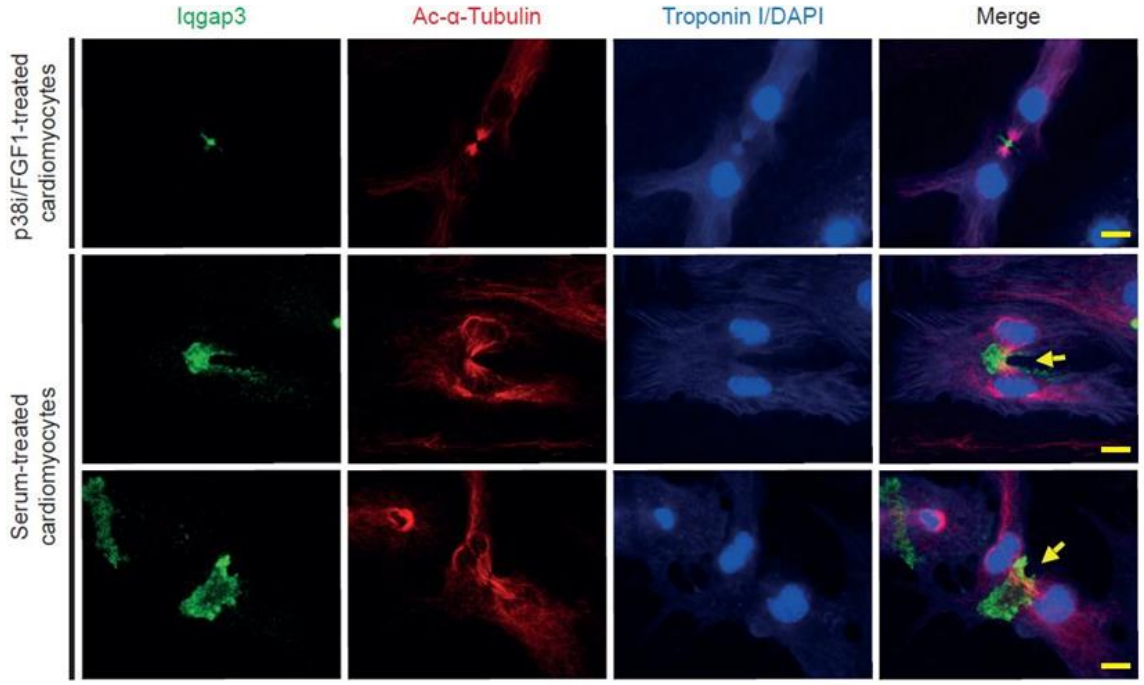

Figure 4.3: Iqgap3 expression and localization during cardiomyocyte cell cycle progression. P3 rat cardiomyocytes were isolated and induced to reenter the cell cycle by p38i/FGF1 treatment and 10% FBS for 72 h. Afterwards cells were stained for Iqgap3 (green), a microtubule marker (Ac-α-Tubulin, red), a cardiac-specific marker (TroponinI, blue) and DNA (DAPI, blue). Yellow arrows indicate asymmetric furrow ingression induced by serum treatment. Scale bar = 10 µm.

These results demonstrate that Iqgap3 is expressed in cardiomyocytes and suggest that Iqgap3 plays a role in cleavage furrow formation.

4.3 IQGAP3 mitotic presence is a conserved localization pattern between different cell lines

To determine whether the observed Iqgap3 localization pattern is cardiomyocyte-specific three different cell lines, HL-1 (mouse atrial tumor cell line), NIH3T3 (mouse embryonic fibroblast cell line), and HeLa (human cervical epithelial tumor cell line) were analyzed (Figure 4.4).

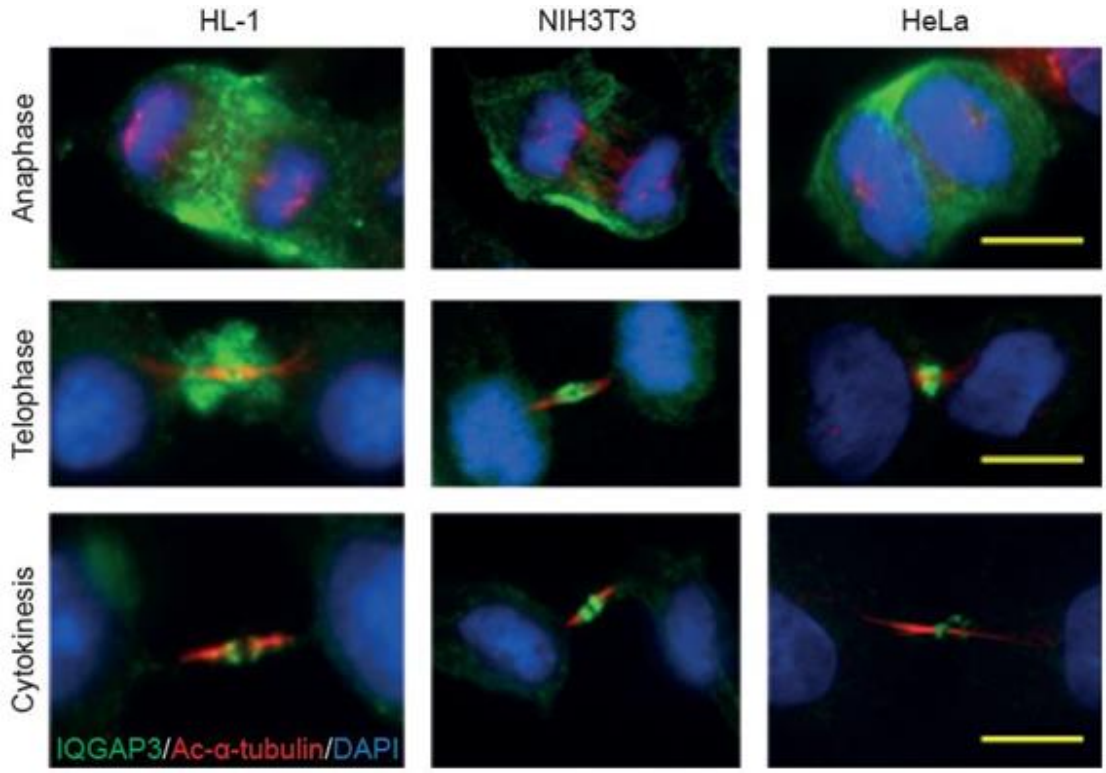

Figure 4.4: IQGAP3 is expressed in a wide variety of cell types with slightly varying expression pattern. Immunofluorescence analyses of HL-1, NIH3T3 and HeLa cells stained for endogenous IQGAP3 (green), a microtubule marker (Ac-α-tubulin, red) and DNA (DAPI, blue). Scale bar = 10 µm.

Immunofluorescence analysis showed that IQGAP3 is present in all three cell types at the cleavage furrow in anaphase. In telophase, IQGAP3 was concentrated at the midbody in NIH3T3 and HeLa cells resembling the expression pattern of bulge proteins such as MKLP1[53]. In contrast, in HL-1 cells IQGAP3 exhibits a much wider expression pattern around the midbody. In the transition from telophase to cytokinesis the microtubule bundle becomes narrowed across its length and IQGAP3 gets concentrated in all three cell lines at the midbody region. While in HeLa cells IQGAP3 localization pattern is conserved during cytokinesis, which is similar to that of bulge proteins, in HL-1 and NIH3T3 cells the IQGAP3 expression pattern resembles now that of flanking proteins (*e.g.* aurora B[53]). These results demonstrate that IQGAP3 is not cardiomyocyte-specific but is expressed in a wide variety of cell types with slightly varying expression patterns.

4.4 IQGAP3 localizes to the cleavage furrow, to the stem body of the midbody and later to the midbody remnant

In order to characterize the dynamics of endogenous IQGAP3 localization from anaphase to post-abscission, HeLa cells were analyzed at several different cell cycle stages by immunofluorescence analysis. To identify the different mitotic stages cells were co-stained for Ac-α-tubulin and DNA (DAPI) (Figure 4.5).

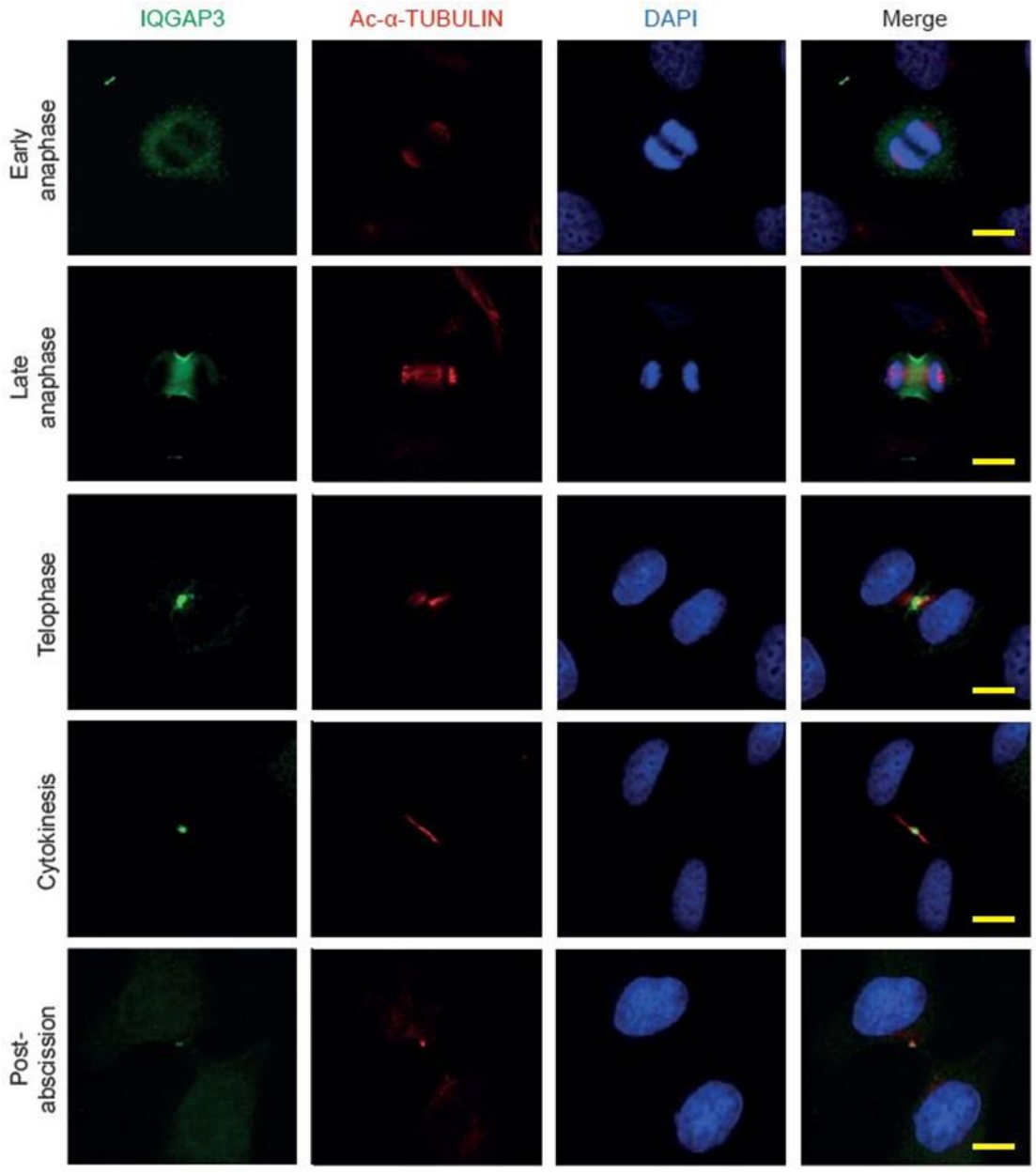

Figure 4.5: IQGAP3 localizes to the cleavage furrow, to the stem body of the midbody and later to the midbody remnant. Immunofluorescence analyses of HeLa cells stained with endogenous IQGAP3 (green), a microtubule marker (Ac-α-TUBULIN, red) and DNA (DAPI, blue). Scale bar = 10 µm.

While IQGAP3 in early anaphase appeared as a diffuse cytoplasmic stain, it localized in late anaphase at the cleavage furrow. After furrow ingression and midzone constriction, it concentrated around the midbody (telophase). In cytokinesis, its localization becomes more evident at the stem body of the midbody, similar to the localization of bulge proteins[53]. After abscission the two tubulin arms are pulled into opposite directions and the Ac-α-tubulin positive midbody remnant generally goes with one arm[58]. The co-localization of IQGAP3 with Ac-α-tubulin indicates that IQGAP3 co-localizes with the midbody remnant. The dynamic change in IQGAP3 localization was further confirmed by both transient and stable transfection experiments. HeLa cells were transiently transfected with a plasmid driving expression of IQGAP3 tagged at the C-terminus with the fluorescent protein TurboGFP (IQGAP3-GFP). After 24 h HeLa cells in different mitotic stages were stained for microtubules (Ac-α-tubulin) and DNA (DAPI) and then analyzed (Figure 4.6). In addition, HeLa cells were stably transfected with a construct driving the expression of IQGAP3 tagged at the C-terminus with myc and analyzed by subsequent immunofluorescence staining of myc, MKLP1, and DNA (DAPI) (Figure 4.7). Finally, a life cell imaging approach verified that in individual cells IQGAP3 localization changes dynamically during mitosis as observed above in still photos Figure 4.8).

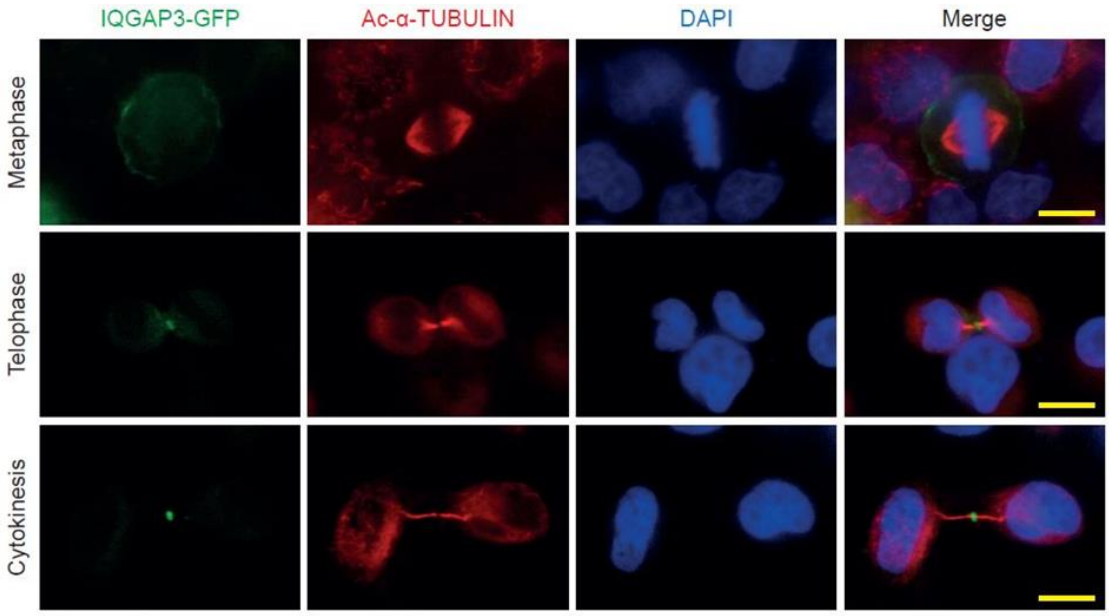

Figure 4.6: Validation of mitotic IQGAP3 localization by transient IQGAP3 overexpression in HeLa cells. HeLa cells were transiently transfected with a plasmid driving expression of IQGAP3 tagged at the C-terminus with the fluorescent protein

TurboGFP (IQGAP3-GFP) (green). After 24 h HeLa cells in different mitotic stages were stained for microtubules (Ac-α-TUBULIN, red) and DNA (DAPI, blue). Scale bar = 10 µm.

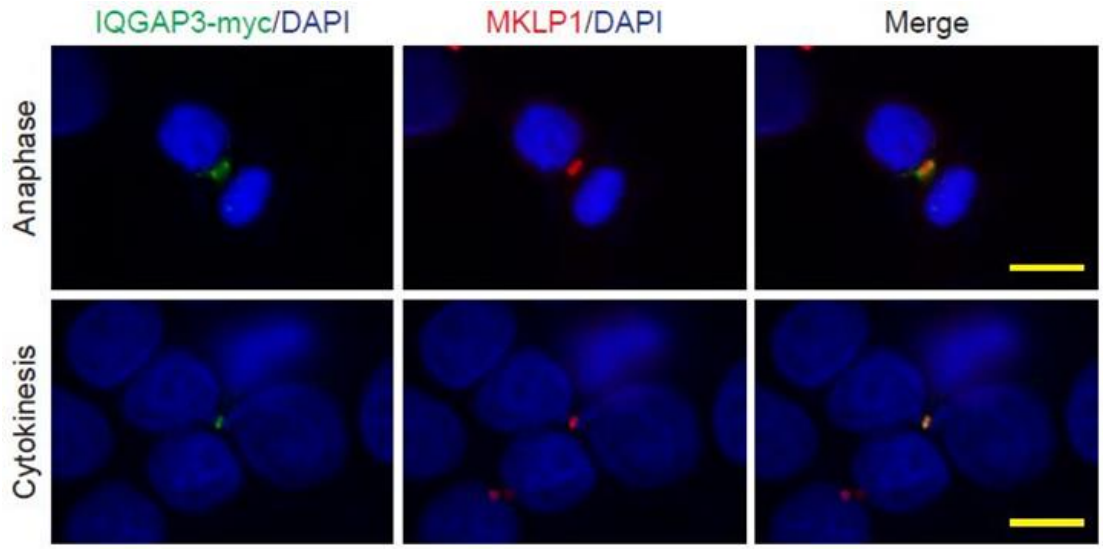

Figure 4.7: Validation of mitotic IQGAP3 localization by stably expressing IQGAP3 in HeLa cells. HeLa cells were stably transfected with a construct driving the expression of IQGAP3 tagged at the C-terminus with myc (IQGAP3-myc) and analyzed by subsequent immunofluorescence staining of myc (green), MKLP1 (red) and DNA (DAPI, blue). Scale bar = 10 µm.

In order to better characterize IQGAP3 localization during different mitotic stages, IQGAP3 (either endogenous or ectopically expressed) was co-stained together with F-actin (Phalloidin), and the mitotic proteins Ect2, aurora B (AIM1), anillin, MKLP1, and Cep55 (Figure 4.9-14). In early anaphase IQGAP3 could in contrast to Ect2, AIM1, and MKLP1 not be detected at the central spindle. Instead it co-localized with anillin at the cell cortex where cleavage furrow ingression will occur. This co-localization was clearer in late anaphase when the cleavage furrow has partially ingressed. In addition, IQGAP3 co-localized with F-actin (Phalloidin) at the site of the actomyosin ring in anaphase. In telophase and later in cytokinesis IQGAP3 was co-stained with the bulge proteins MKLP1, Ect2, anillin, and Cep55. In contrast, it did not co-localize with the “flanking protein” aurora B (AIM1).

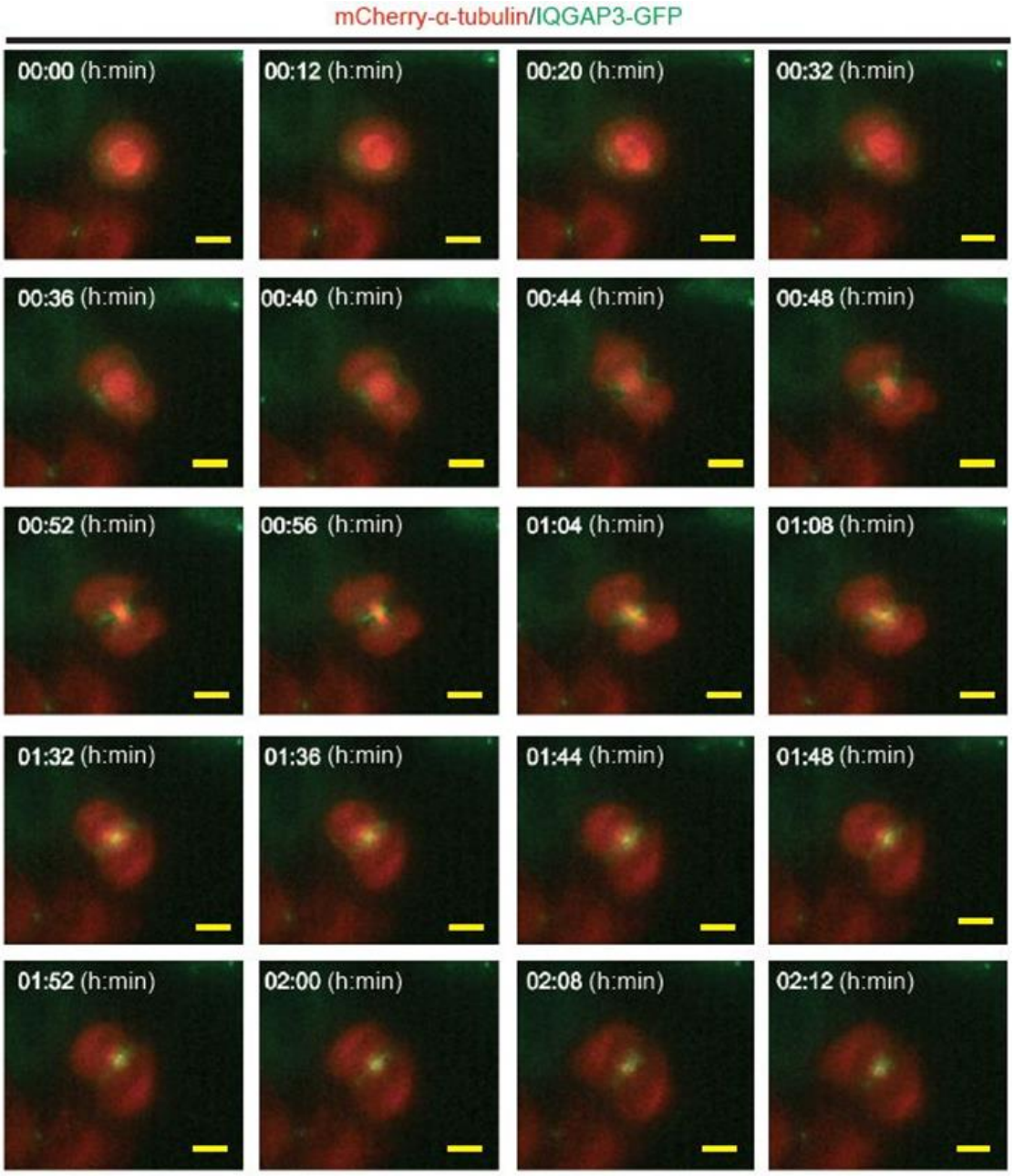

Figure 4.8: The dynamic changes of IQGAP3 during mitosis in HeLa cells. HeLa stably transfected with mCherry-α-tubulin (red) were transiently transfected with a plasmid driving expression of IQGAP3 tagged at the C-terminus with the fluorescent protein TurboGFP (IQGAP3-GFP) (green). Time-lapse movies were taken after 18 h from the transfection. (00:00 = h:min). Scale bar = 10 μm.

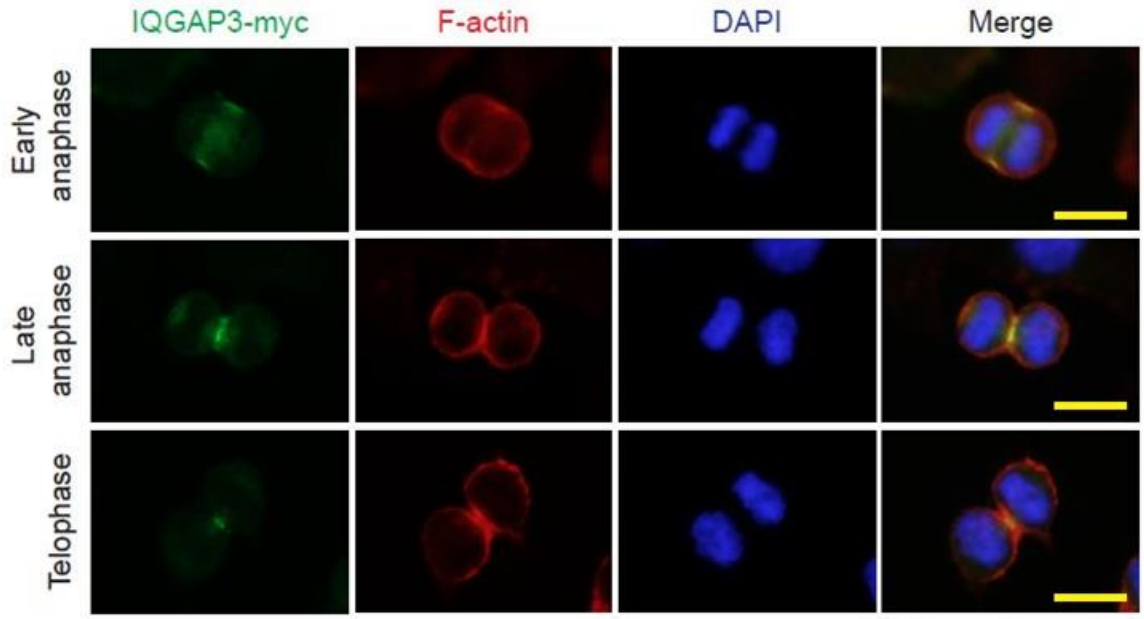

Figure 4.9: IQGAP3 co-localized with F-actin at the site of the actomyosin ring in anaphase. HeLa cells were transiently transfected with a plasmid driving the expression of IQGAP3 tagged at the C-terminus with myc (IQGAP3-myc). After 18 h cells were fixed and stained for myc (green), F-actin (Phalloidin, red) and DNA (DAPI, blue). Scale bar = 10 µm.

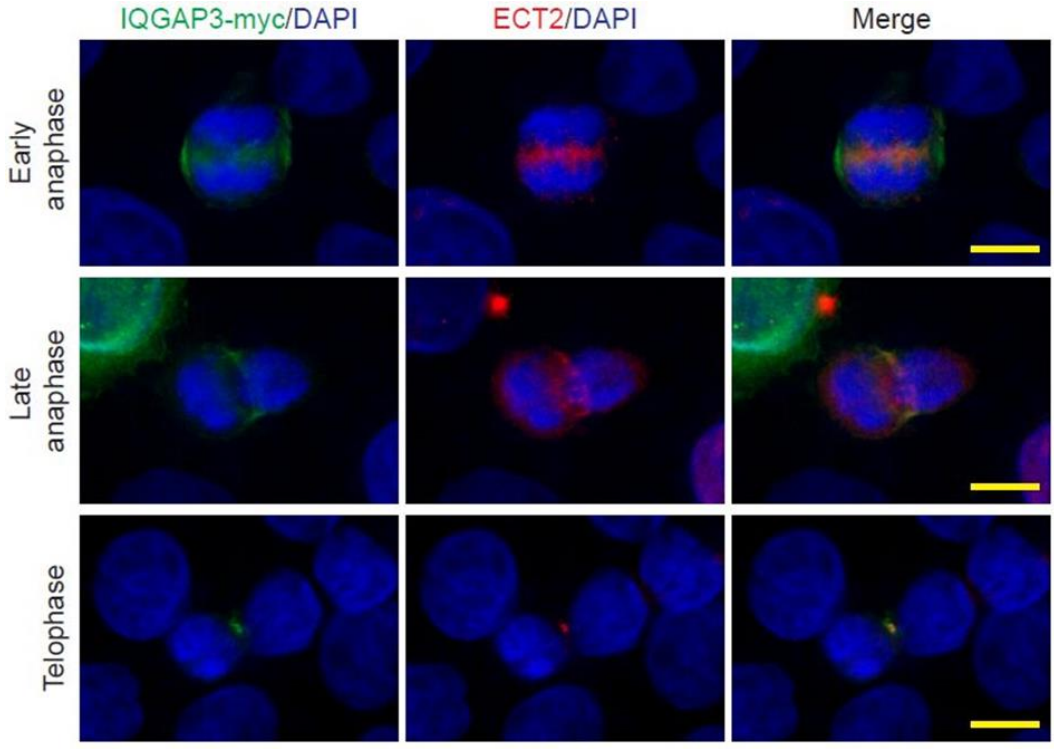

Figure 4.10: IQGAP3 does not co-localize with ECT2 at the cleavage furrow in anaphase, but it does at the stem body of the midbody in telophase. HeLa cells were transiently transfected with a construct driving the expression of IQGAP3 tagged at the C-terminus with myc (IQGAP3-myc). After 18 h cells were fixed and stained for myc (green), ECT2 (red) and DNA (DAPI, blue). Scale bar = 10 µm.

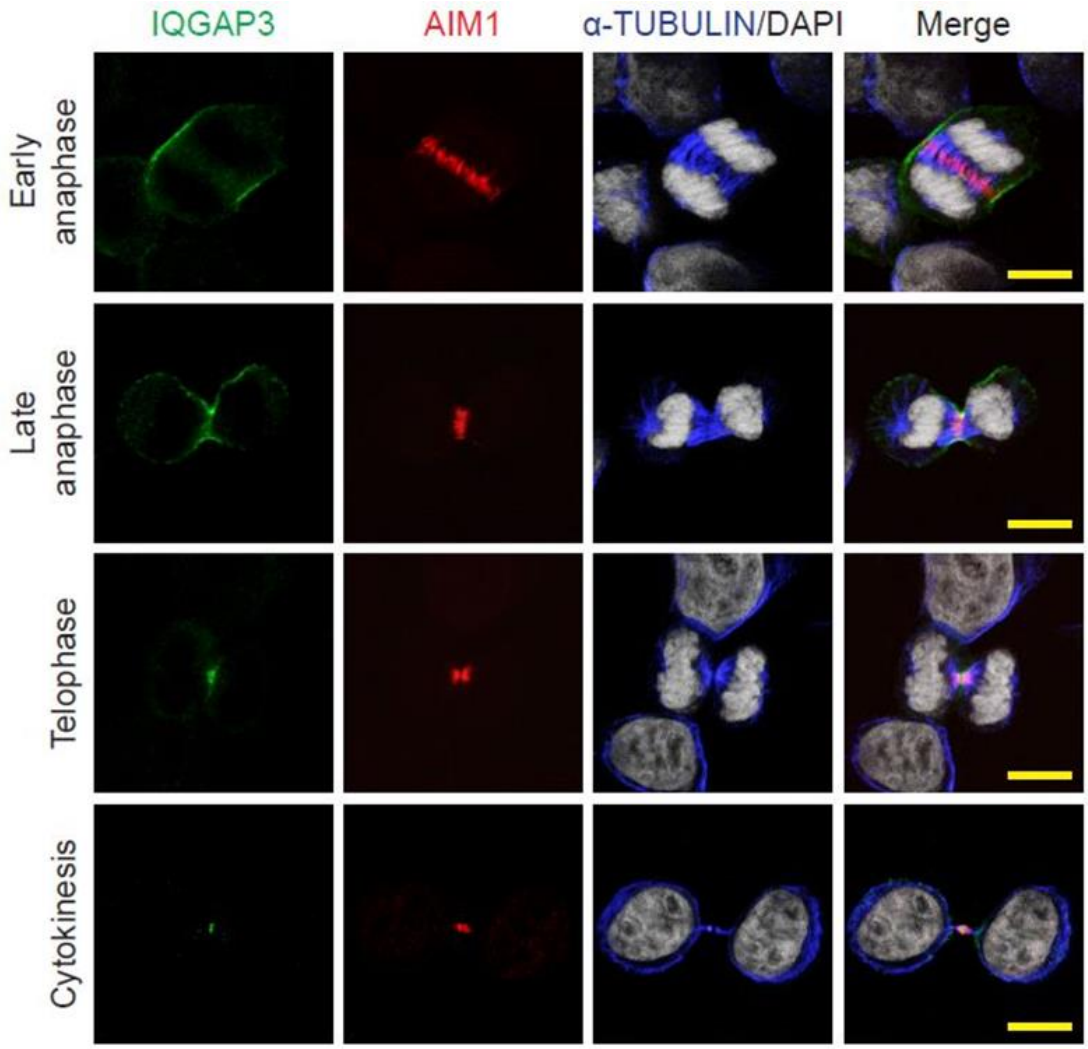

Figure 4.11: IQGAP3 does not co-localize with aurora B neither at the cleavage furrow in anaphase nor at the midbody in telophase and cytokinesis. Confocal microscopy of immunofluorescence stainings for IQGAP3 (green), aurora B (AIM1, red), α-TUBULIN (blue) and DNA (DAPI, grey) in HeLa cells. Scale bar = 10 µm.

As shortly after abscission the midbody was still positive for IQGAP3 (Figure 4.5), it has been investigated whether IQGAP3 remains also several hours after abscission present at the midbody remnant. Co-expression analyses of IQGAP3 (either endogenous or ectopically expressed) with the midbody remnant markers MKLP1 and Cep55 demonstrated that IQGAP3 localizes to the midbody remnant (Figure 4.13-14). Collectively, these data prove that IQGAP3 is a component of the cytokinesis apparatus, because it is present at the cleavage furrow, the stem body of the midbody, as well as the midbody remnant.

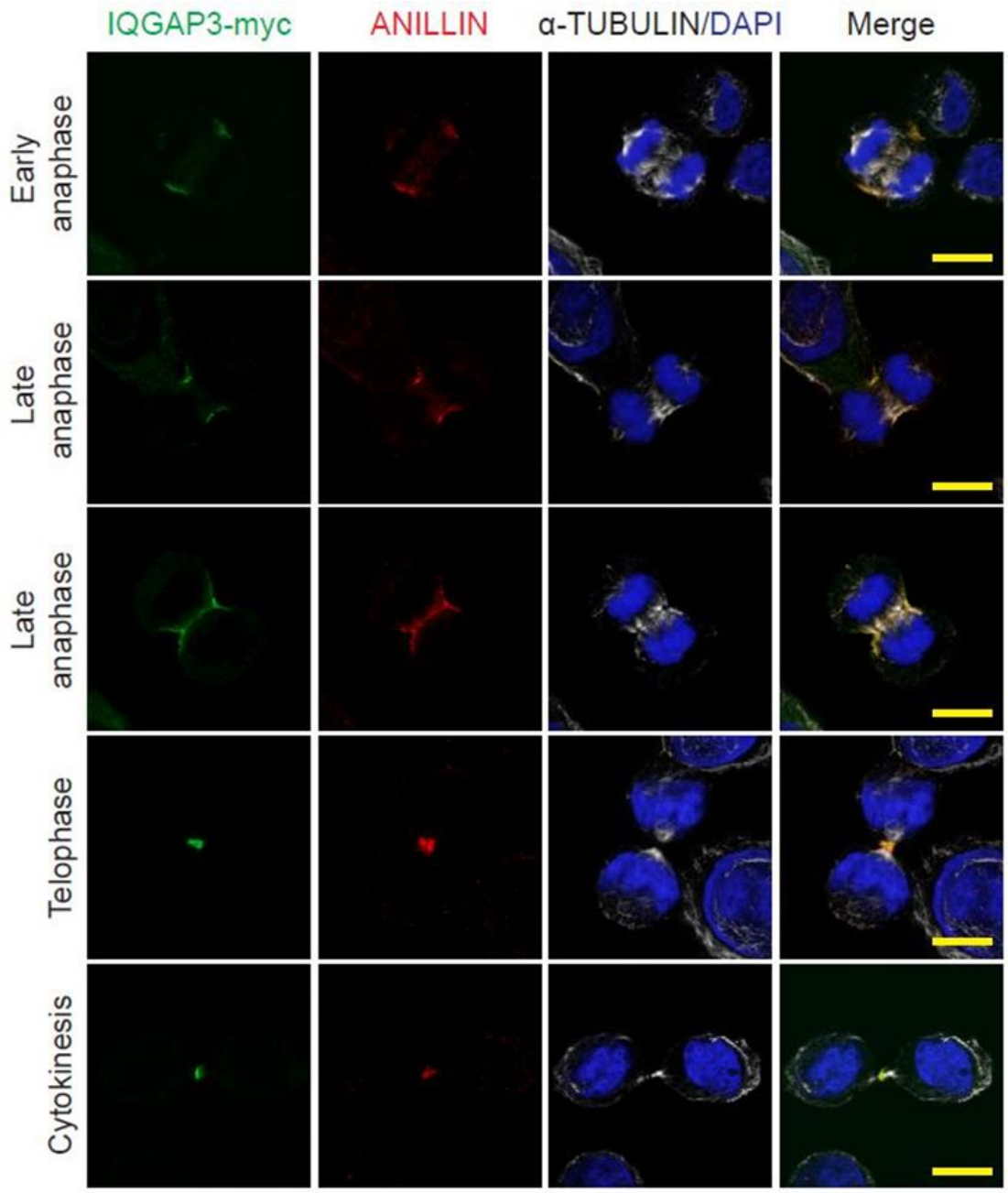

Figure 4.12: IQGAP3 co-localizes with anillin both at the cleavage furrow in anaphase and at the midbody in telophase and cytokinesis. Confocal microscopy of immunofluorescence stainings for IQGAP3 (green), ANILLIN (red), α-TUBULIN (grey) and DNA (DAPI, blue) in HeLa cells. Scale bar = 10 µm.

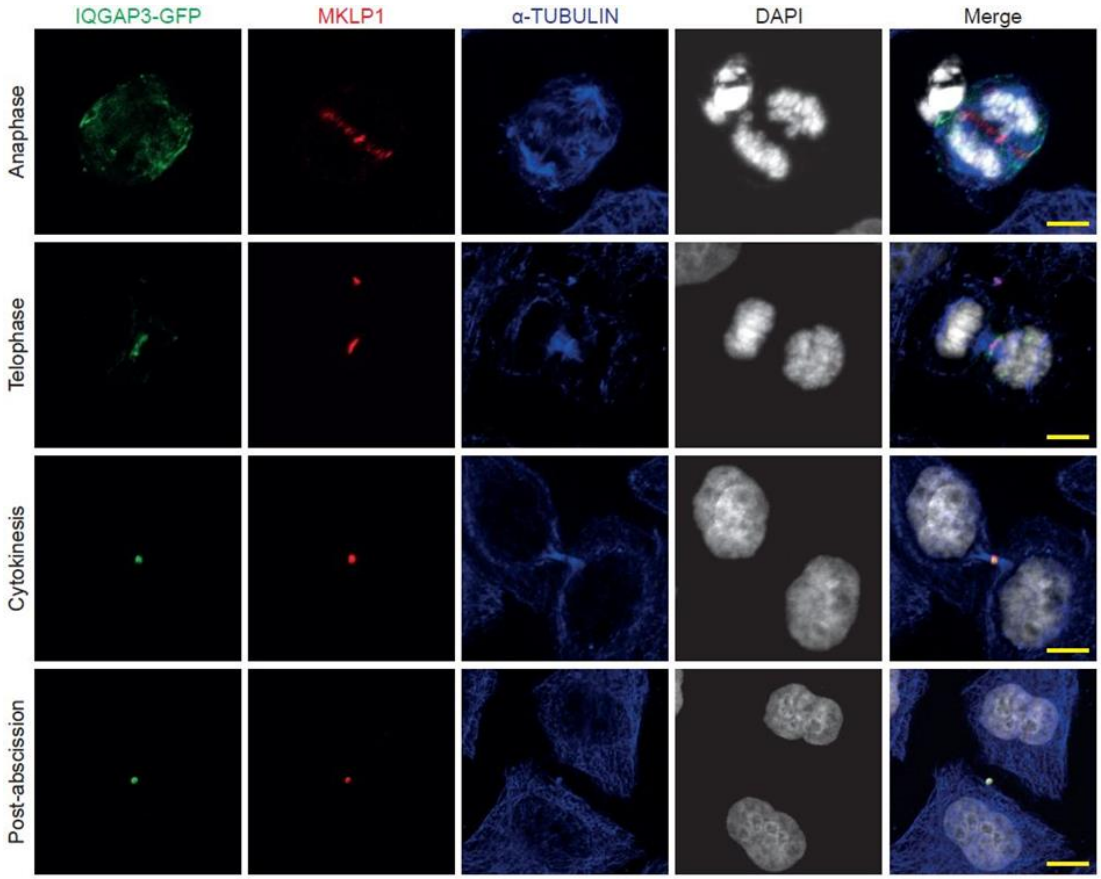

Figure 4.13: IQGAP3 does not co-localize with MKLP1 at the cleavage furrow in anaphase, but it does both at the midbody in telophase/cytokinesis and at the midbody remnant in post-abscission. HeLa cells were transiently transfected with a plasmid driving expression of IQGAP3 tagged at the C-terminus with the fluorescent protein TurboGFP (IQGAP3-GFP) (green). After 18 h cells were fixed and stained for MKLP1 (red), α-TUBULIN (blue) and DNA (DAPI, grey). The stainings were examined by confocal microscopy. Scale bar = 10 µm.

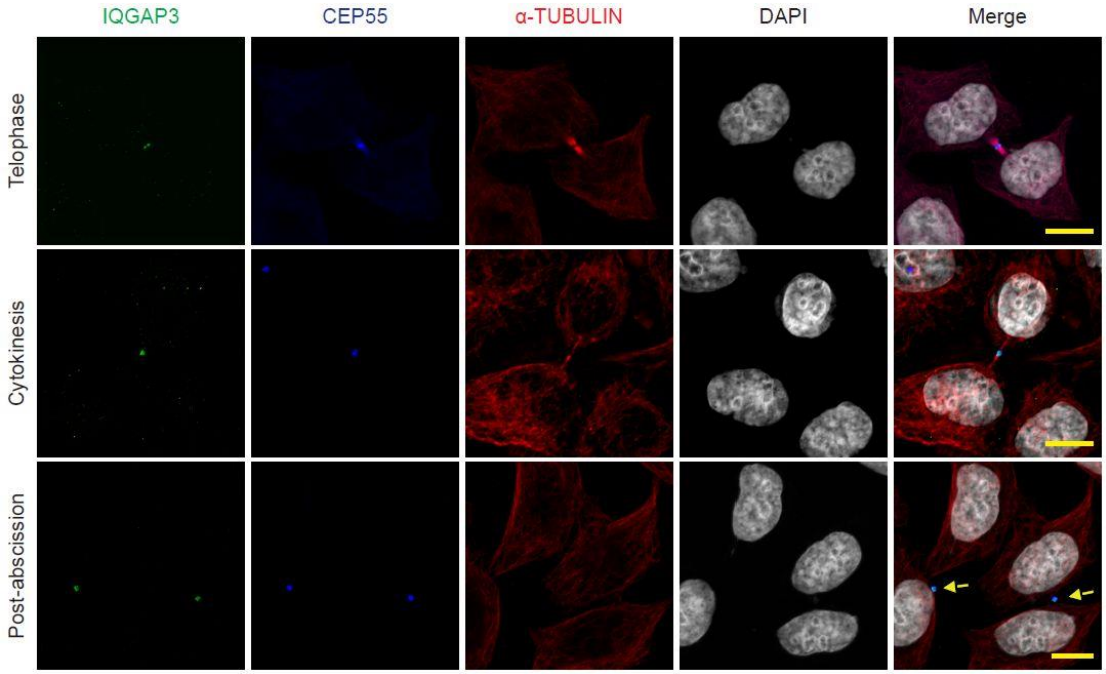

Figure 4.14: IQGAP3 co-localizes with CEP55 both at the midbody in telophase/cytokinesis and at the midbody remnant in post-abscission. Confocal microscopy of immunofluorescence stainings for IQGAP3 (green), CEP55 (blue), α-TUBULIN (red) and DNA (DAPI, grey) in HeLa cells. Yellow arrows indicate midbody remnants. Scale bar = 10 µm.

4.5 IQGAP3 is required for HeLa cell cycle progression

After demonstrating that IQGAP3 is expressed during mitosis, it was tested whether IQGAP3 is required for cell cycle progression. Thus, siRNA-mediated IQGAP3 knockdown was established utilizing the siRNAs si IQ3#1 and a control siRNA (si ctrl). The efficiency and the specificity of this strategy were verified by western blot and immunofluorescence analysis. To increase the efficiency of the knockdown, HeLa cells were transfected with si IQ3#1 and si ctrl during two consecutive days. After 72 h from the last transfection the total cell lysate was collected and analyzed by western blot. The membrane was blotted with anti-IQGAP3 antibody for the knockdown efficiency and anti-IQGAP1 antibody for the knockdown specificity. Pan-actin was used as a loading control (Figure 4.15A).

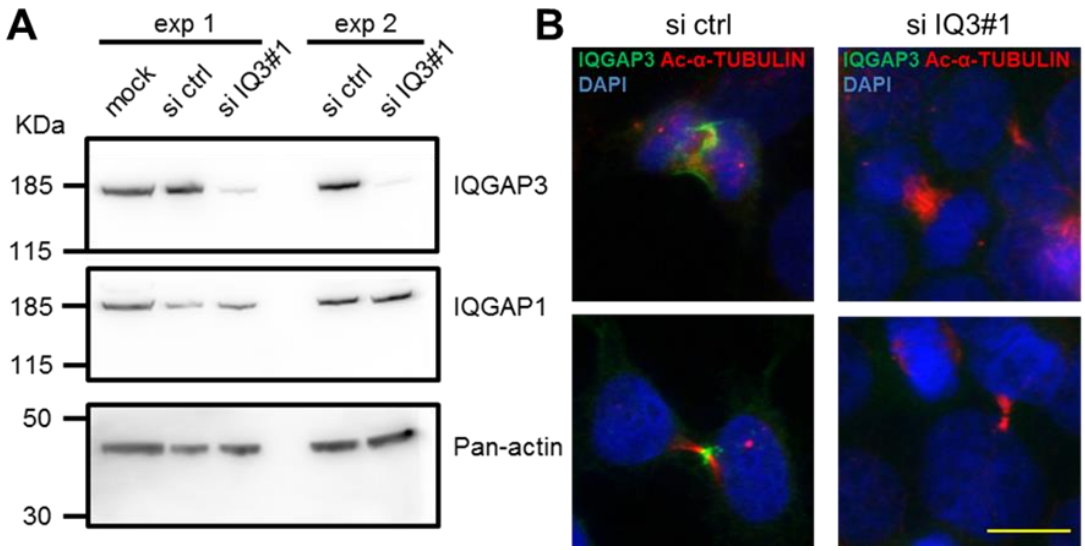

Figure 4.15: The efficiency and the specificity of siRNA-mediated IQGAP3 knockdown strategy. (A) HeLa cells were transfected with either no siRNA molecules (mock) or a control siRNA (si ctrl) or an IQGAP3-specific siRNA (si IQ3#1). After 72 h the total cell lysate was collected and analyzed by western blot. In order to test the efficiency of the siRNA strategy the membrane was blotted against anit-IQGAP3 antibody, while to check the specificity an anti-IQGAP1 antibody was used. Pan-Actin was used as loading control. (B) Confirmation of IQGAP3 knockdown by immunofluorescence analyses. IQGAP3: green, Ac-α-TUBULIN: red, DNA: blue. Scale bar = 10 µm.

The data demonstrate that si ctrl did not affect the endogenous level of IQGAP3 protein since there is no obvious difference in the IQGAP3 protein amount between the samples, si ctrl and mock. In addition, it showed that si IQ3#1 almost abolished IQGAP3 expression but had no obvious effect on the expression level of IQGAP1. Moreover, immunofluorescence data showed that both in anaphase and cytokinesis IQGAP3 was absent in HeLa cells transfected with si IQ3#1 but not si ctrl (Figure 4.15B).

After verifying the chosen knockdown strategy the proliferation assay “Cell Counting kit-8” was utilized to assess whether IQGAP3 is required for HeLa cell proliferation. HeLa cells transfected with either si IQ3#1 or si ctrl were cultured with 10% FBS and the proliferation rate was determined by measuring the increase in cell number over a period of four days. IQGAP3 knockdown reduced the proliferation rate of HeLa cells by around 45% ± 7% (mean ± S.E.M., n = 3, p-value ≤ 0.001) compared to si ctrl-transfected HeLa cells (Figure 4.16).

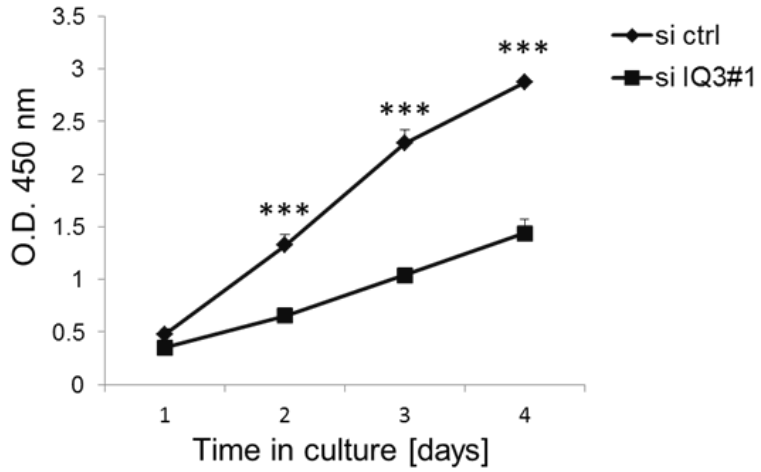

Figure 4.16: IQGAP3 is required for HeLa cell cycle progression. HeLa cells transfected with either a control siRNA (si ctrl) or an IQGAP3-specific siRNA (si IQ3#1) were cultured with 10% FBS and the proliferation rate was determined by measuring the increase in cell number over a period of four days using the kit "Cell Counting kit-8". In the graph data are represented as mean ± S.D (n = 3). ***: *p-value* ≤ 0.001, Student's *t*-test, two-tailed.

To confirm the role of IQGAP3 in regulating proliferation, the proliferation assay was repeated with an additional siRNA against IQGAP3 (si IQ3#3), which resulted in a similar IQGAP3 knockdown as si IQ3#1 (Figure 4.17A). Transfection of HeLa cells with si IQ3#3 reduced the proliferation rate by around 40% compared to si ctrl-treated cells (Figure 4.17B). These data show that both siRNAs significantly reduced the proliferation rate of HeLa cells. To ensure that the effect of these siRNAs is indeed due to the knockdown of IQGAP3 and not some non-related side effect a HeLa cell line was generated that stably expressed an IQGAP3-myc (HeLa IQ3-myc) that is not affected by si IQ3#1, as it lacks the 3'UTR region of the endogenous IQGAP3 targeted by si IQ3#1 (Figure 4.17A). As shown in Figure 4.17C si IQ3#1-mediated knockdown of endogenous IQGAP3 did not affect the proliferation rate of HeLa IQ3-myc cells. Thus, IQGAP3-myc can rescue the si IQ3#1-mediated knockdown of endogenous IQGAP3. Taken together these results indicate that IQGAP3 is required for the proper cell cycle progression of HeLa cells.

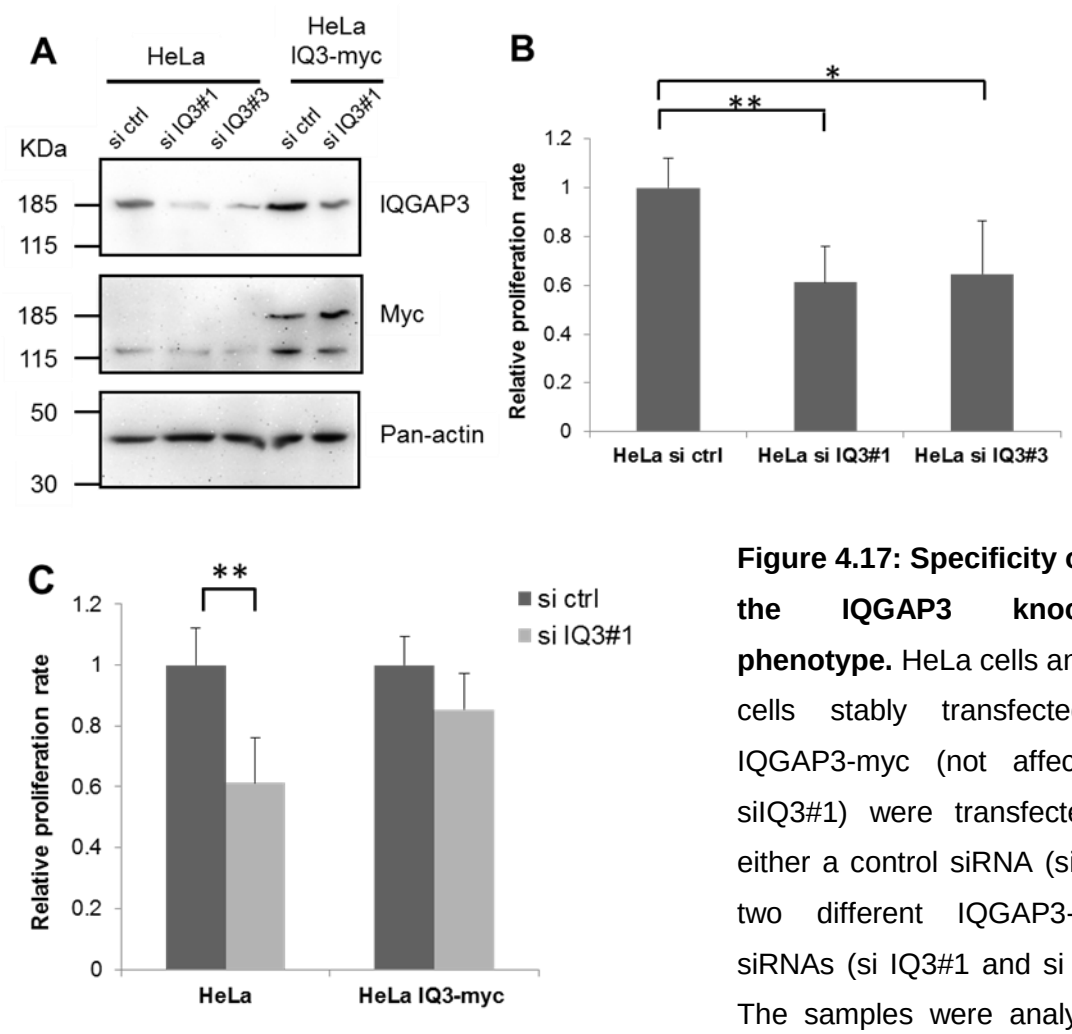

Figure 4.17: Specificity of the IQGAP3 knockdown phenotype. HeLa cells and HeLa cells stably transfected with IQGAP3-myc (not affected by siIQ3#1) were transfected with either a control siRNA (si ctrl) or two different IQGAP3-specific siRNAs (si IQ3#1 and si IQ3#3). The samples were analyzed by western blot. Pan-actin was used as a loading control. (B and C) Proliferation rate was measured by "Cell Counting Kit 8". The data are represented as mean ± S.E.M. (n = 3). ***: p-value* ≤ 0.01; *: *p-value* ≤ 0.05, Student's *t*-test, two-tailed. One-way ANOVA test was performed to compare multiple conditions *vs* control sample in (B) with the result *p-value* ≤ 0.01.

4.6 IQGAP3 depletion fails to induce cytokinesis failure

Knockdown of proteins fundamental for cytokinesis, such as aurora B[9,122] and Plk1[41], causes cytokinesis failure resulting in binucleation. To determine whether the above observed reduced proliferation rate in IQGAP3-depleted cells was due to the accumulation of multinucleated cells, cells were stained three days after the last si ctrl/si IQ3#1 transfection against α-tubulin and DNA (DAPI). The analysis of 500 cells per condition revealed that 2.99% ± 0.002% of si IQ3#1-treated HeLa cells were multinucleated compared to 2.83% ± 0.001% of si ctrl-treated HeLa cells (mean ± S.D., n = 3, p-value > 0.05) (Figure 4.18). Collectively, these data indicate that IQGAP3 plays not a fundamental role in cytokinesis.

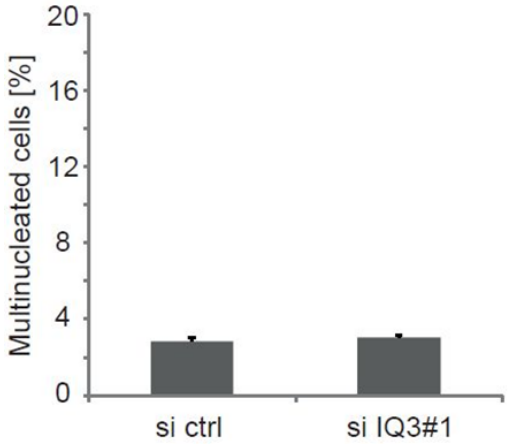

Figure 4.18: IQGAP3 depletion fails to induce cytokinesis failure. HeLa cells were transfected with either a control siRNA (si ctrl) or an IQGAP3-specific siRNA (si IQ3#1) and subsequently cells were stained after three days after from the transfection for α-tubulin and DNA (DAPI). At least 500 cells were counted per condition. The data are represented as mean ± S.D. (n = 3). p-value > 0.05, Student's *t*-test, two-tailed.

4.7 Knockdown of IQGAP3 causes a delay in S and G2/M phase progression

To assess which cell cycle phases are compromised by the knockdown of IQGAP3 resulting in the reduced proliferation rate, FACS analyses were performed. For this purpose HeLa cells transfected with either si ctrl or si IQ3#1 were collected three days after transfection and their DNA content was analyzed by FACS after PI staining. These analyses showed for IQGAP3-depleted HeLa cells an increase of the S phase and the G2/M phase population compared to si ctrl-transfected HeLa cells (si IQ3#1: S = 34% ± 0.06% , G2/M = 13% ± 0.02% *vs.* si ctrl: S = 26% ± 0.02%, G2/M = 10% ± 0.02%) (mean ± S.D., n = 6, p-value ≤ 0.05) (Figure 4.19A-B). Taken together these data indicate that IQGAP3 knockdown impairs the progression through S and G2/M phase in HeLa cells.

IGGAP3 was never observed in the nucleus and none of the performed IQGAP3 stainings indicated a role in S phase. In contrast, all data suggest that IQGAP3 plays a role in mitosis. Thus, it has been hypothesized that the observed S phase delay might be a secondary effect due to some primary mitotic defect in IQGAP3-depleted cells. To prove that IQGAP3 depletion causes a delay in executing mitosis and cytokinesis the duration from pro-metaphase to abscission was measured. For this purpose HeLa cells stably transfected with mCherry-α-tubulin were transfected with either si IQ3#1 or si ctrl. Subsequently, the cells were imaged for 12 h by taking every 5 min a photo between the second and third day after transfection. si IQ3#1-treated HeLa cells required 04:05 ± 00:11(h:min, mean ± S.D., n = 3) to progress to abscission while si ctrl-treated HeLa cells were with 03:37 ± 00:26 (h:min, mean ± S.D., n = 3) significantly faster (Figure 20A-B). Collectively, this

experiment verified that IQGAP3 depletion delays the progression of HeLa cells through mitosis and cytokinesis.

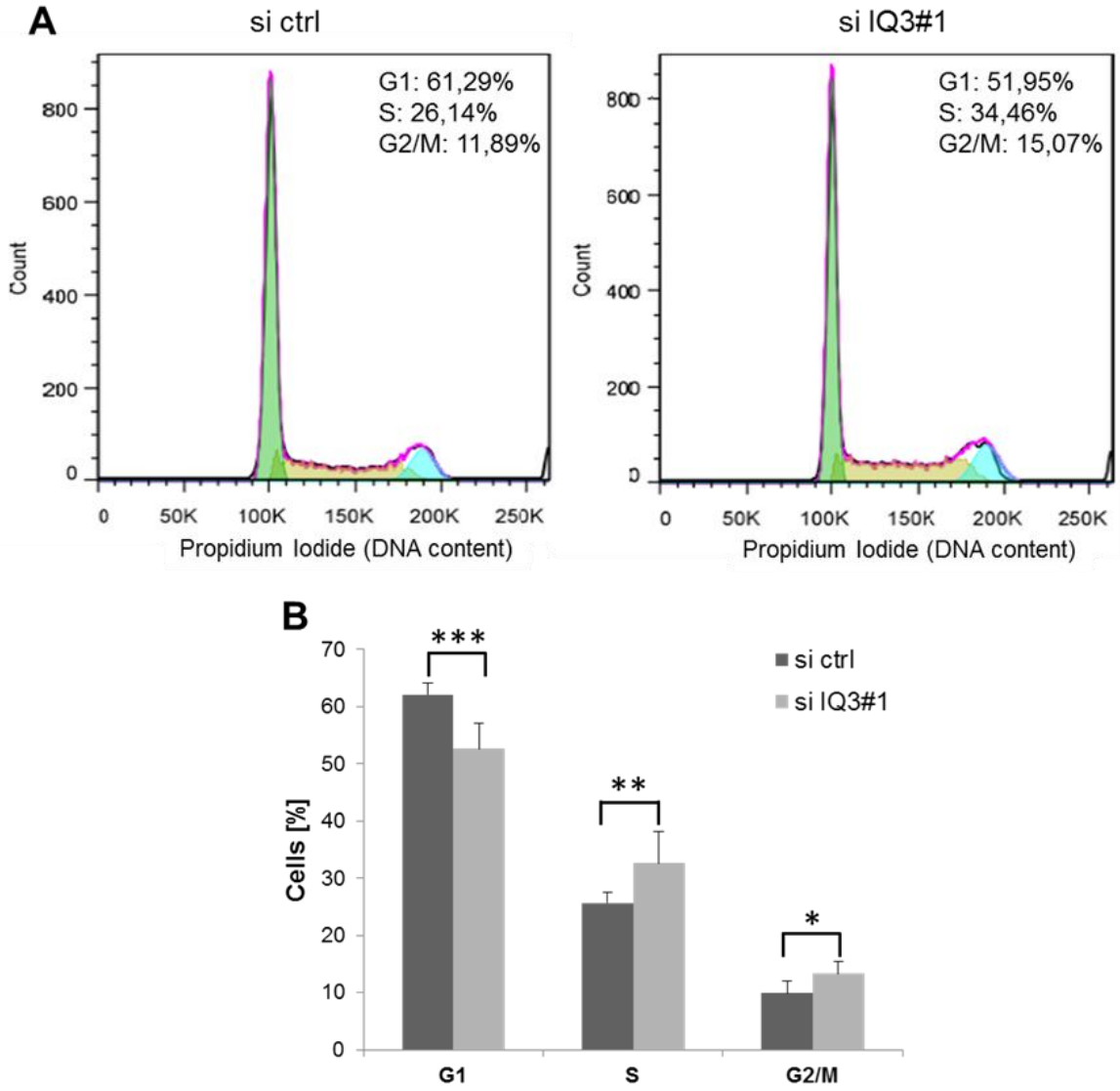

Figure 4.19: Knockdown of IQGAP3 causes a delay in S and G2/M phase progression. (A) The cell cycle in IQGAP3-depleted cells and control cells was analyzed after PI staining by FACS based on DNA content. (B) Quantitative analysis of FACS data described in A. Results are means ± S.D. (n = 6). ***: *p-value* ≤ *0.001; **: p-value* ≤ 0.01; *: *p-value* ≤ 0.05, Student's *t*-test, two-tailed.

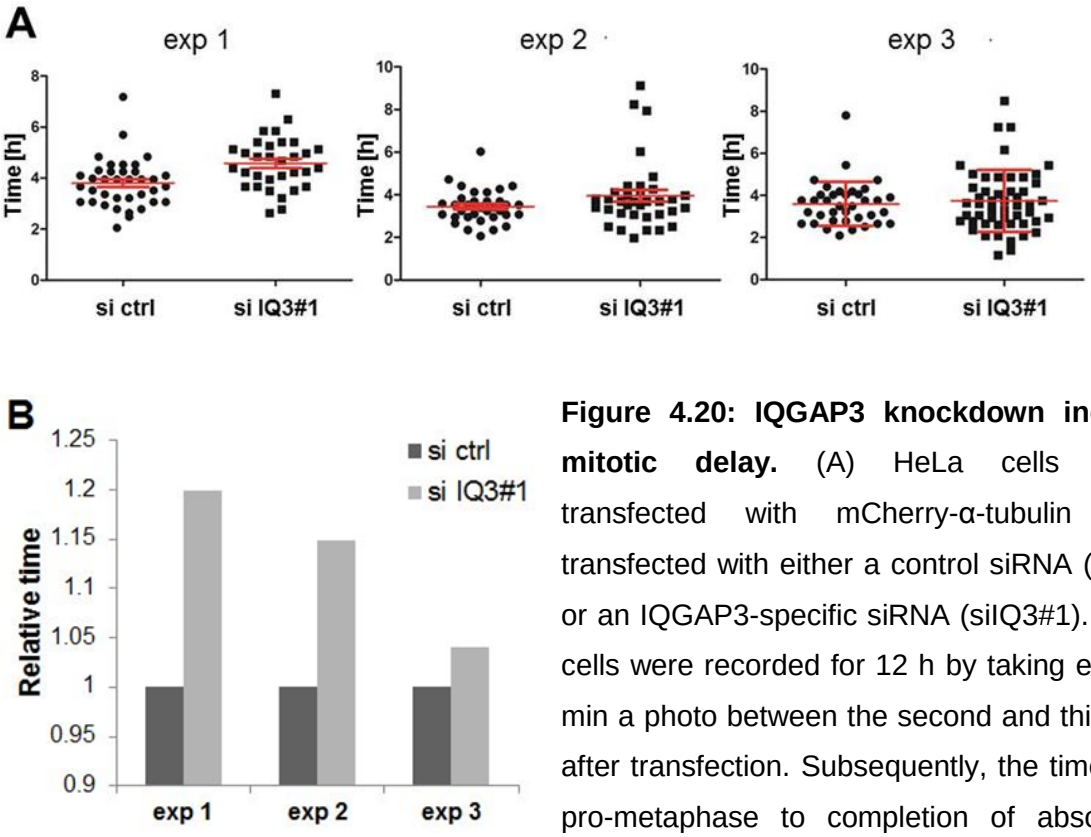

Figure 4.20: IQGAP3 knockdown induces mitotic delay. (A) HeLa cells stably transfected with mCherry-α-tubulin were transfected with either a control siRNA (si ctrl) or an IQGAP3-specific siRNA (siIQ3#1). Then, cells were recorded for 12 h by taking every 5 min a photo between the second and third day after transfection. Subsequently, the time from pro-metaphase to completion of abscission was measured. Per each condition 34 cells were analyzed. Data are represented as mean. (B) Schematic representation of A.

4.8 Knockdown of IQGAP3 leads mitotic multipole formation and aneuploidy

The absence or alteration of the localization or post-translational modification of some fundamental mitotic proteins can cause mitotic delays. Therefore, the expression patterns of F-actin, Ect2, aurora B, anillin, MKLP1 and Cep55 were analyzed in IQGAP3-depleted cells. HeLa cells transfected either with si IQ3#1 or si ctrl were fixed 72 h after transfection and stained. The comparison of the expression patterns of F-actin, Ect2, aurora B, anillin, MKLP1, and Cep55 in si ctrl- and si IQ3#1-transfected cells did not reveal any obvious difference (Figure 4.21-25). These data suggest that IQGAP3 is not required for the proper assembly of the cleavage furrow which is in agreement with the previous finding that IQGAP3 depletion does not result in cytokinesis failure.

As the analysis of the progression of IQGAP3-depleted cells through mitosis based on still photos did not reveal an explanation for the observed mitotic delay time-lapse analysis was performed in order to determine if IQGAP3 depletion affects

the integrity of spindle pole. For this purpose knockdown experiments utilizing si IQ3#1 and si ctrl were performed in HeLa cells stably expressing mCherry-α-tubulin.

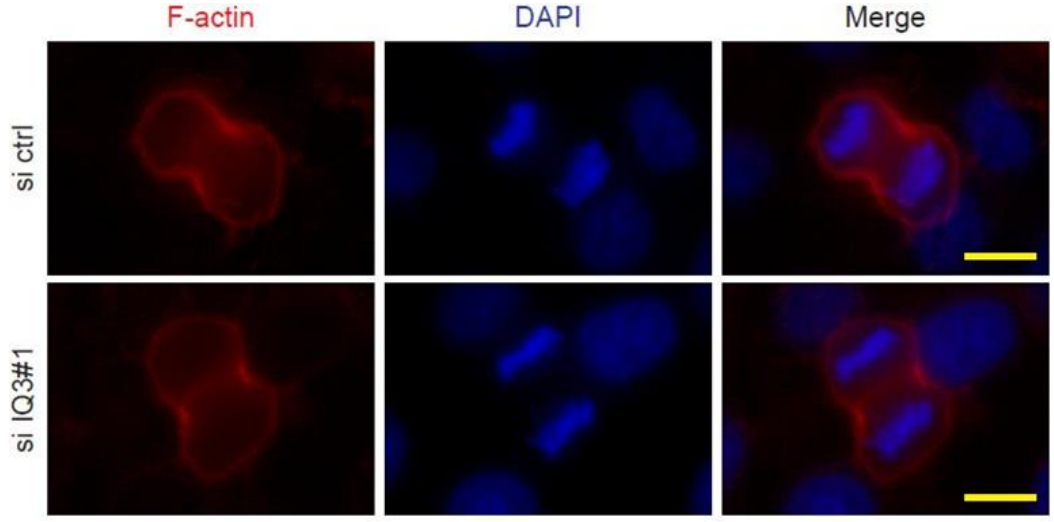

Figure 4.21: IQGAP3 suppression does not cause any alterations of F-actin localization in anaphase. HeLa cells were transfected with either a control siRNA (si ctrl) or an IQGAP3-specific siRNA (si IQ3#1). After three days cells were fixed and stained for F-actin (red) and DNA (DAPI, blue). Scale bar = 10 µm.

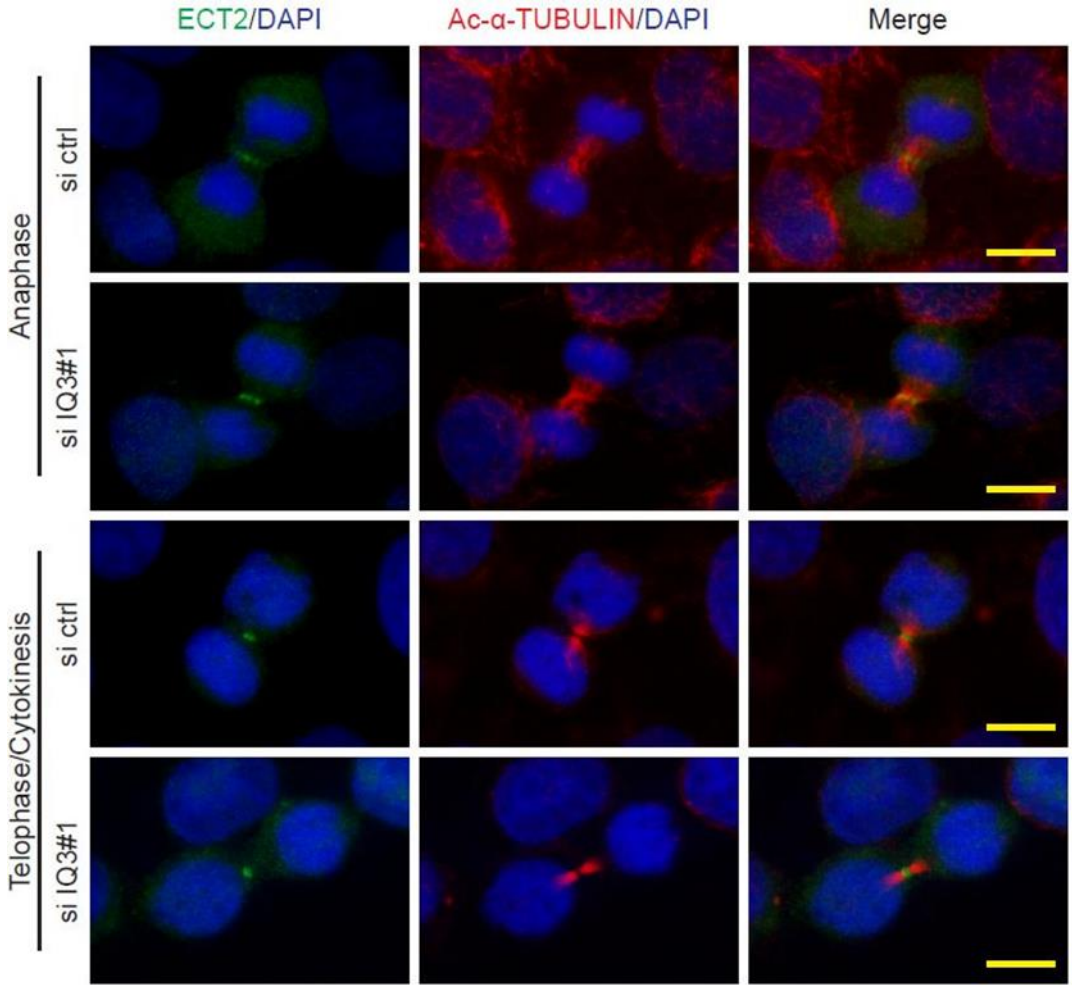

Figure 4.22: Knockdown of IQGAP3 does not lead to any alterations of ECT2 localization both in anaphase and telophase/cytokinesis. HeLa cells were transfected with either a control siRNA (si ctrl) or an IQGAP3-specific siRNA (si IQ3#1). After three days cells were fixed and stained for ECT2 (green), Ac-α-TUBULIN (red) and DNA (DAPI, blue). Scale bar = 10 µm.

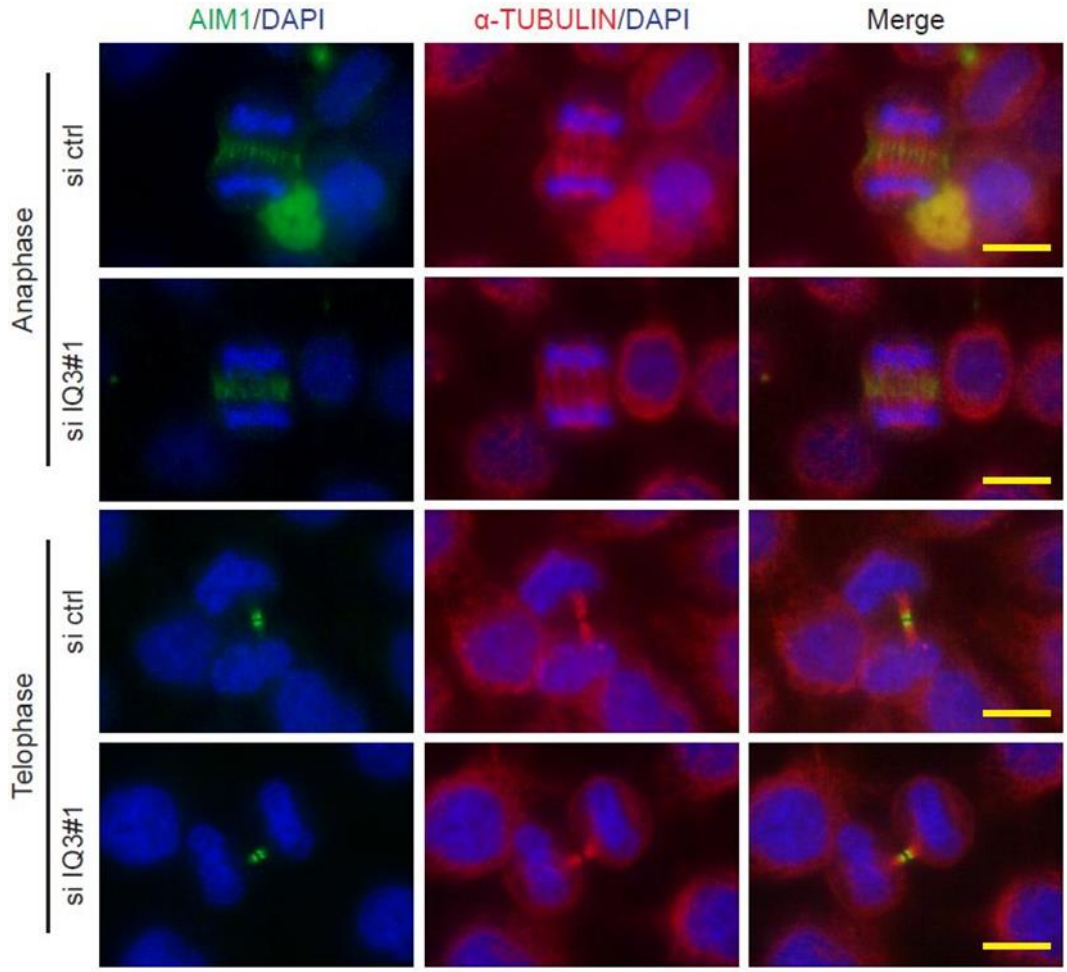

Figure 4.23: IQGAP3 knockdown does not cause any obvious alteration of aurora B localization both in anaphase and telophase. HeLa cells were transfected with either a control siRNA (si ctrl) or an IQGAP3-specific siRNA (si IQ3#1). After three days cells were fixed and stained for AIM1 (green), α-TUBULIN (red) and DNA (DAPI, blue). Scale bar = 10 µm.

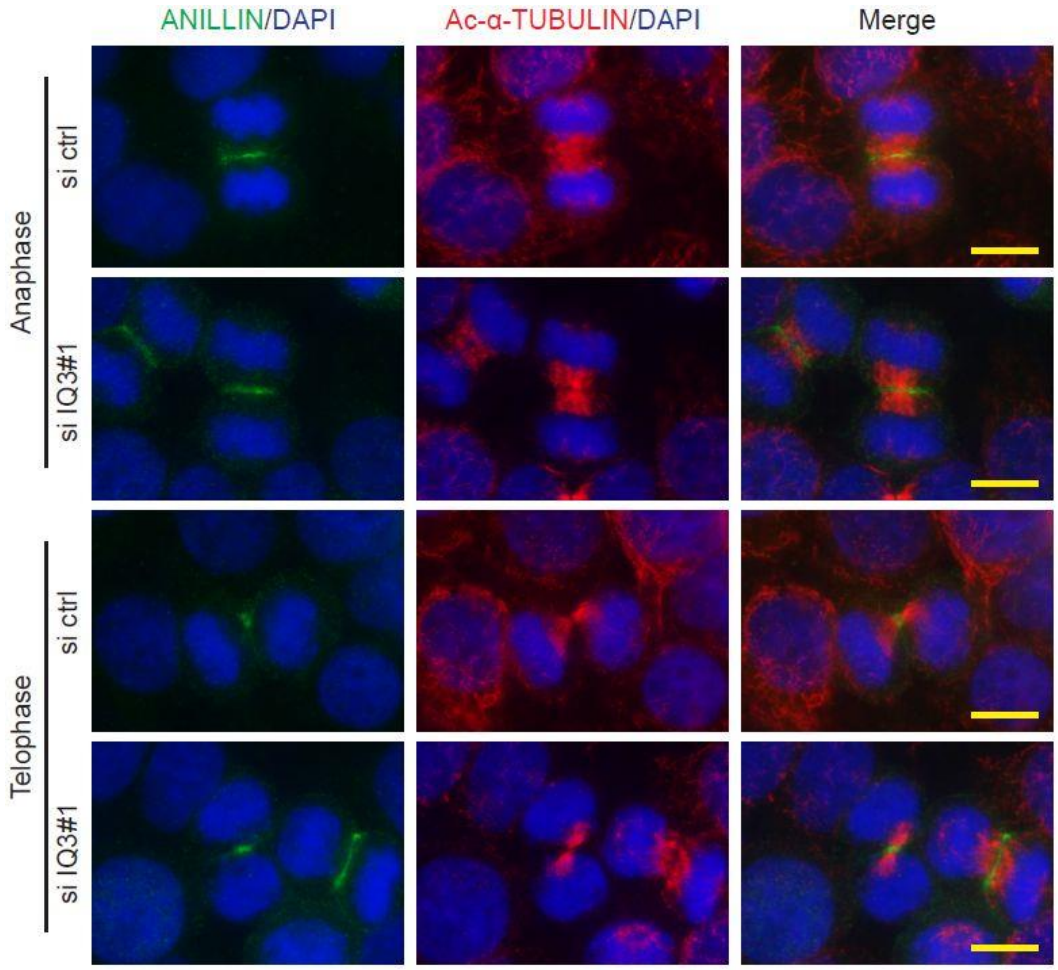

Figure 4.24: IQGAP3 suppression does not cause any alterations of anillin localization both in anaphase and in telophase. HeLa cells were transfected with either a control siRNA (si ctrl) or an IQGAP3-specific siRNA (si IQ3#1). After three days cells were fixed and stained for ANILLIN (green), Ac-α-TUBULIN (red) and DNA (DAPI, blue). Scale bar = 10 µm.

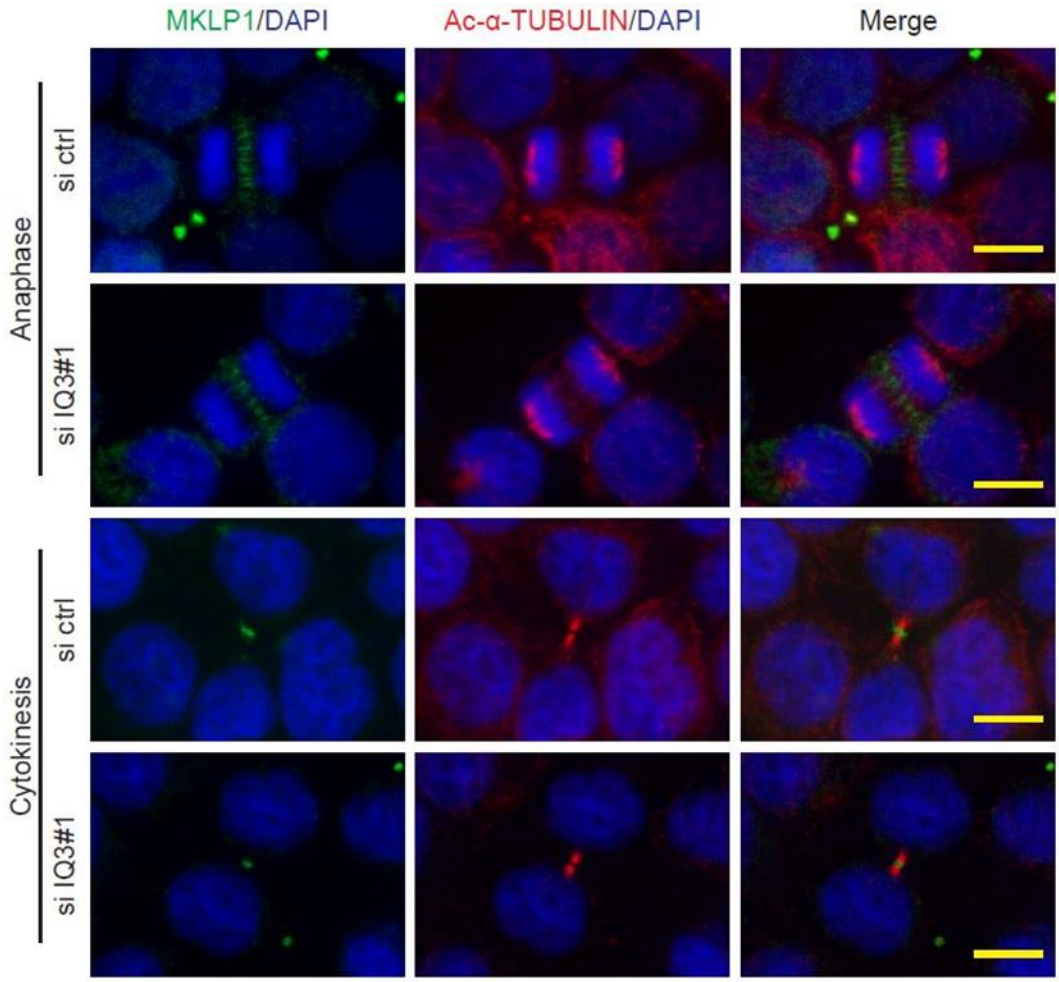

Figure 4.25: Knockdown of IQGAP3 does not lead to any obvious alterations of MKLP1 localization both in anaphase and in cytokinesis. HeLa cells were transfected with either a control siRNA (si ctrl) or an IQGAP3-specific siRNA (si IQ3#1). After three days cells were fixed and stained for MKLP1 (green), Ac-α-TUBULIN (red) and DNA (DAPI, blue). Scale bar = 10 µm.

Time-lapse movies were taken between the second and the third day after transfection and pictures were taken every 5 min. These movies revealed that instead of mitotic bipolar spindles (si ctrl) si IQ3#1-treated HeLa cells formed mitotic multipoles (Figure 4.26A). Quantification of this phenomenon revealed an increase of up to 34% ± 0.02% of mitotic multiples in HeLa si IQ3#1-treated cells compared to 2% ± 0.03% in si ctrl-treated HeLa cells (mean ± S.D., n = 3, p-value ≤ 0.001) (Figure 4.26B). These data suggest that IQGAP3 can affect spindle pole integrity.

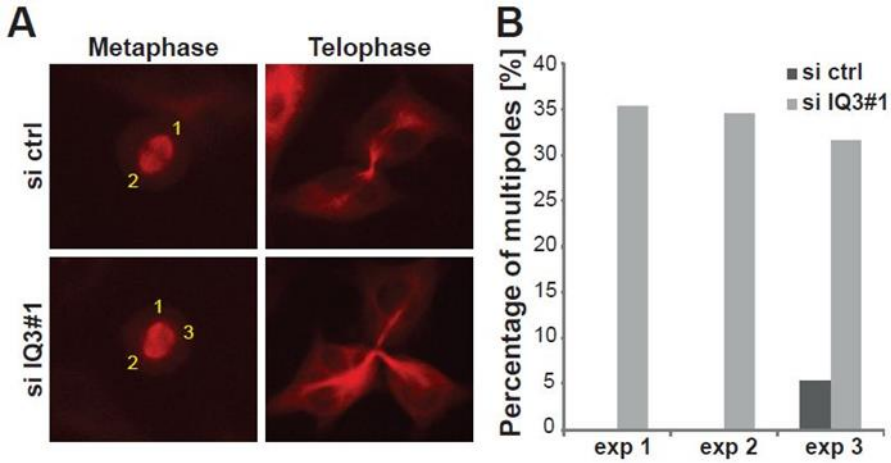

Figure 4.26: Knockdown of IQGAP3 causes mitotic multipole formation. (A) HeLa cells stably transfected with mCherry-α-tubulin were transfected with either a control siRNA (si ctrl) or an IQGAP3-specific siRNA (siIQ3#1). Then, cells were recorded for 12 h by taking every 5 min a photo between the second and third day after transfection. The picture shows a representation of a normal bipolar spindle (si ctrl) *vs.* multipoles (si IQ3#1) in metaphase and telophase. Yellow numbers indicate pole numbers per cell. (B) Percentage of mitotic multipoles in IQGAP3-depleted and control HeLa cells. 34 cells were counted per condition. The data are represented as mean. from three independent experiments. p-value ≤ 0.001, Student's *t*-test, two-tailed.

The formation of multipoles can impair the faithful segregation of the chromosomes during mitosis with the consequence that the subsequent cell division results in two daughter cells with unbalanced genomes (aneuploidy). To determine whether mitotic multipole formation in IQGAP3-depleted cells results in genome instability interphase FISH analysis was performed using centromere-specific chromosome enumerator probe (CEP) probes for chromosome 7 and 8 in the chromosomally stable, diploid HCT116 cells. As chromosome instability is an "accumulative" disorder, IQGAP3 was repeatedly depleted utilizing si IQ3#1 and the 4^{th} generation of cells was analyzed. FISH analysis revealed that IQGAP3-depleted cell populations contain the double amount of cells that diverge (off-mode) from the modal position (the diploid status) for chromosome 7 and 8 (11.15% and 10.26%, respectively *vs.* 5.47% and 5.96% in control cells, p-value ≤ 0.004, Fisher's exact test, n=1) (Figure 4.27A-D). Collectively, even though the FISH experiment was performed only one time these preliminary data suggest that IQGAP3 might be required to maintain genome stability.

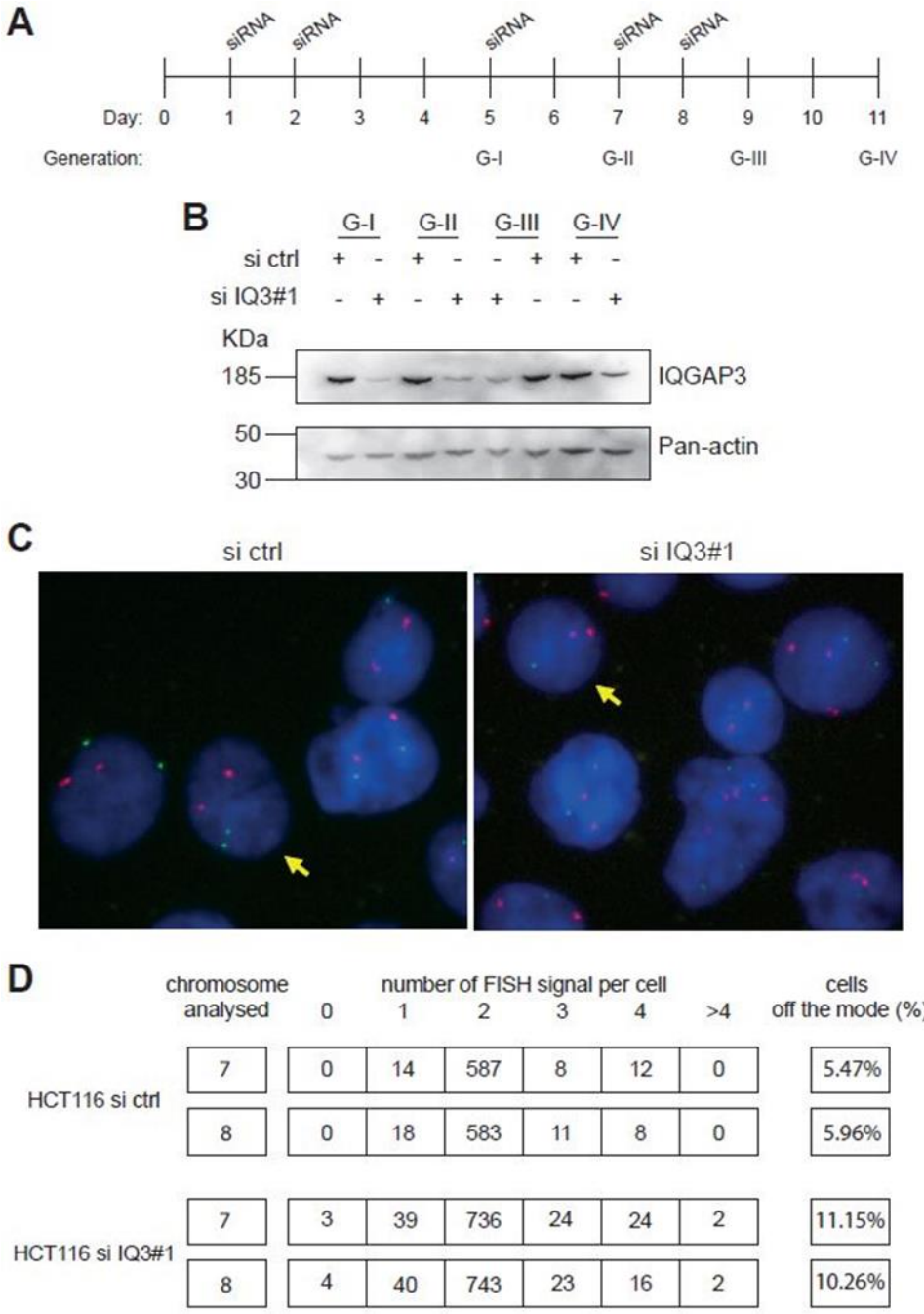

Figure 4.27: IQGAP3 depletion causes aneuploidy. (A) Schematic representation of the experiment. The chromosomally stable, diploid HCT116 cells were repeatedly transfected either with a control siRNA (si ctrl) or an IQGAP3-specific siRNA (si IQ3#1) and kept in culture until the 4th generation. (B) In order to control the efficiency of si IQ3#1 knockdown during the entire length of the experiment the total cell lysate was collected at first, second, third and fourth generations in culture (G-I, G-II ,G-III, G-IV). Pan-Actin was used as loading control. (C) Interphase FISH analysis using centromere-specific, fluorescently labelled probes for chromosome 7 (red) and 8 (green). Nuclei were stained with DAPI. Yellow arrows indicate a diploid cell (si ctrl) and an aneuploidy cell (si IQ3#1). (D) Quantification of FISH signals for chromosome 7 and 8 in si ctrl/si IQ3#1-treated HCT116 cells. Data are represented from only one experiment.

4.9 The N-terminal part of IQGAP3 is important for its localization during mitosis

The role of IQGAP3 in cell cycle control is poorly understood. The characterization of the different domains of IQGAP3 might provide information that will help to elucidate the underlying mechanisms of the above-described IQGAP3 depletion phenotypes. Thus, plasmids driving the expression of two truncated forms of IQGAP3 tagged with TurboGFP were generated. One contains the CH domain and WW repeats (mutA), while the other one contains the IQ and RasGTP domains (mutB) (Figure 4.28).

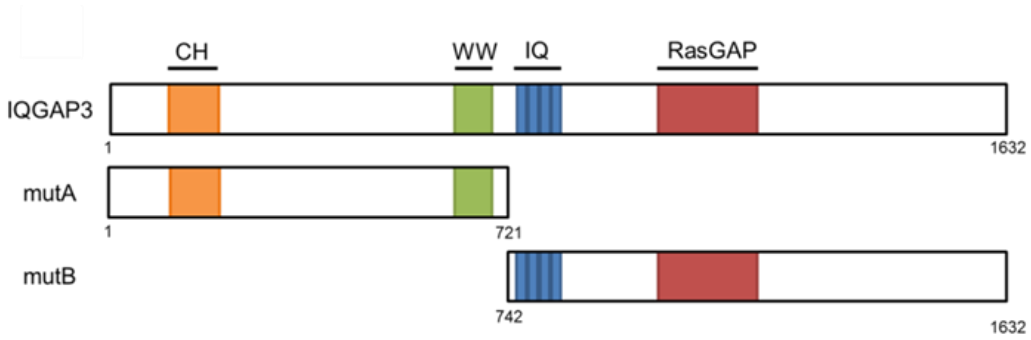

Figure 4.28: Scheme of IQGAP3 protein structure and the two generated truncated forms of IQGAP3 (mutA and mutB). Numbers are the amino acids.

HeLa cells were transfected, and after 24 h stained for Ac-α-tubulin and DNA (DAPI) to analyze the expression pattern of mutA and mutB in different mitotic stages. The N-terminal truncated form of IQGAP3 (mutA-GFP) exhibited the same localization pattern as the full length protein. In contrast, mutB was diffusely localized throughout the cell during all investigated mitotic stages (Figure 4.29A-B). These data suggest that the N-terminus of IQGAP3 contains the domains required to localize IQGAP3 to the cleavage furrow.

To characterize the influence of mutA and mutB on cell proliferation HeLa cells were transiently transfected at day 0 and day 2 and analyzed at day 4. Cells were fixed and stained for α-tubulin and DNA (DAPI). Analysis of the cells indicated that overexpression of mutA, but not mutB, resulted in an increase of multinucleated cells (Figure 30A-D). For a quantitative analysis 100 mutA-GFP-positive cells per condition were counted revealing that mutA overexpression induced multinucleation in 49.40% ± 3.62% of the transfected cells, while in the control (TurboGFP overexpression) 3.67% ± 1.46% multinucleated cells were observed (mean ± S.D., n=3, p-value ≤ 0.001) (Figure 30B). The same quantitative analysis of percentage of multinucleated cells was performed in mutB-GFP-transfected *vs.* TurboGFP-transfected cells (6.52%

± 2.49% *vs.* 6.83% ± 0.94%, respectively, mean ± S.D., n=3, p-value > 0.05) (Figure 30D). These data support the hypothesis that IQGAP3 is required for proper cell cycle progression and suggests that the N-terminal part of IQGAP3 binds to a so far unknown protein that is critical for cytokinesis.

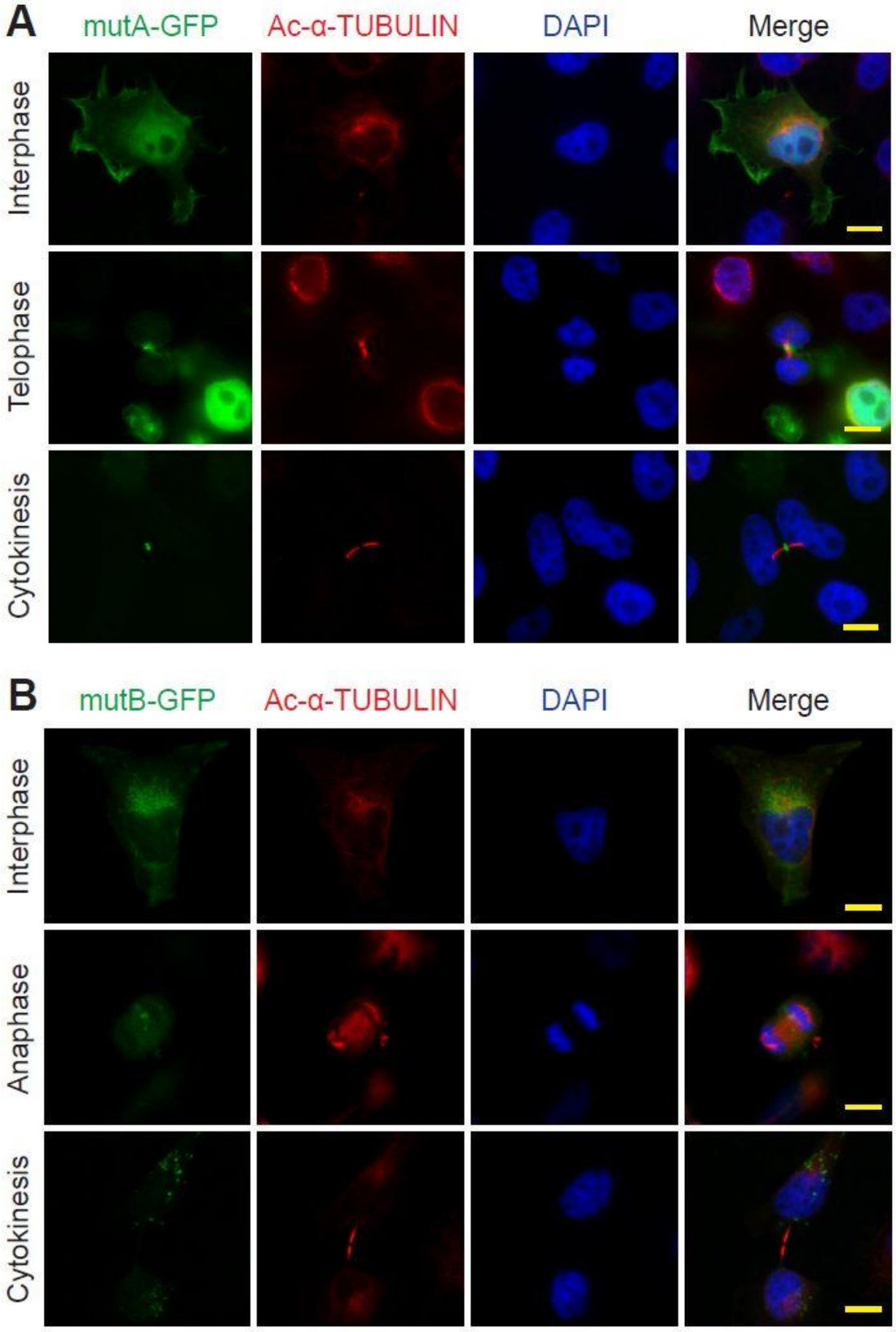

Figure 4.29: The N-terminal part of IQGAP3 is important for its localization during mitosis. (A-B) HeLa cells were transiently transfected with either mutA-GFP or mutB-GFP (green). After 24 h cells were fixed and stained for Ac-α-TUBULIN (red) and DNA (DAPI, blue). Scale bar = 10 µm.

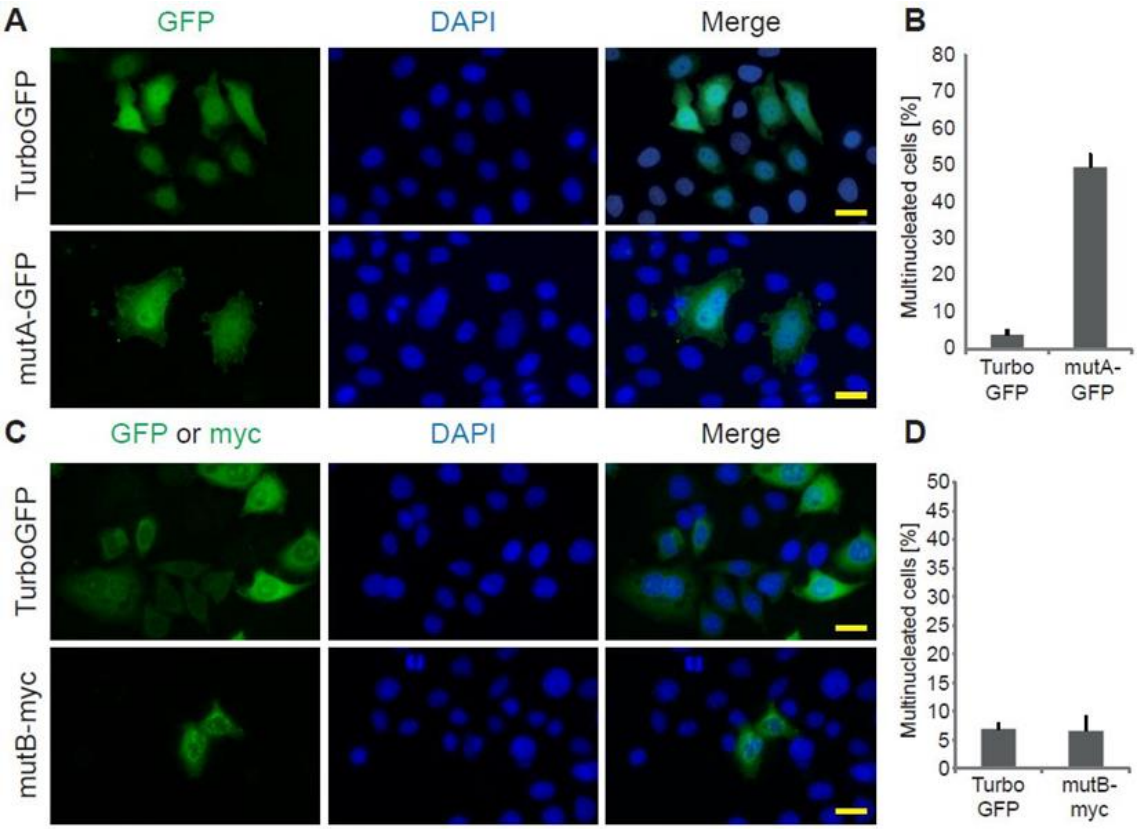

Figure 4.30: Overexpression of mutA-GFP but not mutB-GFP induces multinucleation. (A-D) HeLa cells were transiently transfected at day 0 and day 2 with either mutA-GFP (green) or mutB-myc or pCMV-AC-GFP (TurboGFP) (green) as internal control and analyzed at day 4. Cells were fixed and stained for myc (green) and DNA (DAPI). (A and C) Immunofluorescence analyses of the performed stainings. Scale bar = 20 µm. (B and D) Quantitative analysis of immunofluorescence data shown in A and B. 100 cells were counted per condition. The data are represented as mean ± S.D. from three independent experiments. p-value ≤ 0.001 for mutA-GFP, p-value > 0.05 for mutB-GFP, Student's *t*-test, two-tailed.

5 Discussion and Outlook

The data presented in this thesis revealed that IQGAP3 plays a role in cell proliferation. IQGAP3 is expressed during mitosis in several different cell types localizing to the cleavage furrow and later to the midbody until cytokinesis is completed. However, IQGAP3 is not required for proper cytokinesis in HeLa cells. Instead, IQGAP3 depletion leads to a delay of S and G2/M phase progression resulting in an obvious mitotic delay. A detailed analysis has shown that IQGAP3 deficiency causes in HeLa cells the formation of mitotic multipoles and in HCT116 cells an increase in aneuploid cells. In conclusion, these data demonstrate that IQGAP3 is required for proper cell cycle progression.

5.1 IQGAP3 localization during mitosis

The presented immunofluorescence data in this study show that IQGAP3 is present during mitosis in three different cell lines (HL-1, NIH3T3 and HeLa), but with a slightly different expression pattern. The reason for these different localizations is unknown. Yet, based on previous studies three hypotheses should be considered. First, it has previously suggested that due to different activities of Rho A and septin 7 cytokinesis is executed in a cell type-specific manner[123,124]. Thus, the different observed expression patterns of IQGAP3 might reflect cell type-specific progression through cytokinesis. Another explanation could be the use of different antibodies. In this study two different antibodies were utilized as cell types of different species have been investigated. The antibody targeting the mouse/rat ortholog of IQGAP3 recognizes the IR domains. In contrast, the antibody targeting the human ortholog was generated utilizing the full-length protein and thus it might bind to other epitopes than the IR domain. Finally, it is also possible that there is no difference in cytokinesis among the different studied cell lines. As in this study only still photos have been taken, it might be that the different observed IQGAP3 staining patterns represent the fact that IQGAP3 changes its localization at the midbody during mitosis. However, it appears unlikely that by chance always the same pattern was observed in one distinct cell type. Live cell imaging studies of HL-1 and NIH3T3 cells transiently overexpressing IQGAP3-GFP will resolve this issue. A recent study by Adachi and coworkers confirmed that IQGAP3 is expressed at the cleavage furrow and midbody[101]. Since this study was performed only in HeLa cells their data do not provide any suggestions regarding IQGAP3 localization at the abscission site.

The staining patterns of IQGAP3 in both HL-1 and NIH3T3 cells during cytokinesis suggest a possible function of IQGAP3 in abscission. IQGAP3 shows a similar pattern as flanking proteins. Its localization resembles a coiled-structure that starts from the flanking regions and moves towards a site placed some µm far from the flanking regions. This pattern is comparable to the staining patterns of proteins involved in the ESCRT-III complex, such as CHMP4B. CHMP4B migrates from the midbody to the abscission site that localizes at few µm away from the flanking regions (average: 0.76 µm) forming a coiled structure[54,55,125]. The hypothesis that IQGAP3 localizes to the abscission site is further supported by the fact that the C-terminal part of IQGAP1, a region that shares 75% sequence similarity with IQGAP3, interacts with Tsg101, a member of the ESCRT-III complex[98]. In order to better investigate a possible localization of IQGAP3 at the abscission site, it would be important to perform co-staining or co-immunoprecipitation analyses of IQGAP3 with proteins such as CHMP4B or spastin in HL-1 and NIH3T3 cells. As for some of these proteins no antibodies are available, such as CHMP4B, an alternative is the overexpression of tagged (*e.g.* GFP) versions of such proteins.

5.2 IQGAP3 is not required for cytokinesis progression

The immunofluorescence data demonstrate that IQGAP3 is present at the cleavage furrow, the stem body of the midbody, and the midbody remnants, and thus suggest that IQGAP3 is required for cytokinesis. However, IQGAP3 depletion did not cause any obvious alterations of proteins fundamental for cytokinesis such as F-actin, anillin, Ect2, Cep55, MKLP1, and aurora B. Recently, Adachi and coworkers confirmed that IQGAP3 depletion has no effect on the central spindle proteins MKLP1, MgcRacGAP, and Ect2. In contrast, IQGAP3 depletion caused in their study a slight decrease of the accumulation of Rho A and phospho-myosin light chain 2 (P-MLC) and a strong decrease of the accumulation of anillin at the equatorial cortex during mitosis. Depletion of IQGAP1 enhanced the effect of IQGAP3 depletion on Rho A and P-MLC, but had no significant effect on anillin. This indicated that IQGAP3 might control cytokinesis via anillin. This hypothesis was further supported by the finding that anillin and IQGAP3 co-immunoprecipitated. In addition, the authors demonstrated that anillin knockdown caused mis-localization of IQGAP3 during mitosis. However, it has to be noted that Adachi and coworkers did not study endogenous IQGAP3. Instead, they tested the effect of anillin knockdown on ectopic

expressed IQGAP3. Furthermore the authors speculate that the observed Rho A phenotype caused by the double knockdown of IQGAP proteins is caused by anillin alterations because both IQGAP1 and IQGAP3 don't interact with neither Rho A nor Ect2, a upstream regulator of Rho A. Thus in contrast with these finding, in this study no evidence was found that IQGAP3 depletion affects anillin localization (Figure 4.24), even though the same antibody was utilized as by Adachi and coworkers. Currently, there is no explanation for this discrepancy.

To clarify, if IQGAP3 depletion as suggested by the data from Adachi causes cytokinesis failure the incidence of multinucleation in IQGAP3-depleted cells was investigated. In the present study, siRNA-mediated knockdown of IQGAP3 did not cause the appearance of binucleated cells (n = 3; 500 cells were counted per condition). In contrast, Adachi and coworkers reported that IQGAP3 depletion caused an increase of 5% in multinucleated cells compared to control cells. In addition, depletion of IQGAP3 together with IQGAP1 increased the multinucleation rate to 10%. The authors counted between 600 and 1000 cells per conditions. However, the experiment was repeated only twice without performing a statistical analysis of the results and only in one cell type. Moreover, the authors did not show that IQGAP1 localizes to the cleavage furrow or the midbody during cytokinesis. Taken together it remains unclear why the results presented in this study and published by Adachi and coworkers are different. One reason could be the use of different cells (also different passages or subclones of the same cell type). For example, cells that exhibit an intrinsic multinucleation rate (HeLa cells) might be more sensitive to IQGAP3 depletion in contrast to diploid cells with a stable genome and thus a low multinucleation rate (*e.g.* HCT116). Thus it is important to test the effect of IQGAP3 depletion in a wide variety of cell types including primary cells.

5.3 Characterization of IQGAP3 domains

Expression studies of IQGAP3 mutants have revealed that the N-terminal part of IQGAP3 (mutA) containing the CH domain, IR domain, and WW repeats is sufficient for the proper IQGAP3 localization during mitosis, while the C-terminal part (mutB) containing the IQ domains and RasGAP domain is not required. Adachi and coworkers have performed a more detailed analysis regarding the requirement of the different domains for the localization of IQGAP3 during mitosis. The authors have generated several mutants but only one of their mutants, IQGAP3-ΔCH missing the

CH domain, was present at the cleavage furrow. Among these deletion mutants one, IQGAP3-N1, is highly similar to mutA. Both mutants contain the CH and IR domains. Yet, while mutA contained also the entire WW repeats, IQGAP1-N1 contained only around one third of the domain. As IQGAP1-N1 did not localize to the cleavage furrow, these data indicate that the presence of WW repeats is critical for IQGAP3 localization to the cleavage furrow, possibly through binding to an important cytokinesis protein. Another explanation could be that the WW repeats are required for the proper protein folding of the mutant. Finally it would be interesting to determine whether the CH domain and thus the binding to F-actin is also dispensable in mutA, as shown for IQGAP3-ΔCH, for the localization of IQGAP3 during cytokinesis.

Further characterization of mutA showed that overexpression of this mutA in HeLa cells caused a marked increase of multinucleated cells (50%). This suggests that mutA binds an unknown protein essential for cytokinesis. A similar phenotype was observed by Wang and coworkers after stably overexpressing the IQGAP1 mutants IQGAP1-IR-WW[97], that contains IR domains and WW repeats, as well as IQGAP1-N, that contains in addition the CH domain, in HeLa cells. Overexpression of both mutants resulted in around 50% of multinucleated cells. In contrast, overexpression of full length IQGAP1 or the mutant IQGAP1-C that consists only of the RasGAP domain did not cause multinucleation. These data suggest again that the CH domain might not play an important role in cytokines but the IR domains and WW repeats.

How these mutant proteins impair cytokinesis resulting in cytokinesis failure and multinucleation is unknown. The similar phenotype of the IQGAP3 and the IQGAP1 mutants might be due to the high sequence similarity between the two domains present in all mutants (IR= 52% and WW=41%). Thus, all mutants might bind the same proteins important for cytokinesis. On the other hand, it is also possible that IQGAP3 and IQGAP1 create heterodimers through their IR domains that regulate cytokinesis by binding to other proteins. This hypothesis is supported by the fact that IQGAP1 is known to form homodimers through their IR domains[91,126,127]. In addition, the observation by Adachi and coworkers that IQGAP1 depletion enhances the multinucleation rate of IQGAP3-depleted cells further supports this hypothesis. However, a critical weakness in this hypothesis is that IQGAP1 has so far not been observed during cytokinesis at the cleavage furrow.

Collectively, it will be important to identify in the future binding partners of IQGAP3 to better understand its function during cytokinesis. Whether the analysis of binding partners of mutA will reveal insight into the function of IQGAP3 is unclear as the observed multinucleation rate might be due to an artificial function of the mutant protein. However, such analysis has great potential to learn more about cytokinesis in general. Thus, assays to determine protein-protein interactions such as mass spectrometry studies and/or yeast-two hybrid screens should be performed for IQGAP3, mutA, and mutB (as control). Utilizing more than one method will help to eliminate false-positive hits. In addition, the assays have their individual strengths and weaknesses. The yeast-two hybrid system detects for example only direct interactions while mass spectrometry is used for detecting stable and multi-protein complexes. In addition, the yeast-two hybrid system is more suitable to determine the binding partners for individual domains, while mass spectrometry allows the detection of endogenous interacting partners of the full length IQGAP3[128].

5.4 IQGAP3 is required for proper cell cycle progression

To determine if IQGAP3 is required for proliferation the cell proliferation kit “Cell proliferation Kit-8” was used. This kit measures proliferation indirectly by the presence of living cells, which can convert a salt into a dye. Thus, the quantity of dye is directly proportional to the number of living cells. Thus, if the signal of the dye in a sample is not increasing over time as in the control one can conclude that in the sample are fewer living cells present than in the control. This can be explained by a decreased proliferation rate but also by an increased apoptosis (cell death) rate. In this study, the decreased signal after IQGAP3 depletion was interpreted as reduced proliferation rate. This was further substantiated by FACS analyses revealing a delay in S and G2/M phase progression with a major mitotic delay. Yet, it is possible that IQGAP3 depletion induced also apoptosis. This is supported by the fact that IQGAP3 knockdown induced mitotic multipole formation. Previous studies have demonstrated that multipolarity can create high levels of aneuploidy resulting in cell death[79,80]. Thus, IQGAP3 is required for proper cell cycle progression as its depletion slows down S and G2/M phase and can possibly cause cell death too. To test the hypothesis of increased cell death upon IQGAP3 depletion, the apoptotic index should be calculated with assays such as TUNEL assay. In addition, it should be tested whether multipole formation causes cell death. For this purpose it would be

interesting to determine FACS analyses of TUNEL/PI double stained cells to track in which cell cycle stage apoptosis occurs. Another important assay would be live cell imaging to determine if preferentially multipolar cells undergo cell death.

5.5 IQGAP3 suppression causes mitotic multipoles and aneuploidy

Live cell imaging analyses have revealed that IQGAP3 depletion causes the formation of mitotic multipoles. As outlined in the Introduction, multipolarity can derive from either centrosome amplification dependent or independent mechanisms. The centrosome amplification can be caused by either centriole overduplication or cytokinesis failure. The centrosome amplification independent mechanisms are premature centriole disengagement and PCM fragmentation. As discussed above IQGAP3 depletion did not result in binucleation, which excludes centrosome amplification due to cytokinesis failure as cause for multipole formation. Other causes of multipole formation have not yet been addressed. Thus, in future experiments it would be important to determine if IQGAP3 depletion results in a rosette phenotype, where one mother centriole forms several daughter centrioles. To address this issue, interphase cells should be fixed and stained with a marker for mother centrioles (*e.g.* outer dense fiber of sperm tails 2 (Odf2)) and a marker for daughter centrioles (*e.g.* centrobin). In addition, it should be discriminated between centrosome overduplication, premature centriole disengagement, and PCM fragmentation. For this purpose live cell imaging of a cell line stably expressing centrin (centrosome protein) tagged with GFP and tubulin tagged with mCherry could be performed. To ensure that all changes that the spindle undergoes during pro-metaphase and anaphase are imaged and for a better visualization of possible acentriolar/centriolar poles, images should be taken every 2 to 4 minutes at high resolution (i.e. minimum 60x objective). In addition, the cell chambers used for the videos should be coated with low concentration of fibronectin. This will result in spindle pole formation parallel to the substrate surface[129]. Such time-lapse videos will allow determining whether the multipolarity caused by IQGAP3 knockdown is dependent on centrosome amplification, premature centriole disengagement, or PCM fragmentation. Centrosome amplification should result in two centrin-positive signals at the extra pole. Centriole disengagement can be identified by a single centrin-positive signal at the extra pole. PCM fragmentation will result in a centrin-negative (acentriolar) pole.

Previously, it has been shown that knockdown of CLASP proteins results also in the formation of multipoles, which are characterized by acentriolar poles and generate living aneuploidy daughter cells. Watanabe and coworkers have shown that CLASP2 interacts with IQGAP1[103]. Thus, it can be speculated that IQGAP3 interacts with CLASP proteins or that IQGAP3 has a similar function as CLASPs during mitosis since both IQGAP3 and CLASPs knockdown create mitotic multipoles and generate aneuploidy. To further investigate this it would be interesting to test whether multipolarity is enhanced in IQGAP3-depleted cells by CLASP knockdown. However, it has to be noted that CLASP proteins are found at the centrosomes but not IQGAP3. Yet, PCM fragmentation can also be caused by unbalanced traction forces of microtubules on kinetochores that affect also the centrosome. While IQGAP3 is mainly seen at the cell cortex in the cleavage furrow a weaker signal was also observed in the spindle zone during anaphase. In addition, some data suggest that some spindle pole proteins are less concentrated in the spindle zone in IQGAP3-depleted cells. This hypothesis has to be further investigated employing high-resolution microscopy.

Comparing the low rate of multipolarity with the high rate of aneuploidy suggests that aneuploidy might be independent of multipolarity or that multipolarity was underestimated. A possible reason for an underestimation is that in this study the formation of pseudo bipolar spindles was not considered. As explained in the Introduction, cells with multiple poles can activate a survival pathway resulting in centrosome clustering and pseudo bipolar spindle formation[84,85]. This, however, can cause problems in mitosis resulting in lagging chromosomes, a common cause of aneuploidy. In order to detect the formation of pseudo bipolar spindle a solution could be recording cell lines stably transfected with both a tubulin and a DNA marker (i.e. H2B) tagged with fluorescein proteins. In this way the DNA marker will label eventually lagging chromosomes caused by the formation of pseudo bipolar spindle. Another possibility could be video-recording HeLa stably expressing with centrin-GFP and mCherry-α-tubulin and analyzing the presence of the clustered centrosomes at one pole.

6 References

1 Zhai, Y., Kronebusch, P. J., Simon, P. M. & Borisy, G. G. Microtubule dynamics at the G2/M transition: abrupt breakdown of cytoplasmic microtubules at nuclear envelope breakdown and implications for spindle morphogenesis. *The Journal of cell biology* **135**, 201-214 (1996).

2 Walczak, C. E. & Heald, R. Mechanisms of mitotic spindle assembly and function. *International review of cytology* **265**, 111-158, doi:10.1016/S0074-7696(07)65003-7 (2008).

3 Nogales, E. & Ramey, V. H. Structure-function insights into the yeast Dam1 kinetochore complex. *Journal of cell science* **122**, 3831-3836, doi:10.1242/jcs.004689 (2009).

4 Brinkley, B. R. Microtubule organizing centers. *Annual review of cell biology* **1**, 145-172, doi:10.1146/annurev.cb.01.110185.001045 (1985).

5 Lobrich, M. & Jeggo, P. A. The impact of a negligent G2/M checkpoint on genomic instability and cancer induction. *Nature reviews. Cancer* **7**, 861-869, doi:10.1038/nrc2248 (2007).

6 Wang, Y. *et al.* Centrosome-associated regulators of the G(2)/M checkpoint as targets for cancer therapy. *Molecular cancer* **8**, 8, doi:10.1186/1476-4598-8-8 (2009).

7 Bartek, J. & Lukas, J. Mammalian G1- and S-phase checkpoints in response to DNA damage. *Current opinion in cell biology* **13**, 738-747 (2001).

8 Bertoli, C., Skotheim, J. M. & de Bruin, R. A. Control of cell cycle transcription during G1 and S phases. *Nature reviews. Molecular cell biology* **14**, 518-528, doi:10.1038/nrm3629 (2013).

9 Norden, C. *et al.* The NoCut pathway links completion of cytokinesis to spindle midzone function to prevent chromosome breakage. *Cell* **125**, 85-98, doi:10.1016/j.cell.2006.01.045 (2006).

10 Steigemann, P. & Gerlich, D. W. An evolutionary conserved checkpoint controls abscission timing. *Cell cycle* **8**, 1814-1815 (2009).

11 Pascreau, G., Churchill, M. E. & Maller, J. L. Centrosomal localization of cyclins E and A: structural similarities and functional differences. *Cell cycle* **10**, 199-205 (2011).

12 Pihan, G. A. Centrosome dysfunction contributes to chromosome instability, chromoanagenesis, and genome reprograming in cancer. *Frontiers in oncology* **3**, 277, doi:10.3389/fonc.2013.00277 (2013).

13 Wang, G., Jiang, Q. & Zhang, C. The role of mitotic kinases in coupling the centrosome cycle with the assembly of the mitotic spindle. *Journal of cell science* **127**, 4111-4122, doi:10.1242/jcs.151753 (2014).

14 Doxsey, S., Zimmerman, W. & Mikule, K. Centrosome control of the cell cycle. *Trends in cell biology* **15**, 303-311, doi:10.1016/j.tcb.2005.04.008 (2005).

15 Fishman, M. C. & Chien, K. R. Fashioning the vertebrate heart: earliest embryonic decisions. *Development* **124**, 2099-2117 (1997).

16 DeRuiter, M. C., Poelmann, R. E., VanderPlas-de Vries, I., Mentink, M. M. & Gittenberger-de Groot, A. C. The development of the myocardium and endocardium in mouse embryos. Fusion of two heart tubes? *Anatomy and embryology* **185**, 461-473 (1992).

17 Brand, T. Heart development: molecular insights into cardiac specification and early morphogenesis. *Developmental biology* **258**, 1-19 (2003).

18 Olson, E. N. A genetic blueprint for growth and development of the heart. *Harvey lectures* **98**, 41-64 (2002).

19 High, F. A. & Epstein, J. A. The multifaceted role of Notch in cardiac development and disease. *Nature reviews. Genetics* **9**, 49-61, doi:10.1038/nrg2279 (2008).

20 Xin, M., Olson, E. N. & Bassel-Duby, R. Mending broken hearts: cardiac development as a basis for adult heart regeneration and repair. *Nature reviews. Molecular cell biology* **14**, 529-541, doi:10.1038/nrm3619 (2013).

21 Engel, F. B., Schebesta, M. & Keating, M. T. Anillin localization defect in cardiomyocyte binucleation. *Journal of molecular and cellular cardiology* **41**, 601-612, doi:10.1016/j.yjmcc.2006.06.012 (2006).

22 Soonpaa, M. H., Kim, K. K., Pajak, L., Franklin, M. & Field, L. J. Cardiomyocyte DNA synthesis and binucleation during murine development. *The American journal of physiology* **271**, H2183-2189 (1996).

23 Brodsky, V., Sarkisov, D. S., Arefyeva, A. M., Panova, N. W. & Gvasava, I. G. Polyploidy in cardiac myocytes of normal and hypertrophic human hearts; range of values. *Virchows Archiv : an international journal of pathology* **424**, 429-435 (1994).

24 Herget, G. W., Neuburger, M., Plagwitz, R. & Adler, C. P. DNA content, ploidy level and number of nuclei in the human heart after myocardial infarction. *Cardiovascular research* **36**, 45-51 (1997).

25 Li, F., Wang, X., Capasso, J. M. & Gerdes, A. M. Rapid transition of cardiac myocytes from hyperplasia to hypertrophy during postnatal development. *Journal of molecular and cellular cardiology* **28**, 1737-1746, doi:10.1006/jmcc.1996.0163 (1996).

26 Mollova, M. *et al.* Cardiomyocyte proliferation contributes to heart growth in young humans. *Proceedings of the National Academy of Sciences of the United States of America* **110**, 1446-1451, doi:10.1073/pnas.1214608110 (2013).

27 Kang, M. J. & Koh, G. Y. Differential and dramatic changes of cyclin-dependent kinase activities in cardiomyocytes during the neonatal period. *Journal of molecular and cellular cardiology* **29**, 1767-1777, doi:10.1006/jmcc.1997.0450 (1997).

28 Flink, I. L., Oana, S., Maitra, N., Bahl, J. J. & Morkin, E. Changes in E2F complexes containing retinoblastoma protein family members and increased cyclin-dependent kinase inhibitor activities during terminal differentiation of cardiomyocytes. *Journal of molecular and cellular cardiology* **30**, 563-578, doi:10.1006/jmcc.1997.0620 (1998).

29 Yoshizumi, M. *et al.* Disappearance of cyclin A correlates with permanent withdrawal of cardiomyocytes from the cell cycle in human and rat hearts. *The Journal of clinical investigation* **95**, 2275-2280, doi:10.1172/JCI117918 (1995).

30 Poolman, R. A. & Brooks, G. Expressions and activities of cell cycle regulatory molecules during the transition from myocyte hyperplasia to hypertrophy. *Journal of molecular and cellular cardiology* **30**, 2121-2135, doi:10.1006/jmcc.1998.0808 (1998).

31 Burton, P. B., Yacoub, M. H. & Barton, P. J. Cyclin-dependent kinase inhibitor expression in human heart failure. A comparison with fetal development. *European heart journal* **20**, 604-611 (1999).

32 Pasumarthi, K. B. & Field, L. J. Cardiomyocyte cell cycle regulation. *Circulation research* **90**, 1044-1054 (2002).

33 Sdek, P. *et al.* Rb and p130 control cell cycle gene silencing to maintain the postmitotic phenotype in cardiac myocytes. *The Journal of cell biology* **194**, 407-423, doi:10.1083/jcb.201012049 (2011).

34 Zebrowski, D. C. *et al.* Developmental alterations in centrosome integrity contribute to the post-mitotic state of mammalian cardiomyocytes. *eLife* **4**, doi:10.7554/eLife.05563 (2015).

35 Engel, F. B. *et al.* p38 MAP kinase inhibition enables proliferation of adult mammalian cardiomyocytes. *Genes & development* **19**, 1175-1187, doi:10.1101/gad.1306705 (2005).

36 Harper, J. V. & Brooks, G. The mammalian cell cycle: an overview. *Methods in molecular biology* **296**, 113-153 (2005).

37 Fededa, J. P. & Gerlich, D. W. Molecular control of animal cell cytokinesis. *Nature cell biology* **14**, 440-447, doi:10.1038/ncb2482 (2012).

38 Floyd, S., Pines, J. & Lindon, C. APC/C Cdh1 targets aurora kinase to control reorganization of the mitotic spindle at anaphase. *Current biology : CB* **18**, 1649-1658, doi:10.1016/j.cub.2008.09.058 (2008).

39 Niiya, F., Xie, X., Lee, K. S., Inoue, H. & Miki, T. Inhibition of cyclin-dependent kinase 1 induces cytokinesis without chromosome segregation in an ECT2 and MgcRacGAP-dependent manner. *The Journal of biological chemistry* **280**, 36502-36509, doi:10.1074/jbc.M508007200 (2005).

40 Dai, B. N., Yang, Y., Chau, Z. & Jhanwar-Uniyal, M. Polo-like kinase 1 regulates RhoA during cytokinesis exit in human cells. *Cell proliferation* **40**, 550-557, doi:10.1111/j.1365-2184.2007.00447.x (2007).

41 Petronczki, M., Glotzer, M., Kraut, N. & Peters, J. M. Polo-like kinase 1 triggers the initiation of cytokinesis in human cells by promoting recruitment of the RhoGEF Ect2 to the central spindle. *Developmental cell* **12**, 713-725, doi:10.1016/j.devcel.2007.03.013 (2007).

42 Basant, A. *et al.* Aurora B kinase promotes cytokinesis by inducing centralspindlin oligomers that associate with the plasma membrane. *Developmental cell* **33**, 204-215, doi:10.1016/j.devcel.2015.03.015 (2015).

43 Fu, J., Bian, M., Jiang, Q. & Zhang, C. Roles of Aurora kinases in mitosis and tumorigenesis. *Molecular cancer research : MCR* **5**, 1-10, doi:10.1158/1541-7786.MCR-06-0208 (2007).

44 Green, R. A., Paluch, E. & Oegema, K. Cytokinesis in animal cells. *Annual review of cell and developmental biology* **28**, 29-58, doi:10.1146/annurev-cellbio-101011-155718 (2012).

45 Piperno, G., LeDizet, M. & Chang, X. J. Microtubules containing acetylated alpha-tubulin in mammalian cells in culture. *The Journal of cell biology* **104**, 289-302 (1987).

46 Zhu, C. & Jiang, W. Cell cycle-dependent translocation of PRC1 on the spindle by Kif4 is essential for midzone formation and cytokinesis. *Proceedings of the National Academy of Sciences of the United States of America* **102**, 343-348, doi:10.1073/pnas.0408438102 (2005).

47 Yuce, O., Piekny, A. & Glotzer, M. An ECT2-centralspindlin complex regulates the localization and function of RhoA. *The Journal of cell biology* **170**, 571-582, doi:10.1083/jcb.200501097 (2005).

48 Yoshida, S., Bartolini, S. & Pellman, D. Mechanisms for concentrating Rho1 during cytokinesis. *Genes & development* **23**, 810-823, doi:10.1101/gad.1785209 (2009).

49 Kamijo, K. *et al.* Dissecting the role of Rho-mediated signaling in contractile ring formation. *Molecular biology of the cell* **17**, 43-55, doi:10.1091/mbc.E05-06-0569 (2006).

50 Somers, W. G. & Saint, R. A RhoGEF and Rho family GTPase-activating protein complex links the contractile ring to cortical microtubules at the onset of cytokinesis. *Developmental cell* **4**, 29-39 (2003).

51 Piekny, A. J. & Glotzer, M. Anillin is a scaffold protein that links RhoA, actin, and myosin during cytokinesis. *Current biology : CB* **18**, 30-36, doi:10.1016/j.cub.2007.11.068 (2008).

52 Kechad, A., Jananji, S., Ruella, Y. & Hickson, G. R. Anillin acts as a bifunctional linker coordinating midbody ring biogenesis during cytokinesis. *Current biology : CB* **22**, 197-203, doi:10.1016/j.cub.2011.11.062 (2012).

53 Hu, C. K., Coughlin, M. & Mitchison, T. J. Midbody assembly and its regulation during cytokinesis. *Molecular biology of the cell* **23**, 1024-1034, doi:10.1091/mbc.E11-08-0721 (2012).

54 Elia, N., Sougrat, R., Spurlin, T. A., Hurley, J. H. & Lippincott-Schwartz, J. Dynamics of endosomal sorting complex required for transport (ESCRT) machinery during cytokinesis and its role in abscission. *Proceedings of the National Academy of Sciences of the United States of America* **108**, 4846-4851, doi:10.1073/pnas.1102714108 (2011).

55 Elia, N., Fabrikant, G., Kozlov, M. M. & Lippincott-Schwartz, J. Computational model of cytokinetic abscission driven by ESCRT-III polymerization and remodeling. *Biophysical journal* **102**, 2309-2320, doi:10.1016/j.bpj.2012.04.007 (2012).

56 Bastos, R. N. & Barr, F. A. Plk1 negatively regulates Cep55 recruitment to the midbody to ensure orderly abscission. *The Journal of cell biology* **191**, 751-760, doi:10.1083/jcb.201008108 (2010).

57 Neto, H. & Gould, G. W. The regulation of abscission by multi-protein complexes. *Journal of cell science* **124**, 3199-3207, doi:10.1242/jcs.083949 (2011).

58 Crowell, E. F., Gaffuri, A. L., Gayraud-Morel, B., Tajbakhsh, S. & Echard, A. Engulfment of the midbody remnant after cytokinesis in mammalian cells. *Journal of cell science* **127**, 3840-3851, doi:10.1242/jcs.154732 (2014).

59 Kuo, T. C. *et al.* Midbody accumulation through evasion of autophagy contributes to cellular reprogramming and tumorigenicity. *Nature cell biology* **13**, 1214-1223, doi:10.1038/ncb2332 (2011).

60 Maiato, H. & Logarinho, E. Mitotic spindle multipolarity without centrosome amplification. *Nature cell biology* **16**, 386-394 (2014).

61 Choudhary, A. *et al.* Interphase cytofission maintains genomic integrity of human cells after failed cytokinesis. *Proceedings of the National Academy of Sciences of the United States of America* **110**, 13026-13031, doi:10.1073/pnas.1308203110 (2013).

62 Gabriel, M., Horky, D., Svoboda, A. & Kopecka, M. Cytochalasin D interferes with contractile actin ring and septum formation in Schizosaccharomyces japonicus var. versatilis. *Microbiology* **144 (Pt 8)**, 2331-2344 (1998).

63 Logarinho, E. *et al.* CLASPs prevent irreversible multipolarity by ensuring spindle-pole resistance to traction forces during chromosome alignment. *Nature cell biology* **14**, 295-303, doi:10.1038/ncb2423 (2012).

64 Arquint, C., Sonnen, K. F., Stierhof, Y. D. & Nigg, E. A. Cell-cycle-regulated expression of STIL controls centriole number in human cells. *Journal of cell science* **125**, 1342-1352, doi:10.1242/jcs.099887 (2012).

65 Brownlee, C. W. & Rogers, G. C. Show me your license, please: deregulation of centriole duplication mechanisms that promote amplification. *Cellular and*

molecular life sciences : CMLS **70**, 1021-1034, doi:10.1007/s00018-012-1102-6 (2013).

66 Habedanck, R., Stierhof, Y. D., Wilkinson, C. J. & Nigg, E. A. The Polo kinase Plk4 functions in centriole duplication. *Nature cell biology* **7**, 1140-1146, doi:10.1038/ncb1320 (2005).

67 Tsou, M. F. *et al.* Polo kinase and separase regulate the mitotic licensing of centriole duplication in human cells. *Developmental cell* **17**, 344-354, doi:10.1016/j.devcel.2009.07.015 (2009).

68 Nakamura, A., Arai, H. & Fujita, N. Centrosomal Aki1 and cohesin function in separase-regulated centriole disengagement. *The Journal of cell biology* **187**, 607-614, doi:10.1083/jcb.200906019 (2009).

69 Matsuo, K. *et al.* Kendrin is a novel substrate for separase involved in the licensing of centriole duplication. *Current biology : CB* **22**, 915-921, doi:10.1016/j.cub.2012.03.048 (2012).

70 Holt, L. J., Krutchinsky, A. N. & Morgan, D. O. Positive feedback sharpens the anaphase switch. *Nature* **454**, 353-357, doi:10.1038/nature07050 (2008).

71 Stevens, D., Gassmann, R., Oegema, K. & Desai, A. Uncoordinated loss of chromatid cohesion is a common outcome of extended metaphase arrest. *PloS one* **6**, e22969, doi:10.1371/journal.pone.0022969 (2011).

72 Daum, J. R. *et al.* Cohesion fatigue induces chromatid separation in cells delayed at metaphase. *Current biology : CB* **21**, 1018-1024, doi:10.1016/j.cub.2011.05.032 (2011).

73 Krauss, S. W. *et al.* Downregulation of protein 4.1R, a mature centriole protein, disrupts centrosomes, alters cell cycle progression, and perturbs mitotic spindles and anaphase. *Molecular and cellular biology* **28**, 2283-2294, doi:10.1128/MCB.02021-07 (2008).

74 Kim, K. & Rhee, K. The pericentriolar satellite protein CEP90 is crucial for integrity of the mitotic spindle pole. *Journal of cell science* **124**, 338-347, doi:10.1242/jcs.078329 (2011).

75 Kimura, M. *et al.* Mitotic catastrophe and cell death induced by depletion of centrosomal proteins. *Cell death & disease* **4**, e603, doi:10.1038/cddis.2013.108 (2013).

76 Duensing, S. *et al.* The human papillomavirus type 16 E6 and E7 oncoproteins cooperate to induce mitotic defects and genomic instability by uncoupling centrosome duplication from the cell division cycle. *Proceedings of the National Academy of Sciences of the United States of America* **97**, 10002-10007, doi:10.1073/pnas.170093297 (2000).

77 Shekhar, M. P., Lyakhovich, A., Visscher, D. W., Heng, H. & Kondrat, N. Rad6 overexpression induces multinucleation, centrosome amplification, abnormal mitosis, aneuploidy, and transformation. *Cancer research* **62**, 2115-2124 (2002).

78 Meraldi, P., Honda, R. & Nigg, E. A. Aurora-A overexpression reveals tetraploidization as a major route to centrosome amplification in p53-/- cells. *The EMBO journal* **21**, 483-492 (2002).

79 Marthiens, V., Piel, M. & Basto, R. Never tear us apart--the importance of centrosome clustering. *Journal of cell science* **125**, 3281-3292, doi:10.1242/jcs.094797 (2012).

80 Ganem, N. J., Godinho, S. A. & Pellman, D. A mechanism linking extra centrosomes to chromosomal instability. *Nature* **460**, 278-282, doi:10.1038/nature08136 (2009).

81 Chan, J. Y. A clinical overview of centrosome amplification in human cancers. *International journal of biological sciences* **7**, 1122-1144 (2011).

82 Boveri, T. Concerning the origin of malignant tumours by Theodor Boveri. Translated and annotated by Henry Harris. *Journal of cell science* **121 Suppl 1**, 1-84, doi:10.1242/jcs.025742 (2008).

83 Steinbeck, R. G. Pathologic mitoses and pathology of mitosis in tumorigenesis. *European journal of histochemistry : EJH* **45**, 311-318 (2001).

84 Kramer, A., Maier, B. & Bartek, J. Centrosome clustering and chromosomal (in)stability: a matter of life and death. *Molecular oncology* **5**, 324-335, doi:10.1016/j.molonc.2011.05.003 (2011).

85 Quintyne, N. J., Reing, J. E., Hoffelder, D. R., Gollin, S. M. & Saunders, W. S. Spindle multipolarity is prevented by centrosomal clustering. *Science* **307**, 127-129, doi:10.1126/science.1104905 (2005).

86 Gregan, J., Polakova, S., Zhang, L., Tolic-Norrelykke, I. M. & Cimini, D. Merotelic kinetochore attachment: causes and effects. *Trends in cell biology* **21**, 374-381, doi:10.1016/j.tcb.2011.01.003 (2011).

87 Silkworth, W. T., Nardi, I. K., Scholl, L. M. & Cimini, D. Multipolar spindle pole coalescence is a major source of kinetochore mis-attachment and chromosome mis-segregation in cancer cells. *PloS one* **4**, e6564, doi:10.1371/journal.pone.0006564 (2009).

88 Duensing, S., Duensing, A., Crum, C. P. & Munger, K. Human papillomavirus type 16 E7 oncoprotein-induced abnormal centrosome synthesis is an early event in the evolving malignant phenotype. *Cancer research* **61**, 2356-2360 (2001).

89 Thein, K. H., Kleylein-Sohn, J., Nigg, E. A. & Gruneberg, U. Astrin is required for the maintenance of sister chromatid cohesion and centrosome integrity. *The Journal of cell biology* **178**, 345-354, doi:10.1083/jcb.200701163 (2007).

90 Briggs, M. W. & Sacks, D. B. IQGAP proteins are integral components of cytoskeletal regulation. *EMBO reports* **4**, 571-574, doi:10.1038/sj.embor.embor867 (2003).

91 Shannon, K. B. IQGAP Family Members in Yeast, Dictyostelium, and Mammalian Cells. *International journal of cell biology* **2012**, 894817, doi:10.1155/2012/894817 (2012).

92 Nojima, H. *et al.* IQGAP3 regulates cell proliferation through the Ras/ERK signalling cascade. *Nature cell biology* **10**, 971-978, doi:10.1038/ncb1757 (2008).

93 Johnson, M., Sharma, M., Brocardo, M. G. & Henderson, B. R. IQGAP1 translocates to the nucleus in early S-phase and contributes to cell cycle progression after DNA replication arrest. *The international journal of biochemistry & cell biology* **43**, 65-73, doi:10.1016/j.biocel.2010.09.014 (2011).

94 Johnson, M. A., Sharma, M., Mok, M. T. & Henderson, B. R. Stimulation of in vivo nuclear transport dynamics of actin and its co-factors IQGAP1 and Rac1 in response to DNA replication stress. *Biochimica et biophysica acta* **1833**, 2334-2347, doi:10.1016/j.bbamcr.2013.06.002 (2013).

95 Lee, I. J., Coffman, V. C. & Wu, J. Q. Contractile-ring assembly in fission yeast cytokinesis: Recent advances and new perspectives. *Cytoskeleton* **69**, 751-763, doi:10.1002/cm.21052 (2012).

96 Machesky, L. M. Cytokinesis: IQGAPs find a function. *Current biology : CB* **8**, R202-205 (1998).

97 Wang, J. B., Sonn, R., Tekletsadik, Y. K., Samorodnitsky, D. & Osman, M. A. IQGAP1 regulates cell proliferation through a novel CDC42-mTOR pathway. *Journal of cell science* **122**, 2024-2033, doi:10.1242/jcs.044644 (2009).

98 Morita, E. *et al.* Human ESCRT and ALIX proteins interact with proteins of the midbody and function in cytokinesis. *The EMBO journal* **26**, 4215-4227, doi:10.1038/sj.emboj.7601850 (2007).

99 Skop, A. R., Liu, H., Yates, J., 3rd, Meyer, B. J. & Heald, R. Dissection of the mammalian midbody proteome reveals conserved cytokinesis mechanisms. *Science* **305**, 61-66, doi:10.1126/science.1097931 (2004).

100 Tekletsadik, Y. K., Sonn, R. & Osman, M. A. A conserved role of IQGAP1 in regulating TOR complex 1. *Journal of cell science* **125**, 2041-2052, doi:10.1242/jcs.098947 (2012).

101 Adachi, M., Kawasaki, A., Nojima, H., Nishida, E. & Tsukita, S. Involvement of IQGAP family proteins in the regulation of mammalian cell cytokinesis. *Genes to cells : devoted to molecular & cellular mechanisms* **19**, 803-820, doi:10.1111/gtc.12179 (2014).

102 Le Clainche, C. *et al.* IQGAP1 stimulates actin assembly through the N-WASP-Arp2/3 pathway. *The Journal of biological chemistry* **282**, 426-435, doi:10.1074/jbc.M607711200 (2007).

103 Watanabe, T. *et al.* Phosphorylation of CLASP2 by GSK-3beta regulates its interaction with IQGAP1, EB1 and microtubules. *Journal of cell science* **122**, 2969-2979, doi:10.1242/jcs.046649 (2009).

104 Rittmeyer, E. N., Daniel, S., Hsu, S. C. & Osman, M. A. A dual role for IQGAP1 in regulating exocytosis. *Journal of cell science* **121**, 391-403, doi:10.1242/jcs.016881 (2008).

105 White, C. D., Brown, M. D. & Sacks, D. B. IQGAPs in cancer: a family of scaffold proteins underlying tumorigenesis. *FEBS letters* **583**, 1817-1824, doi:10.1016/j.febslet.2009.05.007 (2009).

106 Sbroggio, M. *et al.* ERK1/2 activation in heart is controlled by melusin, focal adhesion kinase and the scaffold protein IQGAP1. *Journal of cell science* **124**, 3515-3524, doi:10.1242/jcs.091140 (2011).

107 Sbroggio, M. *et al.* IQGAP1 regulates ERK1/2 and AKT signalling in the heart and sustains functional remodelling upon pressure overload. *Cardiovascular research* **91**, 456-464, doi:10.1093/cvr/cvr103 (2011).

108 Jin, S. H. *et al.* IQGAP2 inactivation through aberrant promoter methylation and promotion of invasion in gastric cancer cells. *International journal of cancer. Journal international du cancer* **122**, 1040-1046, doi:10.1002/ijc.23181 (2008).

109 Schmidt, V. A., Chiariello, C. S., Capilla, E., Miller, F. & Bahou, W. F. Development of hepatocellular carcinoma in Iqgap2-deficient mice is IQGAP1 dependent. *Molecular and cellular biology* **28**, 1489-1502, doi:10.1128/MCB.01090-07 (2008).

110 White, C. D. *et al.* IQGAP1 and IQGAP2 are reciprocally altered in hepatocellular carcinoma. *BMC gastroenterology* **10**, 125, doi:10.1186/1471-230X-10-125 (2010).

111 Xie, Y. *et al.* IQGAP2, A candidate tumour suppressor of prostate tumorigenesis. *Biochimica et biophysica acta* **1822**, 875-884, doi:10.1016/j.bbadis.2012.02.019 (2012).

112 Logue, J. S., Whiting, J. L., Tunquist, B., Langeberg, L. K. & Scott, J. D. Anchored protein kinase A recruitment of active Rac GTPase. *The Journal of biological chemistry* **286**, 22113-22121, doi:10.1074/jbc.M111.232660 (2011).

113 Ghaleb, A. M. *et al.* IQ Motif-Containing GTPase-Activating Protein 2 (IQGAP2) Is a Novel Regulator of Colonic Inflammation in Mice. *PloS one* **10**, e0129314, doi:10.1371/journal.pone.0129314 (2015).

114 Sugano, Y. *et al.* The Rho-GTPase binding protein IQGAP2 is required for the glomerular filtration barrier. *Kidney international*, doi:10.1038/ki.2015.197 (2015).

115 Wang, S. *et al.* IQGAP3, a novel effector of Rac1 and Cdc42, regulates neurite outgrowth. *Journal of cell science* **120**, 567-577, doi:10.1242/jcs.03356 (2007).

116 Kunimoto, K. *et al.* Involvement of IQGAP3, a regulator of Ras/ERK-related cascade, in hepatocyte proliferation in mouse liver regeneration and development. *Journal of cellular physiology* **220**, 621-631, doi:10.1002/jcp.21798 (2009).

117 Yang, Y. *et al.* IQGAP3 promotes EGFR-ERK signaling and the growth and metastasis of lung cancer cells. *PloS one* **9**, e97578, doi:10.1371/journal.pone.0097578 (2014).

118 Monteleon, C. L. *et al.* IQGAP1 and IQGAP3 Serve Individually Essential Roles in Normal Epidermal Homeostasis and Tumor Progression. *The Journal of investigative dermatology* **135**, 2258-2265, doi:10.1038/jid.2015.140 (2015).

119 Huang da, W., Sherman, B. T. & Lempicki, R. A. Systematic and integrative analysis of large gene lists using DAVID bioinformatics resources. *Nature protocols* **4**, 44-57, doi:10.1038/nprot.2008.211 (2009).

120 Kuo, T. C., Chang, P. Y., Huang, S. F., Chou, C. K. & Chao, C. C. Knockdown of HURP inhibits the proliferation of hepacellular carcinoma cells via downregulation of gankyrin and accumulation of p53. *Biochemical pharmacology* **83**, 758-768, doi:10.1016/j.bcp.2011.12.034 (2012).

121 Engel, F. B. *et al.* A mammalian myocardial cell-free system to study cell cycle reentry in terminally differentiated cardiomyocytes. *Circulation research* **85**, 294-301 (1999).

122 Gully, C. P. *et al.* Antineoplastic effects of an Aurora B kinase inhibitor in breast cancer. *Molecular cancer* **9**, 42, doi:10.1186/1476-4598-9-42 (2010).

123 Menon, M. B. *et al.* Genetic deletion of SEPT7 reveals a cell type-specific role of septins in microtubule destabilization for the completion of cytokinesis. *PLoS genetics* **10**, e1004558, doi:10.1371/journal.pgen.1004558 (2014).

124 Yoshizaki, H. *et al.* Cell type-specific regulation of RhoA activity during cytokinesis. *The Journal of biological chemistry* **279**, 44756-44762, doi:10.1074/jbc.M402292200 (2004).

125 Schiel, J. A. *et al.* FIP3-endosome-dependent formation of the secondary ingression mediates ESCRT-III recruitment during cytokinesis. *Nature cell biology* **14**, 1068-1078, doi:10.1038/ncb2577 (2012).

126 Mateer, S. C. *et al.* The mechanism for regulation of the F-actin binding activity of IQGAP1 by calcium/calmodulin. *The Journal of biological chemistry* **277**, 12324-12333, doi:10.1074/jbc.M109535200 (2002).

127 Mateer, S. C., Wang, N. & Bloom, G. S. IQGAPs: integrators of the cytoskeleton, cell adhesion machinery, and signaling networks. *Cell motility and the cytoskeleton* **55**, 147-155, doi:10.1002/cm.10118 (2003).

128 Causier, B. Studying the interactome with the yeast two-hybrid system and mass spectrometry. *Mass spectrometry reviews* **23**, 350-367, doi:10.1002/mas.10080 (2004).

129 Doorenbos, C. J., Blauw, G. J. & van Brummelen, P. Arterial and venous effects of atrial natriuretic peptide in the human forearm. *American journal of hypertension* **4**, 333-340 (1991).

130 Mardin, B.R., Schiebel E. Breaking the ties that bind: New advances in centrosome biology. *The Journal of Cell Biology* **197**, 11-18, doi: 10.1083/jcb.201108006 (2012).

Acknowledgments

I would like to thank all the people who gave me their huge support (psychological and emotional) during all these years of my PhD study.

I'm particularly thankful to my doctoral supervisor Prof. Dr. Felix Engel who accepted me as IMPRS PhD student in his laboratory at Max Plank Institute of Heart and Lung Research. I will be always thankful for his kind guidance, encouragement and motivation. In particular I would like to thank him for believing in me and in my research.

I'm especially thankful to my university supervisor Prof. Dr. Frasch who supports my PhD application at the FAU from the first day. I would be always thankful for his immediate help, for his support in solving all my bureaucratic and not problems and at last but not least, for his constructive criticisms.

My gratitude goes also to Prof. Dr. Gaubatz who was always opened to share materials, ideas and knowledge of the "cytokinesis word". I would be never thankful enough for his support. Special thanks go to two members of his working group, Marc Fackler and Patrick Wolter, for being always present to share ideas and solve technical issues even though the physical distance.

I would like to thank all my working colleagues from Prof. Engel's laboratory for their help and assistance in these last two years of my PhD. They become more than only colleagues. So big thanks go to: Dr. David Zebrowski for sharing the "responsibilities" of building the new laboratory in Erlangen from scratch; Dr. Silvia Vergarajauregui for helping in my research and supporting me and my ideas; Gentian Musa and Robert Becker for bringing more "fun" in the routine work; Melanie Schubert for assisting me with her perfect efficiency and organization; Michaela Kümmel and Jana Petzold for organizing perfectly the second moving and for being constantly a daily help; Anna-Maria Herrmann for organizing the laboratory in Univesitätsstrasse.

Particular thanks go to Dr. Fulvia Ferrazzi and Marco Moraschini for helping in all the bioinformatics analyses.

I would like to thank all the organizers and the PhD students of the doctoral program IMPRS at the Max Plank Institute for Heart and Lung research for providing me the possibility to improve my skills with workshops and mainly for organizing the annual PhD retreats.

My warm thanks go to Adriana Contreras, Piera De Gaspari, Elisabetta Gamen and Diya Hasan for becoming my “replacement family” and being always next to me as a family does despite the distance in these last years.

Special thanks go to Frederic Strobl for being always present in bad and good moments of this new experience, for supporting me continuously and for sharing with me such beautiful moments.

It is my pleasure to thank also my “new” Erlangen friends, Chirine El Baba, Jelena Ivanovska and Marko Ivkovic who make me feel not alone during the first year of the moving in Erlangen. Other thanks go to Elena Irollo who makes me feel “home” at the TRC center.

I would like to thank also all my closest friends from Naples who always believe in me and help me with their life suggestions: Margherita, Mariangela, Sarah, Rossella and Azzurra.

Finally, I would like to deeply thank all my “enlarged family” for their constant support and huge love: my mother, Patrizia, and my sister, Stefania, all the members of the Roselli family (Nonna Viviana, Roberto, Stefania, Pierpaolo, Cinzia, Nevio, Francesco, Marina, Franco, Rosanna e Vera) and Leone family (Riccardo, Alberta, Alexandra, Gustavo, Lorenzo e Manuela) and the friends, Stefano, Paolo, Silvia, Gianluca, Bruna, Ornella, Massimo, Paola, Ape, Giorgio, Alessandro, Valeria, Paola e Francesco.

Curriculum Vitae

Name: Marina Leone **Date:** September 2, 2015

Date of Birth: 03.06.1986 **Place of Birth:** Naples, Italy

Office Address: Universitätsklinikum Erlangen
Schwabachanlage 12 (TRC center), Erlangen, 91054, GERMANY

Home Address: Schobertweg 5, Erlangen, 91056, GERMANY

E-Mail: marina.leone@uk-erlangen.de **Phone:** +49 (0) 9131 85 25701

Education

01.09.2005-04.11.2008	BSc degree in Biotechnology for healthcare, Federico II, Naples (Italy), mark: 110/110 cum laude.
04.11.2008-29.10.2010	MSc degree in Medical Biotechnologies, Federico II, Naples (Italy), mark: 110/110 cum laude, Host laboratory for MSc thesis: Dr. Missero, CEINGE, Naples.
2011-Present	PhD student, Max Planck Institute for Heart and Lung research, IMPRS PhD program (International Max Planck research School) /Friedrich-Alexander-University Erlangen-Nürnberg (FAU) university, Bad Nauheim/ Erlangen (Germany)

Academic

2014	Supervisor of Bachelor student

Awards and Honors

2013	ImmunoTools Award 2013 (ImmunoTools GmbH, Germany)
2013	Student Sponsorship 2013 (Primer designLtd, UK)

2014 PhD coordinator of the CYDER (Cell cycle in Disease and Regeneration), EFI (Emergency Fields Initiative)

Professional Societies

since 2014 Member of Biochemical Society

Original publications:

- **Leone M,** Magadum A, Engel FB. "Cardiomyocyte proliferation in cardiac development and regeneration – a guide to methodologies and interpretations". AJP-Heart and Circulatory Physiology. (Review) (accepted)
- Zebrowski DC, Vergarajauregui S, Wu CC, Piatkowski T, Becker R, **Leone M**, Hirth S, Ricciardi F, Falk N, Giessl A, Just S, Braun T, Weidinger G, Engel FB "Developmental alterations in centrosome integrity contribute to the post-mitotic state of mammalian cardiomyocytes". *eLife.* 2015 Aug 6; PMID: 26247711.
- Mishra HK, Prots I, Havlicek S, Kohl Z, Perez-Branguli F, Boerstler T, Anneser L, Minakaki G, Wend H, Hempl M, **Leone M**, Brückner M, Klucken J, Reis A, Boyer L, Schuierer G, Behrens J, Lampert A, Engel FB, Gage FH, Winkler J and Beate Winner. "GSK3/ß-dependent dysregulation of neurodevelopment in SPG11-linked hereditary spastic paraplegia". *Science Translational Medicine.* (submitted)
- Stopp S, Fackler M, **Leone M**, Frantz S, Engel FB and Gaubatz S."A role for GAS2L3 in cytokinesis". (in preparation)

Conference contributions

Poster:

1) 3rd IMPRS Annual Retreat
   Marina Leone, Ajit Magadum, Mortimer Korf-Klingebiel, Kai Wollert, Felix B. Engel; **Systems biology approach to promote cardiac regeneration**; 2011, Kleinwalsertal, Austria.
2) 4th IMPRS Annual Retreat

Leone, M., Ferrazzi, F., Korf-Klingebiel, M., Wollert, K., Engel, F.B.; **System biology approach to promote cardiac regeneration**; 2012, Kloster Hoechst, Germany.

3) The Dynamic Cell 2014
   Leone, M., Engel, F.B.; **IQGAP3 is a novel player in cytokinesis**; 2014, Cambridge, UK
4) Cell Cycle: bridging scales in cell division
   Leone, M., Engel, F.B.; **IQGAP3 is a novel player in cytokinesis**; 2014, Roscoff (Brittany), France.
5) DGZ: International Meeting of the German Society for Cell Biology
   Leone, M., Ferrazzi, F., Engel, F.B.; **IQGAP3 is a novel player in cytokinesis**; 2015, Cologne, Germany.

Talk:

1) 5th IMPRS Annual Retreat
   Leone, M., Engel, F.B.; **IQGAP3 is a novel player in cytokinesis**; 2013, Kleinwalsertal, Austria.

Training courses:

1) Whole Transcriptome Data Analysis; 2012, EMBL, Germany.